

## INFORMATION TO USERS

This manuscript has been reproduced from the microfilm master. UMI films the text directly from the original or copy submitted. Thus, some thesis and dissertation copies are in typewriter face, while others may be from any type of computer printer.

**The quality of this reproduction is dependent upon the quality of the copy submitted.** Broken or indistinct print, colored or poor quality illustrations and photographs, print bleedthrough, substandard margins, and improper alignment can adversely affect reproduction.

In the unlikely event that the author did not send UMI a complete manuscript and there are missing pages, these will be noted. Also, if unauthorized copyright material had to be removed, a note will indicate the deletion.

Oversize materials (e.g., maps, drawings, charts) are reproduced by sectioning the original, beginning at the upper left-hand corner and continuing from left to right in equal sections with small overlaps. Each original is also photographed in one exposure and is included in reduced form at the back of the book.

Photographs included in the original manuscript have been reproduced xerographically in this copy. Higher quality 6" x 9" black and white photographic prints are available for any photographs or illustrations appearing in this copy for an additional charge. Contact UMI directly to order.

# UMI

A Bell & Howell Information Company  
300 North Zeeb Road, Ann Arbor MI 48106-1346 USA  
313/761-4700 800/521-0600



University of Alberta

A Direct Method for Determination of No-Flow Boundaries  
in Rectangular Reservoirs Using Pressure Buildup Data

by

Dorothy Greenidge



A thesis submitted to the Faculty of Graduate Studies and  
Research in partial fulfillment of the requirements for the degree of  
Doctor of Philosophy  
in  
Petroleum Engineering

Department of Civil and Environmental Engineering

Edmonton, Alberta  
Fall 1998



National Library  
of Canada

Acquisitions and  
Bibliographic Services

395 Wellington Street  
Ottawa ON K1A 0N4  
Canada

Bibliothèque nationale  
du Canada

Acquisitions et  
services bibliographiques

395, rue Wellington  
Ottawa ON K1A 0N4  
Canada

*Your file Votre référence*

*Our file Notre référence*

The author has granted a non-exclusive licence allowing the National Library of Canada to reproduce, loan, distribute or sell copies of this thesis in microform, paper or electronic formats.

The author retains ownership of the copyright in this thesis. Neither the thesis nor substantial extracts from it may be printed or otherwise reproduced without the author's permission.

L'auteur a accordé une licence non exclusive permettant à la Bibliothèque nationale du Canada de reproduire, prêter, distribuer ou vendre des copies de cette thèse sous la forme de microfiche/film, de reproduction sur papier ou sur format électronique.

L'auteur conserve la propriété du droit d'auteur qui protège cette thèse. Ni la thèse ni des extraits substantiels de celle-ci ne doivent être imprimés ou autrement reproduits sans son autorisation.

0-612-34771-0

Canada

**University of Alberta**

**Library Release Form**

**Name of Author:** Dorothy Greenidge

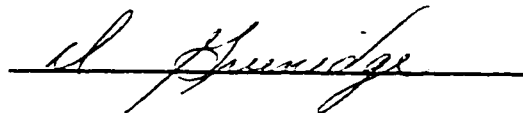
**Title of Thesis:** A Direct Method for Determination of No-Flow Boundaries in Rectangular Reservoirs Using Pressure Buildup Data

**Degree:** Doctor of Philosophy

**Year this Degree Granted:** 1998

Permission is hereby granted to the University of Alberta Library to reproduce single copies of this thesis and to lend or sell such copies for private, scholarly, or scientific research purposes only.

The author reserves all other publication and other rights in association with the copyright in the thesis, and except as hereinbefore provided, neither the thesis nor any substantial portion thereof may be printed or otherwise reproduced in any material form whatever without the author's prior written permission.



64 Hawksley Crescent N.W.  
Calgary, Alberta  
Canada  
T3G 3C4

Dated July 30, 1998

***Courage is the price that Life  
extracts for granting  
peace.***

***The soul that knows it not,  
knows no release  
from little things.***

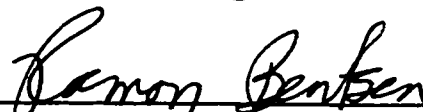
***Amelia Earhart***

***(1897 - 1937)***

University of Alberta

Faculty of Graduate Studies and Research

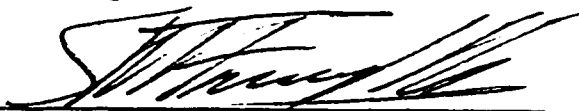
The undersigned certify that they have read, and recommend to the Faculty of Graduate Studies and Research for acceptance, a thesis entitled A Direct Method for Determination of No-Flow Boundaries in Rectangular Reservoirs submitted by Dorothy Greenidge in partial fulfillment of the requirements for the degree of Doctor of Philosophy in Petroleum Engineering.



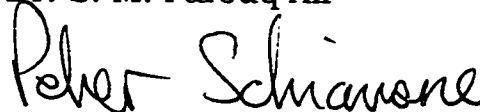
Supervisor Dr. R.G. Bentsen



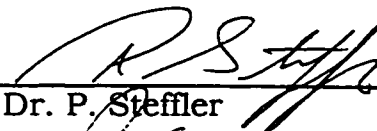
Co-Supervisor Mr. L. Mattar



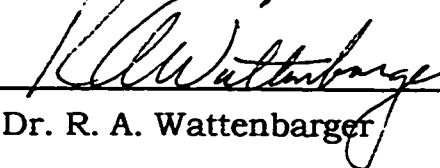
Dr. S. M. Farouq Ali



Dr. P. Schiavone



Dr. P. Steffler



Dr. R. A. Wattenbarger

Dated May 25, 1998

## **ABSTRACT**

Detection of no-flow boundaries is an integral and important aspect of well test analysis. Identification of no-flow boundaries assists in defining the reservoir system and is used in determining the areal extent of a reservoir. Existing procedures for detection of boundaries rely heavily on the use of type curves. These type curves have been derived for use with drawdown data, and do not necessarily work with buildup data.

A direct method for detecting no-flow boundaries in rectangular reservoirs using only buildup data, without reference to drawdown type curves, has been developed. This direct method of boundary detection introduces the concept of Boundary Influenced Difference of Pressure, or BIDP, which relies on using an infinite acting reservoir as a frame of reference. The BIDP is defined as the difference between the "Infinite-Acting Reservoir" pressure and the "Boundary Influenced" pressure. This differencing procedure removes the effect of the infinite-acting behaviour and accentuates the boundary effects. The BIDP thus contains the "boundary information". Additionally, by utilizing the semi-log derivative of the BIDP the number of boundaries is indicated and the distance to those boundaries may be calculated.

Furthermore, this method does not rely on the duration of producing time, as do the existing traditional methods of boundary detection. This direct method depends only on the duration of shut-in time, and is not affected by the duration of producing time. Thus boundaries can be detected for relatively short producing times and longer shut-in times.

The method is illustrated with examples using synthetic data. The application of the method to "noisy" data is also demonstrated.



## **ACKNOWLEDGEMENTS**

Success is seldom a solitary journey. This work is no exception. There are many people who encouraged me to continue when things looked rather bleak, and I thank you all.

In particular, my heartfelt gratitude to my husband, Keith Drysdale. Without your support and encouragement this would never have come to pass.

I am grateful to Louis Mattar for his many hours of discussion, and his guidance and understanding throughout this research. Also, thanks to Louis's wife, Shelia, for her cheerful encouragement and many cups of tea.

Thank you Dr. Bentsen for all your kindness and assistance. I truly appreciated your thought provoking questions, many discussions, and the meticulous editing of this work.

To all my friends, especially Ron and Sonia Tibbatts, Karl and Jennifer Schulze, Kimi Rutz, Bonnie Cook, and Lynn Becker, thanks for your support and friendship during the course of this work.

## **TABLE OF CONTENTS**

<b>Chapter</b>	<b>Page</b>
1.0 Introduction	1
2.0 Review of Literature	5
2.1 Background	5
2.2 Type Curves	8
2.3 Deconvolution	12
2.4 Boundary Conditions and Solutions	17
3.0 Statement of the Problem	20
4.0 Development of the Boundary Detection Method	23
4.1 General Assumptions of the Method	25
4.2 General Concepts of the Method	26
4.2.1 Radial Diffusivity Equation and Superposition	27
4.2.2 Method of Images	29
4.2.3 Radius of Investigation	31
4.2.4 Infinite-Acting Reservoir Frame of Reference	33
4.3 Variation from the Infinite Case	37
4.4 Description of d(BIDP) Curve	41
4.5 Single No-Flow Boundary	55
4.6 Two Intersecting No-Flow Boundaries	61
4.7 Two Parallel No-Flow Boundaries	65
4.8 Three Intersecting No-Flow Boundaries	69
4.9 Four Intersecting No-Flow Boundaries	77
4.10 Summary of Method of Boundary Determination	88
4.11 Discussion of Computer Programs	89

5.0	Results and Discussion	91
5.1	Semi-Infinite Reservoir d(BIDP) Curves	92
5.2	Finite Reservoir d(BIDP) Curves	95
5.3	Effects of Wellbore Storage and Skin	98
5.4	Effect of Changing Permeability $k$	103
5.5	Effect of Changing Flow Rate $q$	109
5.6	Multiple Equidistant Boundaries	112
5.7	Effect of Producing time $t_p$	115
5.8	Effect of Shut-In Time $\Delta t$	120
5.9	Use of the d(BIDP) Method with Noisy Data	122
6.0	Conclusions and Recommendations	126
6.1	Conclusions	126
6.2	Recommendations	128
7.0	References	129
	Appendix	137
	Solution to the Radial Diffusivity Equation for Constant Flow Rate in an Infinite Medium	137
	Key to Reservoir Configurations used in Figures	142
	Distance to Boundary - Sample Calculation	144
	Computer Program Listings	145

## **LIST OF FIGURES**

Figure	Page
4.2.2.1 Example of Method of Images	30
4.2.4.1 Pressure Difference $\Delta p_{\text{drawdown}}$ and $\Delta p_{\text{buildup}}$	34
4.2.4.2 Pressure Difference $\Delta p_{\text{BDIP}}$	36
4.3.1 Boundary Influenced Difference of Pressure	38
4.3.2 BIDP for Different Boundary Conditions	40
4.4.1 Regions of the d(BIDP) Curve	43
4.4.2 d(BIDP) Curve for a Reservoir with a Single No-Flow Boundary	46
4.4.3 d(BIDP) Curve for a Reservoir with Two No-Flow Boundaries	47
4.4.4 d(BIDP) Curve for a Reservoir with Three No-Flow Boundaries	49
4.4.5 d(BIDP) Curve for a Reservoir with Four No-Flow Boundaries	51
4.4.6 d(BIDP) Curve for a Reservoir with Four No-Flow Boundaries - expanded scale	53
4.5.1 Method of Images for a Single No-Flow Boundary	55
4.5.2 d(BIDP) Curve for Single Boundary	58
4.5.3 Comparison of Difference Techniques	60
4.6.1 Method of Images Two Intersection Boundaries	61
4.6.2 d(BIDP) Curve for Reservoir with Two Intersecting Boundaries	64

4.7.1	Method of Images for Two Parallel Boundaries	65
4.7.2	d(BIDP) Curve for Two Parallel No-Flow Boundaries	68
4.8.1	Method of Images for Three No-Flow Boundaries	69
4.8.2	d(BIDP) Curve for Three No-Flow Boundaries	75
4.9.1	Method of Images for Four No-Flow Boundaries	77
4.9.2	d(BIDP) Curve for Four No-Flow Boundaries	86
5.1.1	Single Boundary Reservoir	93
5.2.1	Finite Reservoir	96
5.3.1	Single Boundary Reservoir without Wellbore Storage or Skin	99
5.3.2	Single Boundary Reservoir With Wellbore Storage and Skin	100
5.4.1	Single Boundary Reservoir with Permeability of 1md	104
5.4.2	Single Boundary Reservoir with Permeability of 10md	105
5.4.3	Single Boundary Reservoir with Permeability of 100md	106
5.4.4	Single Boundary Reservoir with Permeability of 1000md	107
5.5.1	Single Boundary Reservoir - Flow Rate of 10m <sup>3</sup> /d	110
5.5.2	Single Boundary Reservoir - Flow Rate of 25 m <sup>3</sup> /d	111
5.6.1	Multiple Equidistant Boundaries	113
5.7.1	Effect of Producing Time $t_p$ - Single Boundary Reservoir	116

5.7.2	Effect of Producing Time $t_p$ - Four Boundary Case - Part 1	118
5.7.3	Effect of Producing time $t_p$ - Four Boundary Case - Part 2	119
5.9.1	$d(BIDP)$ Curve of “Noisy” Data	123
5.9.2	Application of Bourdet Smoothing Algorithm	124
5.9.3	Comparison of Smoothed and Synthetic Data	125

## **NOMENCLATURE<sup>1</sup>**

$B$	=	formation volume factor
$BIDP$	=	Boundary Influenced Difference in Pressure
$C_D$	=	dimensionless wellbore storage
$c_t$	=	total compressibility
$d$	=	distance to a boundary
$Ei$	=	exponential integral function
$h$	=	formation thickness
$I$	=	counter for infinite series
$J$	=	counter for infinite series
$k$	=	formation permeability
$p$	=	pressure
$p_i$	=	initial reservoir pressure
$p_w$	=	bottomhole pressure in a well
$p_{wf}$	=	flowing bottomhole pressure in a well
$p_{wfs}$	=	flowing bottomhole pressure in a well at the instant of shut-in
$p_{ws}$	=	shut-in bottomhole pressure in a well
$p_{wsb}$	=	shut-in bottomhole pressure in a well in a reservoir system with a boundary
$p_{ws\infty}$	=	shut-in bottomhole pressure in a well in an infinite-acting reservoir
$p_{well}$	=	bottomhole pressure in a well

---

1     The equations in this work are presented in a consistent set of units. Thus, the units of variables and parameters are not specified here.

$p_{\infty}$	=	bottomhole pressure in a well in an infinite-acting reservoir
$q$	=	flow rate of a well
$r$	=	radius
$r_i$	=	radius of investigation
$r_w$	=	wellbore radius
$s$	=	skin
$t$	=	time
$t_p$	=	producing time
$w$	=	distance to a boundary
$x$	=	distance to a boundary
$y$	=	distance to a boundary
$z$	=	distance to a boundary

### *Greek Symbols*

$\alpha$	=	group of variables used to simplify equations
$\beta$	=	group of variables used to simplify equations
$\Delta p$	=	difference in pressure
$\Delta p_{\text{BIDP}}$	=	boundary influenced difference in pressure
$\Delta p_{\text{buildup}}$	=	difference in pressure during buildup
$\Delta p_{\text{drawdown}}$	=	difference in pressure during drawdown
$\Delta t$	=	shut-in time
$\phi$	=	porosity
$\mu$	=	viscosity
$\gamma$	=	Euler's Constant = 1.781



## **1.0 Introduction**

The analysis of pressure data has been a subject of interest to petroleum engineers for many decades. Pressure data can be analyzed to determine reservoir parameters and flow characteristics. Measurement of bottom hole pressure data is one of the few ways of acquiring “real time” data from a reservoir. Furthermore, this data can be obtained with a high degree of accuracy for a very reasonable cost. Hence there is much interest in acquiring and interpreting pressure data.

The theory of pressure transient analysis is derived from the solution of the radial diffusivity equation for a fluid of small but constant compressibility flowing at a constant rate. From the general solution, using various boundary conditions which represent different well/reservoir geometries, dimensionless drawdown type curves have been developed. These drawdown type curves give the analyst the opportunity to compare the raw data with the analytical solution and thus, qualitatively and quantitatively, determine the reservoir system in which the well is located.

The graphical comparison of measured bottom hole pressure data to these standard dimensionless type curves is known as Type Curve Matching. This is a straight forward, well documented and accepted procedure. It applies equally well to simple and complex systems in drawdown tests.

Type curve matching has two main results: (1) Reservoir Parameter Estimation, and (2) Reservoir Model Identification. Here “reservoir parameters” are quantities such as reservoir permeability, wellbore storage effects and skin. “Reservoir model” refers to the reservoir-well system which would produce the specific pressure-time data recorded. Examples of reservoir models include: a circular reservoir with constant pressure boundaries with the producing well located in the center; channel reservoirs with the producing well very close to one boundary; dual porosity systems; and multi-layered composite systems.

Reservoir parameter estimation is usually done using the portion of the measured data that is “infinite-acting”, or transient. Reservoir model identification depends upon the interpretation of boundary effects that are considered to be in the late time region of the data.

The majority of the published solutions apply to single rate drawdown tests. Variable rate and multi-rate tests are treated simply by application of the Principle of Superposition. Buildup tests are considered to be a special case of a multi-rate drawdown test where the last rate is zero.

From a practical point of view, buildup tests are preferred. Drawdown data are collected while the well is flowing. As a result the data are subject to wellbore dynamics and wellbore effects. This causes drawdown data to be noisy, even at the best of times.

Often, the drawdown data are so noisy that they cannot be analyzed successfully. By contrast, buildup data are collected when the well is shut-in. During the early time period, wellbore effects and afterflow affect the data. However, these phenomena generally quickly disperse, and the reservoir signal is often apparent thereafter.

Furthermore, with the cessation of afterflow, a constant sandface flowrate is achieved. Theoretically, then, the buildup data can be analyzed as a superposition of drawdown solutions.

For buildup data, currently there are no type curves published in the literature. The current procedure for analyzing buildup data is to mathematically manipulate the time variable to force buildup data to match the drawdown type curves. Using this hybrid time variable, the buildup data are then analyzed as if they were a drawdown test. This temporal superposition process works very well for infinite-acting, homogeneous reservoirs.

This process also works reasonably well to determine reservoir parameters in more complex reservoir models, if the infinite-acting portion of the data can be identified. However, the reservoir model itself may not be readily identified in these cases. The buildup data set, even after it has been mathematically manipulated, represents boundaries or heterogeneities very differently than does drawdown data. Furthermore, if the infinite-acting portion of the data cannot be identified, the technique of

using drawdown type curves to analyze buildup data fails miserably.

Reservoir model identification for buildup data is currently a trial and error method. Measured data are compared to theoretical or numerical solutions of various reservoir configurations until a suitable match is found. This is an imprecise and time consuming process. The starting reservoir configuration is a “best guess” guided by the analyst’s previous experience. Refining the initial configuration to match the actual data is very much dependent on the analyst’s previous experience and exposure to various reservoir models and their representation in buildup data.

As the majority of well tests currently conducted are buildup tests, a rigorous and direct methodology for reservoir model identification would be advantageous.

## **2.0 Review of Literature**

### **2.1 Background**

The analysis of buildup data began with Horner [1951]. Horner suggested a semi-log analytical method of determining formation permeability. A plot of the shut-in bottom hole pressure versus the logarithm of  $\{(t_p + \Delta t) / \Delta t\}$  resulted in a straight line with a slope that was inversely proportional to the permeability. With the assumptions of radial flow in an infinite acting reservoir, a constant formation permeability, a single phase fluid of small and constant compressibility, and constant viscosity, this semi-log plot has provided the foundation for traditional pressure buildup analysis.

Horner also showed that, for wells in closed drainage systems, reservoir pressure eventually became static. This static pressure provided an estimate of the average pressure within the drainage area of the well.

Additionally, Horner showed that for a well located near a no-flow linear barrier, the buildup pressures in the late time period would show a marked increase. This increased pressure formed a second linear trend with a slope that was twice that of the initial semi-log straight line.

Miller, Dyes, and Hutchinson [1950] presented a study of wells located in closed (bounded) reservoirs and constant pressure boundary reservoirs. This study assumed that the wells had been produced to pseudosteady state or steady state prior to shut-in. Miller et al. concluded that a plot of buildup pressures versus the logarithm of shut-in time produced a straight line with a slope that was inversely proportional to the permeability. Also, for either boundary condition (closed or constant pressure), the pressure data reached a static value. This value was indicative of the average pressure in the drainage area of the well.

Miller et al. also studied wellbore storage phenomena. Because the well is shut-in at surface, the sandface flow rate does not instantaneously fall to zero. Fluid continues to enter the wellbore until the formation pressure becomes static. Miller et al. coined the term “afterflow” to describe this phenomenon. Previously, this phenomenon had been termed “annulus unloading” by van Everdingen and Hurst [1949], for the case where a well is opened at surface and produced.

A different method of determining average pressure in the drainage area of the well was presented by Matthews, Brons, and Hazebroek (MBH) [1954]. Matthews et al. developed dimensionless curves for wells at various locations in drainage areas of various shapes. Using the extrapolated pressure from the Horner plot, the average pressure in the drainage area can be determined from the MBH dimensionless curves.

The advantage of the MBH method is that it is applicable to a wide variety of drainage area shapes. This method has two disadvantages. First, it requires previous knowledge about the shape and size of the drainage area, and second, it requires a knowledge of the location of the well within the drainage area. This method also relies on estimates of reservoir and fluid properties that may not be known with great accuracy.

Slider [1971] presented a paper that outlined a new buildup analysis method for a well that had reached either pseudosteady-state or stabilized flow. The method is based on the change in pressure caused by the negative rate effect due to shutting in the well. The two advantages attributed to the Slider method are: first, a complete analysis can be accomplished without prior knowledge of the porosity or effective compressibility and second, a straight line pressure plot exists for much longer time periods than other methods. The disadvantage of this method is that the answer depends heavily on the extrapolation of the drawdown data. This is a semi-log method, after the fashion of Horner.

A paper by Ramey [1976] provides an excellent summary of advances in well testing theory to that time. It provides a view of the historical trend of research in pressure transient analysis and gives some predictions of future directions. As in most areas of scientific research, the historical trend was to build on previous concepts and trains of thought, sometimes not stopping to consider new tools that are available.

## **2.2 Type Curves**

Drawdown type curves including storage and skin were first published by Agarwal, Al-Hussainy, and Ramey [1970]. These type curves allowed a graphical method of determining reservoir parameters; but, more importantly, allowed a description of the reservoir/well system model. These drawdown curves worked well for drawdown tests, but were not applicable for buildup data because producing time effects were not taken into account.

The focus of the work on pressure buildup type curves, documented in the literature, has been to manipulate the time function to allow buildup data to fit the existing drawdown curves, rather than developing specific type curves for buildup data. This, no doubt, is because drawdown type curves were readily available and understood.

Agarwal [1980] devised the concept of “equivalent time” which accounts for the dependence of buildup behaviour on the duration of the producing time. This allowed a time shift of buildup data so that the drawdown type curves could be used for analysis. The method accounts for the effects of producing time, and in that respect is similar to the Horner method. It may be used to determine formation permeability, skin, and reservoir pressure. This type of analysis works well for buildup data during the infinite acting or transient portion of the flow period. Beyond



the infinite-acting range of data the equivalent time manipulation does not work.

McKinley [1971] presented a paper that detailed a method for determining wellbore transmissibility from afterflow dominated pressure data. While afterflow is generally regarded as a nuisance, it is reasonable to assume that the afterflow data contains valuable information. Pressure change during afterflow reflects a balance between the wellbore storage capacity and the ability of the formation to flow fluid to the wellbore.

McKinley's method uses real time, not dimensionless time, and relies not on "correcting" the measured pressure data, but rather on utilizing a set of type curves generated for a homogeneous, radially finite reservoir to calculate the near wellbore transmissibility. Wellbore transmissibility is an indicator of the ease with which the formation supplies fluid to the wellbore. The manner in which the measured data deviates from the type curve gives an indication of the transmissibility of the bulk formation as compared to the wellbore transmissibility. This type curve analysis provides a comparative index of transmissibility which gives an indication of damage or improvement (skin) near the wellbore. This method focuses on the early time data and is used primarily for well tests that are dominated by afterflow.

Raghavan, Meng, and Reynolds [1980] presented a new procedure to analyze pressure buildup data following a short flow

period by utilizing drawdown type curves. By converting buildup data to equivalent drawdown data a larger data set for drawdown type curve matching is obtained. The method of conversion is to assume that the drawdown extension  $\Delta p$  for a given value of shut-in time,  $\Delta t$ , is  $(p_i - p_{wf}(t_p)) + (p_i - p_{ws}(\Delta t))$ , where  $t_p$  and  $\Delta t$  have the same numerical value. This results in an extension of the drawdown data that can be matched to the drawdown type curve. The authors state that a longer band of data will result in a more reliable match. This method requires that pressure-rate data prior to buildup are available, and an estimate of the initial reservoir pressure is needed.

The most recent major advances in type curve matching and analysis came from Bourdet, Whittle, Douglas, and Pirard (1983) with the introduction of derivative type curves. Following the earlier concepts of finding the slopes of the semi-log plots, derivative type curves are plots of the derivative of the semi-log curve plotted on a log-log scale. Derivative curves allowed for determination of the reservoir parameters, as well as the identification of well and reservoir flow behaviour.

Derivative curves provide unique "signatures" that enable the identification of flow regime. For example, one can identify radial, linear, or bi-linear flow by observing the value of the slope of the derivative curve. These signatures are a significant advance over the traditional type curves.

The derivative curves necessarily depend greatly on the quality of the measured data to achieve a smooth derivative curve. With the advent of modern electronic pressure gauges this is no longer a major concern due to the accuracy of the electronic gauges and the number of data points it is now possible to record. However, the measured data still often needs to be “smoothed”. Bourdet, Ayoub, and Pirard (1989) did address this concern and offered some methods for smoothing the recorded data.

## **2.3 Deconvolution**

Through the 1980's there was another approach to the analysis of buildup data. This involved the inverse use of Duhamel's principle or deconvolution. By definition, deconvolution is a mathematical technique for extracting the effect of the time-dependent input data from the output data. From a pressure transient analysis standpoint, deconvolution extracts the drawdown data that underlie the buildup data. Because the tools to analyze the drawdown data are available, the reservoir system could then be described.

Inherently, deconvolution has two drawbacks. Mathematically, it is a highly unstable, inverse problem. When the deconvolution algorithms work, the resulting data has a high degree of scatter. Secondly, from a more practical point of view, application of deconvolution to pressure transient analysis depends on the measurement of the downhole (sandface) flow rate. This is a very uncommon measurement that is subject to many inaccuracies, and one that is relatively expensive to obtain.

Papers which illustrate the development of deconvolution as a tool for the analysis of buildup data are summarized as follows:

Stewart, Wittmann, and Meunier [1983] and Meunier, Wittmann, and Stewart [1983] presented a discussion on the use of deconvolution in well test analysis using data (pressure and flow

rate) measured downhole. Measurement of the downhole flow rate allows for elimination or minimization of wellbore storage and afterflow effects. The identification of storage directly means almost twice the amount of data is available at early time for analysis compared to other methods.

For deconvolution, the continuously measured variable rate is replaced by a piecewise linear approximation. The resulting convolution integral has an analytical solution. For radial flow, a plot of rate normalized pressure versus a modified logarithmic time function is linear. The flow capacity and skin can be determined from the slope and intercept, in a similar fashion to the constant rate case. Thus the authors develop the theoretical basis for the analysis of simultaneous, continuously variable bottomhole pressure and bottomhole flow rate data. This model eliminates the simplifying assumption of constant wellbore storage. However, for application to buildup data, extrapolations of pressure and manipulated time functions are invoked to allow the use of drawdown theory.

Thompson and Reynolds [1986] presented a paper that proposed three methods of application of Duhamel's principle to well test data. They considered both drawdown and buildup data, but concentrated on the drawdown solutions. Unique to this work is the idea that the methods presented use Duhamel's principle to convert the variable sandface rate - pressure data to the equivalent pressure data that would have been obtained if production had

been at a constant sandface rate. This equivalent constant rate data can then be analyzed using standard procedures. Furthermore, Thompson and Reynolds extended the previous methods of planar radial flow to a more general case that could be used for fractured wells or heterogeneous reservoirs. The biggest limitation to their methods is that sandface flow rates must be available.

Moser [1987] suggested a modified Gladfelter method to account for changing flow rates. This improvement is to correct the time function in a continuous fashion, after the fashion of Horner, rather than in discrete units. Moser points out that the method is more intuitively based, rather than based on mathematical derivation. However, the method did give excellent results in the examples provided. The limitation is the reliance on measured sandface flow rates.

The first use of convolution data in type curves was presented by Ayestaran, Mimhas, and Kuchuk [1988]. Based on the rate normalized pressure deconvolution developed by Gladfelter, Tracy, and Wilsey [1955], a method for identifying system characteristics and estimating reservoir parameters was developed. Furthermore, it was shown that an “automatic type curve matching”, that included the effect of prior production history, could be achieved. While the proposed technique worked well on synthetic data, noise in the gathered data or oscillations in the flow rate caused the model to break down to the extent that it

could not be used for model identification. This method used sandface flow rates and pressures. To incorporate surface flow rates, the model was found to be very dependent on wellbore storage. This effect could not always be effectively incorporated in the model.

Kuchuk, Carter, and Ayestaran [1990] and Kuchuk [1990-a] suggested that the ability to deconvolve pressure and flow data would be of use in many reservoir problems. Particularly in the area of pressure transient analysis, data trends may be masked by more prominent time-dependent effects, and the reservoir data are lost. For example, in hydraulically fractured wells the characteristic half slope, because it occurs at early times, may be masked by wellbore storage or rate variations. The authors go on to describe deconvolution methods that are numerical solutions to the convolution integral. These techniques are very successful with “synthetic” data, but fail when even small amounts of noise are introduced into the data.

As research progressed on the deconvolution of pressure-flow data, it became apparent that if downhole flow rates, rather than surface flow rates, were used in deconvolution the mathematical results would be less subject to data scatter. While this was an improvement, obtaining the downhole flow rates was subject to its own set of problems. The gauges were affected by wellbore effects and fluid movement in the wellbore. Kuchuk [1990-b] presented a comparison of convolution/deconvolution

interpretation techniques and standard techniques by utilizing two field cases. It was noted that the deconvolution formula is recursive; that is, previously computed values are used to compute the next value. Thus small perturbations in initial data result in large perturbations in the computed solutions. Kuchuk concluded that the downhole flow rate is crucial for system identification and parameter estimation. Furthermore, deconvolved pressure derivative data can be an effective system identification tool.

In 1994 Baygun, Kuchuk, and Arikan [1994] presented a constrained least-squares deconvolution method which should be useful for noisy data. The constraints considered were autocorrelation constraints and derivative of energy constraints. In the numerical examples presented, the deconvolution result oscillated about the true influence function, but was not biased away, in any direction, from the true solution. Also, the magnitude of the oscillations was significantly suppressed compared to earlier techniques.



## **2.4 Boundary Conditions and Solutions**

For the purpose of building a computer model to generate solutions for various boundary conditions and flow regimes, the literature was reviewed for existing solutions, both analytical and numerical. The following is a description of some of the more applicable papers:

Ramey and Cobb [1971] presented a general theory for pressure buildup in a closed drainage area, and compared the Muskat method, the MDH method, and the Horner method, for wells in the center of a closed square. For each of the methods the length of producing time was considered a variable. For the Muskat and MDH methods, the length of time the well was produced had a significant impact on the values of permeability and average reservoir pressure computed. For the Horner method, for all producing times considered the correct slope was achieved, and the correct value of permeability was calculated. For those cases where the producing time resulted in pseudosteady state flow prior to shut-in, and the shut-in time was long enough to see a buildup to pseudosteady-state, the average reservoir pressure calculated was correct.

One of the more interesting conclusions in this work was that the Horner method straightens buildup data to much longer shut-in times than does the MDH method, and because of this the

Horner method appears to be much more useful than the MDH method.

The work of Ramey and Cobb [1971] was extended by Cobb and Smith [1975] to develop a correlation between the time required to reach the end of the semi-log straight lines as a function of the time the well was produced prior to shut-in and well geometry. By extension, this allowed for an estimate of the minimum time the well must be shut in before the effects of the boundaries become pronounced.

Correa and Ramey [1986] presented a new approach to solve the problem of pressure buildup following constant pressure production. By using the unit step function to combine boundary effects the problem was solved analytically. This solution was obtained by solving the diffusivity equation with a single inner boundary condition that included the mixed conditions for flow and buildup. The solution was obtained using regular Laplace transformation techniques. The authors emphasized that the solution does not involve the use of superposition, nor does it involve a temporal transformation. However, the use of the unit step function in this manner is an elementary form of convolution [Wylie 1975].

Moser [1983, 1987] proposed a method of semi-log type curve analysis for drawdown data after the fashion of Horner. For the analysis of buildup data Moser proposed a temporal

desuperposition to extract drawdown data which can then be analyzed using traditional methods. Restrictions on this desuperposition were that the initial pressure must be known and that the duration of the buildup was at least twice that of the drawdown period.

### **3.0 Statement of the Problem**

The objective of this research is to develop a rigorous and direct methodology to identify no-flow boundary effects in rectangular reservoirs using pressure buildup data.

The theory of pressure transient analysis is derived from the solution of the diffusivity equation for a fluid of small but constant compressibility, flowing at a constant rate. From the general solution, using various boundary conditions which represent different well/reservoir geometries, dimensionless drawdown type curves have been developed. "Reservoir Model Identification" and "Reservoir Parameter Estimation" by the graphical comparison of bottomhole pressure data to standard dimensionless type curves is known as Type Curve Matching. It is a well defined and accepted procedure and applies equally well to simple and complex reservoir systems for drawdown data.

There are no published dimensionless type curves for pressure buildup data. If the transient portion of the data can be recognized, the reservoir parameters can be estimated from the drawdown type curves, but, in many instances, no conclusions can be drawn about the reservoir-well system.

Currently, the method used for model identification is to generate "synthetic" solutions for various reservoir models and then to compare the measured data to the synthetic solution. (A

synthetic solution is one which is generated by supplying all the reservoir parameters and solving the radial diffusivity equation for a specific boundary condition.) This is a tedious and time consuming method of trial and error. There are no guidelines for choosing a model with which to start nor, once a model is chosen, how to proceed to achieve an acceptable match to the synthetic solution.

To add further complexity to this problem when using the current methods, it is known that the “characteristic shape” of response of a given system, in buildup data, is influenced by the duration of flow preceding the pressure buildup.

The majority of well tests currently conducted are buildup tests, due to the resulting high quality data achieved. However, it is very difficult to identify reservoir systems from buildup data using the current analytical techniques.

Rectangular reservoirs were chosen as the primary subject of this study primarily because it was felt that a boundary detection method developed for rectangular reservoirs could be readily extended to other reservoir configurations. Rectangular reservoirs offer a wide range of configurations, and an infinite number of well/boundary situations that can be studied. Also these reservoirs can be mathematically represented in several ways. As a result, this reservoir configuration offers several approaches for development of a boundary detection methodology.

The last decade has seen a significant change in the operation and production of the Western Canadian Sedimentary Basin. There is much more interest in exploiting shallow formations which are hydrocarbon bearing. Most of these were formed in a river or channel environment and have resulted in rectangular shaped reservoirs. The ability to determine the boundaries in these formations has great application to the development of this resource.

Thus, the objective of this research is to develop a rigorous and direct methodology to identify no-flow boundary effects in rectangular reservoirs using pressure buildup data.

## **4.0 Development of the Boundary Detection Method**

Pressure transient analysis, or well testing, is the most frequently used method to gather “real time” data about a well in a reservoir system. The data gathered from a well test are analyzed to determine reservoir parameters such as permeability, skin, and wellbore storage effects, and to some extent to determine the reservoir model.

By identifying various portions of the data, such as early time, infinite acting (transient) and late time, the reservoir parameters and reservoir model may be determined. For example, early time data is analyzed to give wellbore storage and skin effects. The transient portion is analyzed to give flow regime and permeability, while the late time data are analyzed to determine boundaries and hence the reservoir model.

These results are most often obtained using a technique known as type curve matching. Type curve matching is the graphical comparison of measured bottom hole pressure data to standard dimensionless type curves. The standard type curves are solutions of the radial diffusivity equation for a fluid of small and constant compressibility, flowing at a constant rate, and various boundary conditions. Type curve matching is a straight forward, well documented and accepted procedure.

The majority of the published type curves apply to single rate drawdown tests. Variable rate and multi-rate tests are treated simply by application of the Principle of Superposition. Buildup tests are considered to be a special case of multi-rate drawdown where the last rate is zero.

It has been previously stated that buildup tests are preferred due to the quality of the resulting data. Analysis of the buildup data follows the same methodology as that of drawdown data. In fact, drawdown data type curves are used analyze buildup data. This is accomplished by mathematically manipulating the time variable (temporal superposition) to force the buildup data to match the drawdown type curves.

While this method works reasonably well for the analysis of early time data, and the infinite-acting data, the late time data and hence boundaries cannot be analyzed successfully. The buildup data, even after mathematical manipulation, represent boundaries quite differently than drawdown data.

The objective of this chapter is to detail the development of a direct method for determining boundaries in rectangular reservoirs using buildup data.



## **4.1 General Assumptions of the Method**

The focus of this research is to investigate boundary effects so that a reservoir model may be determined. Thus, for the purpose of developing a boundary detection model, it is assumed that early, transient and late time portions of the data have been identified. Further, from the early and transient portions of the data, the reservoir parameters of wellbore storage, skin effect, and permeability have been determined and are available. It is also assumed that reasonable estimates of porosity, net thickness, total compressibility, and fluid viscosity are available.

Essentially, the analysis for the early time and transient portions of the data have been completed as for a well in an infinite-acting reservoir. It is now when the trial and error process of reservoir model identification begins.

The model has been developed for a reservoir flowing a single phase light crude oil of small but constant compressibility. It was assumed that there was a connate water saturation, but that water is immovable. Gas was considered to be solution gas only.

To assist in understanding the development of the method, the effects of wellbore storage and skin have been omitted from the development of the equations. The effect of wellbore storage and skin are discussed in the chapter titled "Results and Discussion".

## **4.2 General Concepts of the Method**

There are five main concepts which are key to the understanding of the derivation of the method. These are:

1. The Radial Diffusivity Equation
2. Method of Images
3. The Principle of Superposition
4. Radius of Investigation, and
5. An Infinite-Acting Reservoir Frame of Reference.

The Radial Diffusivity Equation is the basis for all solutions in pressure transient analysis.

The Method of Images is a mathematical technique which allows no-flow boundaries to be constructed at specific distances from a flowing well.

The Principle of Superposition will be used in two ways. Firstly, with the radial diffusivity equation to represent all boundary conditions. Secondly, with the Method of Images to simulate no-flow boundaries.

The Radius of Investigation concept gives an indication of the distance a pressure signal has travelled in a specific reservoir during a finite amount of time.

An Infinite-Acting Reservoir Frame of Reference is the key element of this method of boundary detection. Traditional methods of analysis use a pressure measurement during the flowing portion of the well test as a reference for the difference in pressure used in the solution of the radial diffusivity equation. This method uses the response from an identical well in an infinite-acting reservoir as the reference pressure.

A more detailed discussion of each of these concepts follows.

#### **4.2.1 Radial Diffusivity Equation and Superposition**

The theory of Pressure Transient Analysis is derived from the solution to the Radial Diffusivity Equation for a fluid of small but constant compressibility flowing at a constant rate.

The Radial Diffusivity Equation is:

$$\frac{\partial^2 p}{\partial r^2} + \frac{1}{r} \frac{\partial p}{\partial r} = \frac{\phi \mu c_t}{k} \frac{\partial p}{\partial t} \quad \text{.....(4.2.1.1)}$$

It is derived by combining the Law of Conservation of Mass, Darcy's Law, and an Equation of State. (see Matthews and Russell [1967] for the full derivation). To solve this equation for a well flowing at a constant rate in an infinite, homogeneous reservoir, the boundary and initial conditions are:

$$r \frac{\partial p}{\partial r} = \frac{q\mu}{2\pi kh} \quad \text{for } t > 0 \text{ and } r \rightarrow r_w, \quad \text{.....(4.2.1.2)}$$

$$p = p_i \quad \text{as } r \rightarrow \infty, \quad \text{and} \quad \text{.....(4.2.1.3)}$$

$$p = p_i \quad \text{at } t = 0. \quad \text{.....(4.2.1.4)}$$

The solution to the radial diffusivity equation for a well flowing in an infinite, homogeneous reservoir is:

$$p_i - p = \frac{q\mu}{4\pi kh} \left( - \text{Ei} \left( - \frac{\phi\mu c_t r_w^2}{4kt} \right) \right). \quad \text{.....(4.2.1.5)}$$

(See the Appendix for the complete solution.) This solution is an exact analytical solution.

There is no disputing that an infinite acting homogeneous reservoir is a very ideal case. However, solutions for other boundary conditions may be obtained by use of the Principle of Superposition. Mathematically, the Principle of Superposition states that the addition of two or more solutions of a linear differential equation results in a new solution of the equation. This new solution is valid for a different set of boundary conditions than those of the original equation (Crank 1975). Thus, by combining solutions to the radial diffusivity equation, various reservoir configurations can be modelled.

#### **4.2.2 Method of Images**

The change in pressure at any point in a reservoir is the sum of the changes in pressure at that point caused by flow in each of the wells in the reservoir. This is a direct application of the Principle of Superposition. Using this concept, no-flow boundaries can be constructed mathematically.

Consider the pressure behaviour of a well producing in a reservoir located a distance “ $d$ ” from a single no-flow boundary. Mathematically, this is the same problem as two identical wells producing at a distance of “ $2d$ ” apart, as illustrated in Figure 4.2.2.1. The second well is considered to be an “image” well. It can be shown that a line equidistant from each of the wells has a pressure gradient of zero, which means that there is no flow. This line, then, represents a no-flow boundary.

Expanding this technique, many no-flow boundary configurations can be represented. An array of image wells influencing the actual well will effectively represent these no-flow boundary configurations. For further details on the method, see Earlougher (1977).

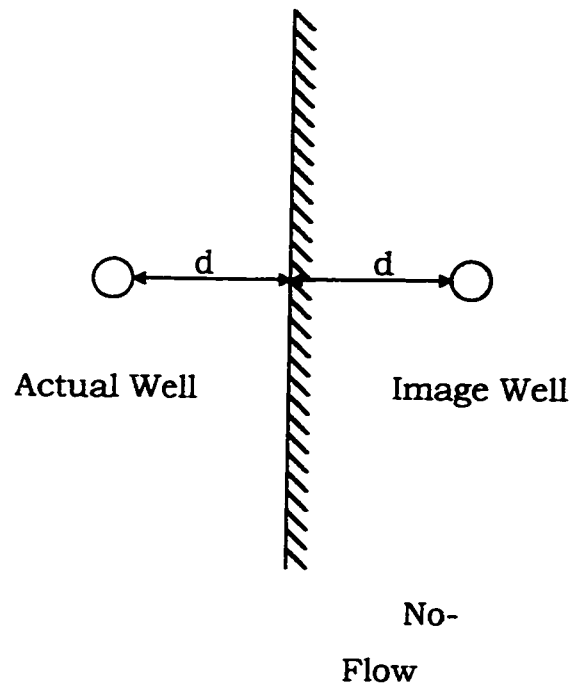


Figure 4.2.2.1 Example of Method of Images

### 4.2.3 Radius of Investigation

It is possible to estimate the distance to the no-flow boundary from the characteristic curve by applying the concept of "Radius of Investigation". Radius of investigation is the distance, measured in a radial direction from the well, over which there is a measurable change in pressure due to production or injection at the well.

There are a number of expressions which define the concept of radius of investigation based on what is considered to be a measurable change in pressure. Van Poollen (1964) reviewed various definitions of radius of investigation and provided advice on their use. Each of the definitions is valid given the underlying assumptions. However, the resulting radius of investigation is at best, an estimate.

For the purpose of this work, the radius of investigation is defined as the distance a pressure transient has moved into a formation following an instantaneous rate change in a well. (Lee (1982)) It is given by the equation:

$$r_i = \sqrt{\frac{4kt}{\gamma\phi\mu c_t}} \quad \text{.....(4.2.3.1)}$$

Equation [4.2.3.1] describes the time it takes the maximum pressure disturbance to reach a distance of  $r_i$  from the well

following an instantaneous change in the rate. The radius of investigation equation also describes the distance a significant pressure disturbance has propagated into a formation by production or injection at a constant rate.

Shutting in a well is a significant rate change. The pressure disturbance propagated as a result of this action can be traced using the shut-in time  $\Delta t$ . Using a specific  $\Delta t$  in the radius of investigation equation enables the calculation of the distance the pressure disturbance, caused by shutting in the well, has travelled in the reservoir.

For the purpose of finding the distance to the boundary using shut-in time, the radius of investigation equation can be written as:

$$d = \sqrt{\frac{4k\Delta t}{\gamma\phi\mu c_t}} \quad \text{.....(4.2.3.2)}$$

where “d” is the distance to the no-flow boundary.



#### 4.2.4 Infinite-Acting Reservoir Frame of Reference

Traditional methods of well test analysis rely on the solution to the radial diffusivity equation which can be expressed as:

$$\Delta p = -\frac{qB\mu}{4\pi kh} \left[ Ei \left( -\frac{\phi\mu c_t r_w^2}{4kt} \right) \right] \quad \text{.....(4.2.4.1)}$$

This representation expresses a difference in pressure as a function of the other reservoir variables. In a drawdown test, the pressure difference is expressed as the difference between the initial pressure,  $p_i$ , and the flowing bottom hole pressure,  $p_{wf}$ . For a buildup test, the pressure difference is expressed as the difference between the wellbore pressure in the shut-in well,  $p_{ws}$ , and the flowing bottomhole pressure at the instant of shut-in,  $p_{wfs}$ . This is illustrated in Figure 4.2.4.1.

The basis for the direct method of boundary determination developed herein is to use a different frame of reference for the pressure difference. Instead of using the flowing well condition as a frame of reference, this new method relies on an “infinite-acting reservoir” frame of reference. The pressure difference is expressed as the difference between a well in an ideal, infinite-acting, homogeneous reservoir, and an identical well in a specific reservoir configuration. For this method  $\Delta p$  in the solution to the radial diffusivity equation is expressed as  $\Delta p = p_\infty - p_{well}$  at any given time. This pressure difference is referred to as the Boundary

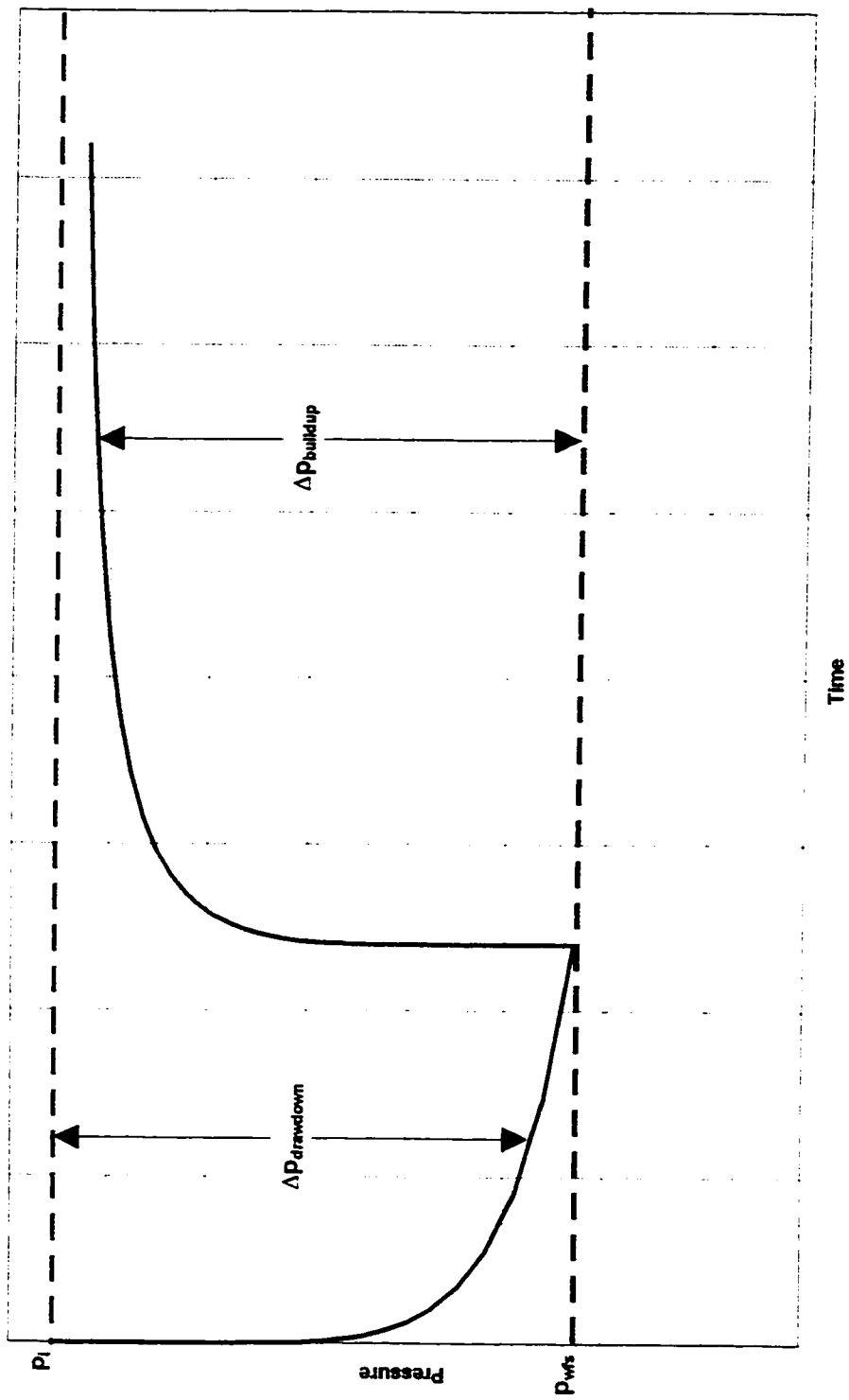


**Figure 4.2.4.1 Pressure Difference  $\Delta p_{drawdown}$  and  $\Delta p_{buildup}$**

Influenced Difference of Pressure or BIDP. Figure 4.2.4.2 illustrates this difference of pressure.

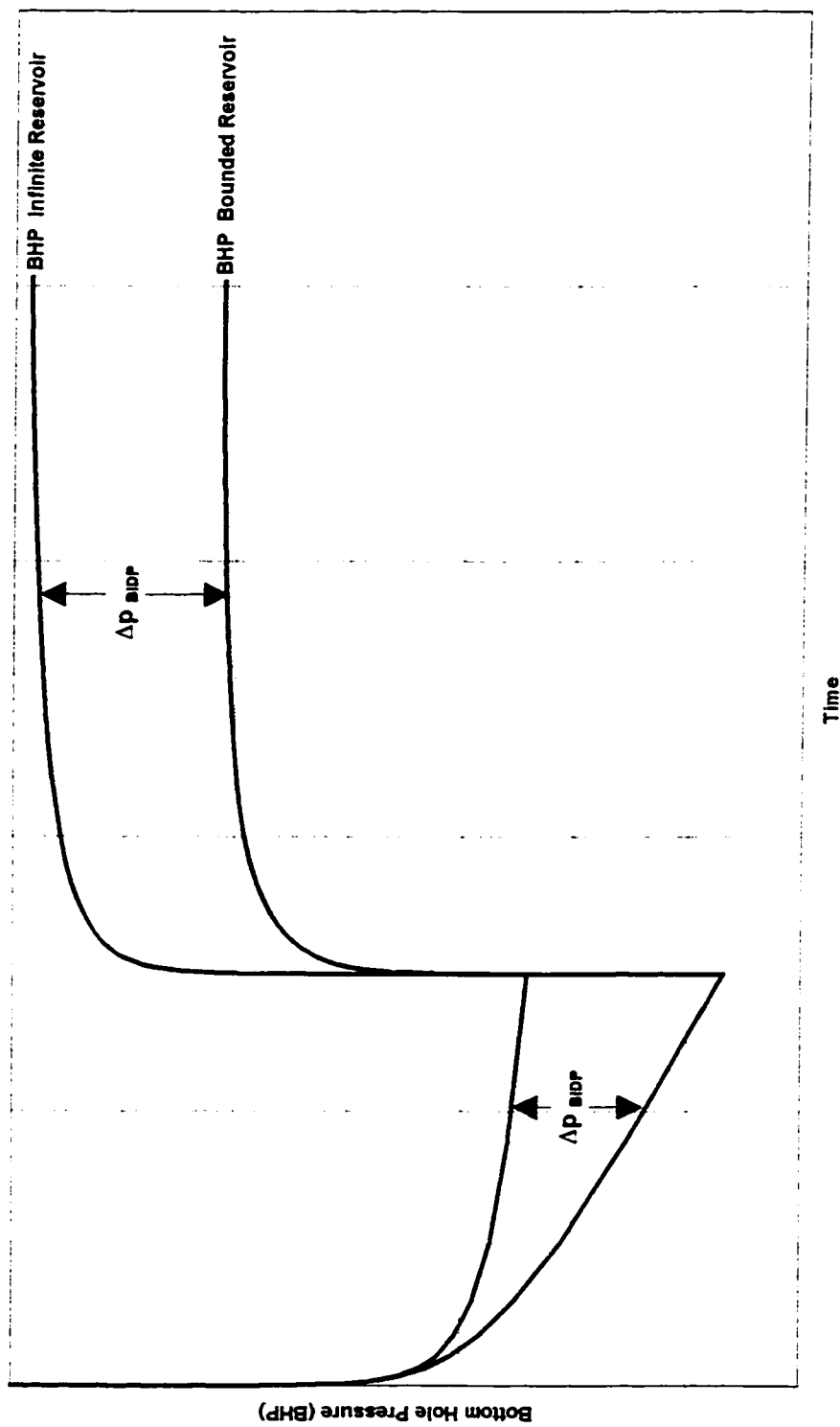


**Figure 4.2.4.2 Pressure Difference  $\Delta p_{\infty DP}$**

### **4.3 Variation from the Infinite Case**

Consider a plot of the solution of the radial diffusivity equation for an infinite homogeneous reservoir. Now, if a boundary is imposed, the solution will vary from the infinite case. The difference of the pressures in these two cases will contain information that will uniquely describe the boundary condition. The pressure difference in this case is the difference between a well flowing in an infinite reservoir of given reservoir parameters, and a well flowing at the same rate in a reservoir with identical reservoir parameters having a no-flow boundary. This pressure difference is referred to in this work as the Boundary Influenced Difference in Pressure (BIDP).

Due to the previously mentioned preference to use buildup data for the analysis of well tests, in this work from this point forward the discussion will focus on buildup data and its use in describing boundaries.

Figure 4.3.1 shows the Boundary Influenced Difference in Pressure in a semi-infinite reservoir. A semi-infinite reservoir is one which has at least one side unbounded. The plot shows that the pressure difference is constant for a period of time, then increases, and finally decreases asymptotically to zero.

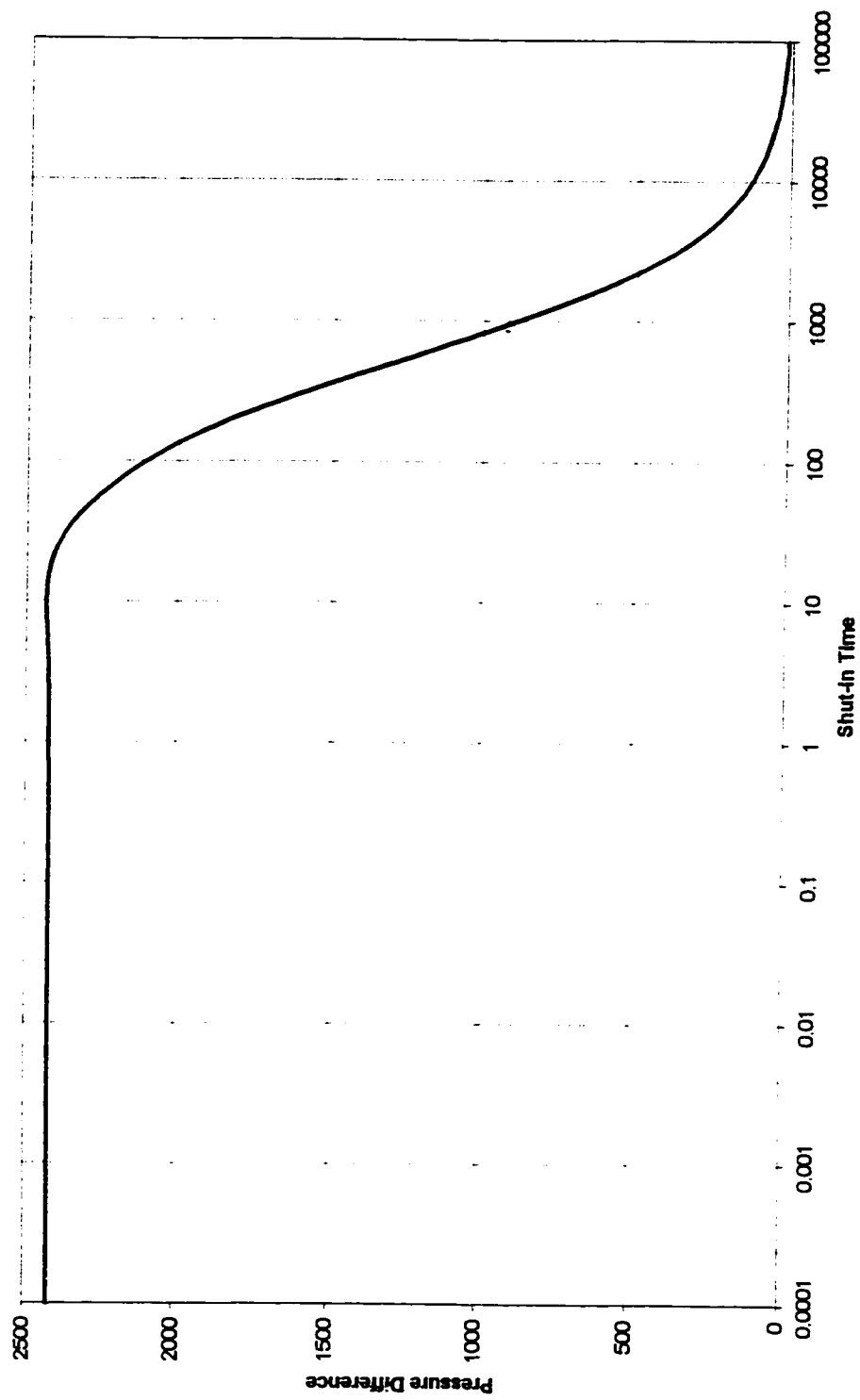


**Figure 4.3.1 Boundary Influenced Difference of Pressure**

Figure 4.3.2 shows the BIDP for several cases, each of which describes a different boundary condition. All these curves have the same general shape and do not display any unique characteristic which could be used to identify the particular boundary configuration of each system. The issue of an unique characteristic can be overcome by plotting the semi-log derivative of the BIDP versus the log of time. This is a technique similar to that described by Bourdet et al. (1983).

The derivative curve developed by Bourdet et al. (1983) has gained prominence in conventional well test analysis because it clearly identifies features which are not evident in other plotting techniques. The derivative by its very nature serves to magnify subtle changes in trends. These subtle changes can be interpreted and the result is a curve from which some reservoir characteristics may be identified.

A key to the reservoir configurations used in this work is given in the Appendix.

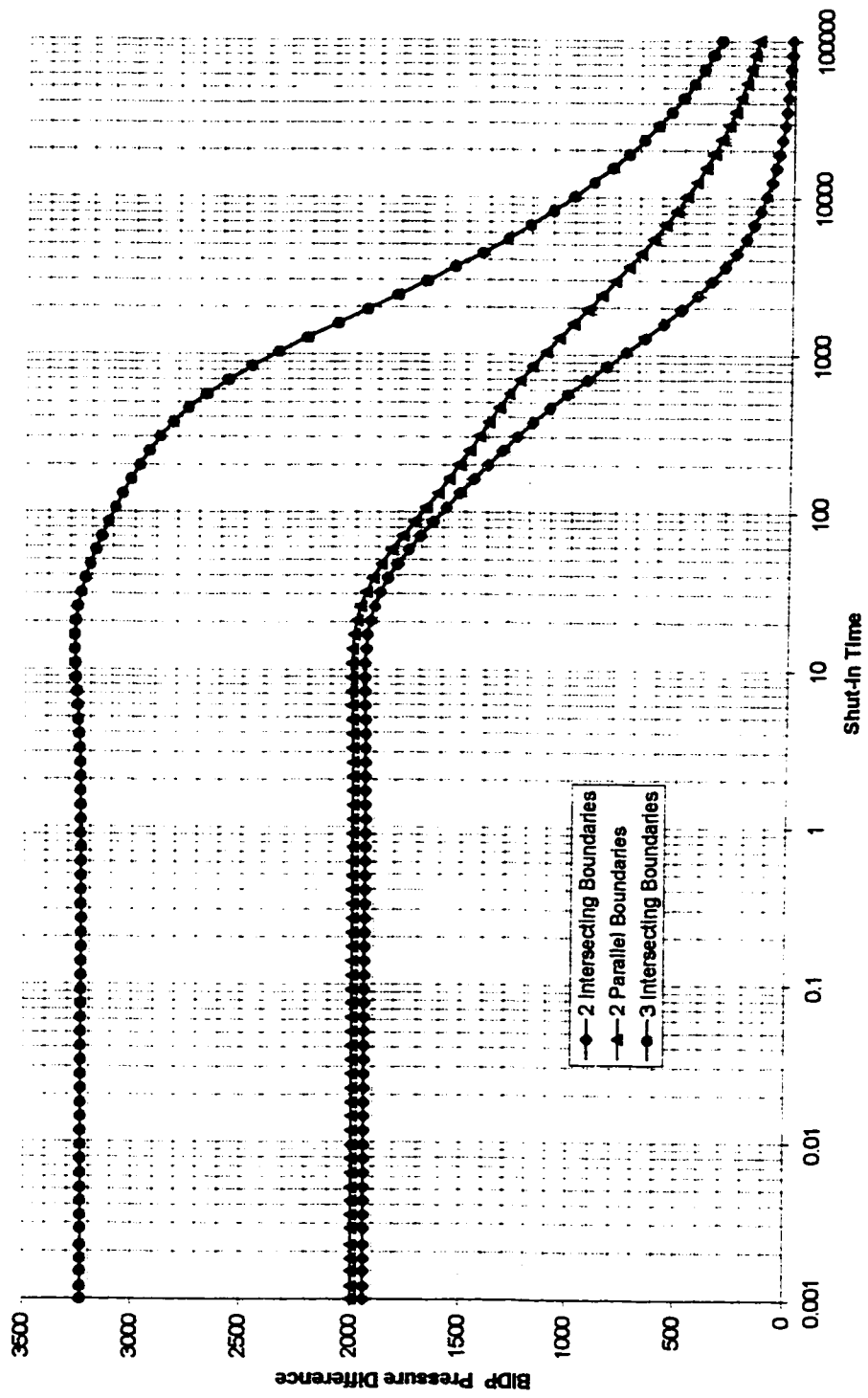


**Figure 4.3.2 BIDP for Different Boundary Conditions**



#### **4.4 Description of d(BIDP) Curve**

The d(BIDP) curve is the plot of the semi-log derivative of BIDP versus the log of shut-in time,  $\Delta t$ . The BIDP is defined as the difference between buildup pressures in an infinite acting reservoir and buildup pressures in a bounded reservoir. A description of the d(BIDP) curve and how it relates qualitatively to what is physically occurring in the reservoir is presented below. Further a discussion of how boundaries are reflected in the d(BIDP) curve and how to calculate the distance to each boundary is included.

The d(BIDP) curve describes the time rate of change of the pressure difference between a well flowing in a reservoir system with no-flow boundaries and a well flowing in an infinite-acting reservoir with identical reservoir flow characteristics. While this is a simple statement summarizing the mathematics behind the d(BIDP) curve, it represents a complex set of physical events. As illustrated in Figure 4.2.4.2, the bottom hole pressure in the bounded reservoir is not only different in magnitude from that in the infinite-acting reservoir, but the rate of change of the bottom hole pressure in the bounded reservoir is different as well. Both the magnitude of the bottom hole pressure and the rate of change of the bottom hole pressure are influenced by the specific boundary configuration present. The d(BIDP) curve captures these subtle differences and accentuates them.

Figure 4.4.1 illustrates the  $d(\text{BDP})$  curve for a well in a reservoir with a single boundary. The curve is divided into four regions. The first region of the example curve in Figure 4.4.1 is at shut-in times of less than 0.1000 hours. In this region, the curve is flat with a  $d(\text{BDP})$  value of zero. This represents a constant difference in pressure between the infinite-acting reservoir and the bounded reservoir. In effect the bounded reservoir is mimicking the behaviour of the infinite-acting reservoir. The buildup response in the bounded reservoir has not yet been influenced by any boundary. It is acting as true radial flow in the reservoir.

The second region of the example curve is at shut-in times between 0.1000 hours and 11.0 hours. This region illustrates an increasing difference in pressure and an increasing rate of change of that difference. The physical interpretation of this trend is that the reservoir is recharging the depleted area between the well and the no-flow boundary from the unbounded portion of the reservoir. The reservoir is no longer acting in true radial flow.

The third region of the example curve is at shut-in times between 11.0 hours and 120 hours. This region illustrates a decreasing difference in the pressure between the infinite-acting reservoir and the bounded reservoir, and a decrease in the rate of change of that difference. The physical interpretation is that the infinite portion of the reservoir, which is at a higher pressure, is equalizing the pressure across the entire reservoir including that part of the reservoir between the well and the boundary.

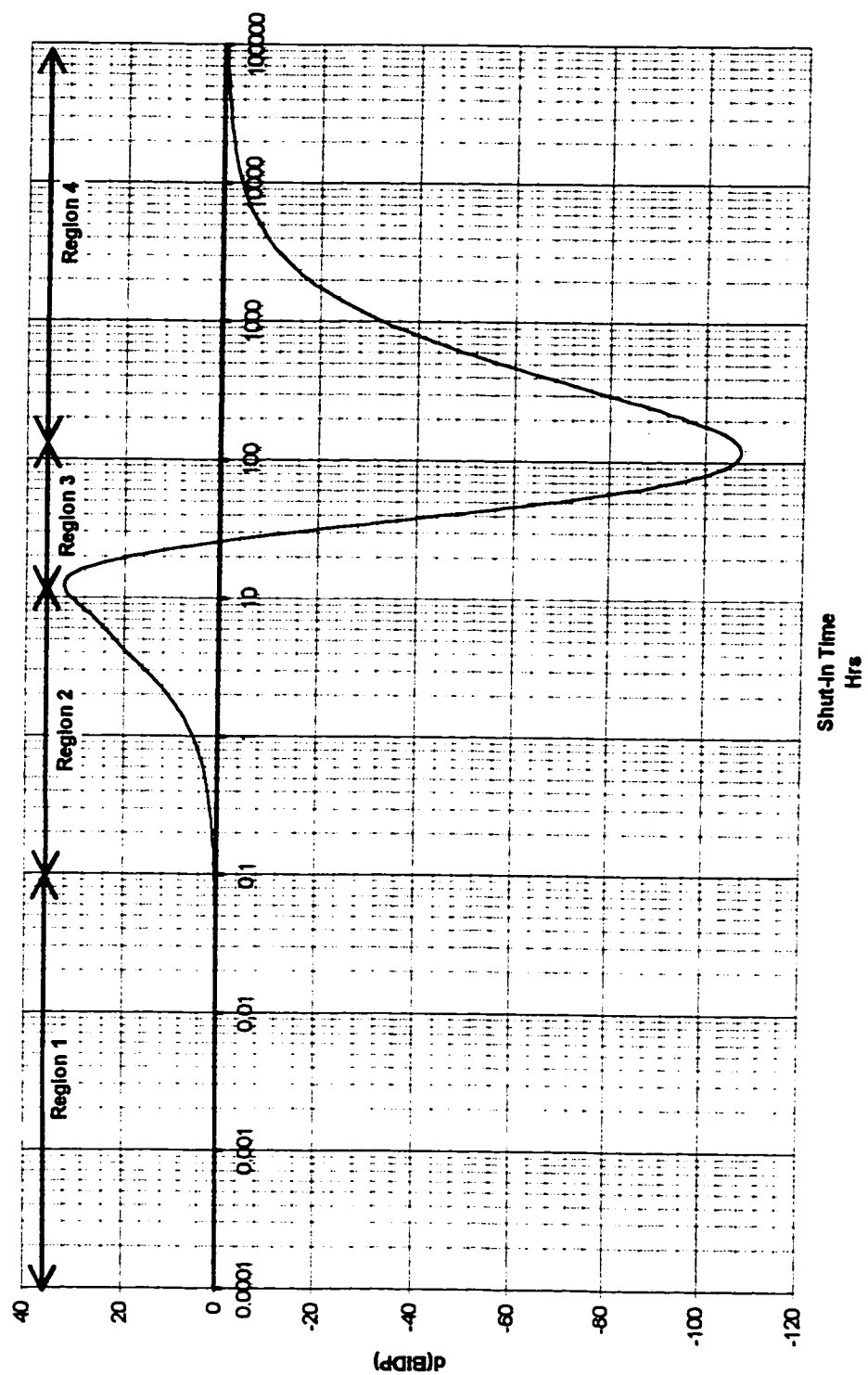


**Figure 4.4.1 Regions of the  $d(BIPR)$  Curve**

The fourth region of the example curve is at shut-in times greater than 120 hours. This region shows an ever decreasing difference in pressure between the infinite-acting reservoir pressure and the bounded reservoir pressure, and the rate of change of this difference asymptotically approaches zero as the shut-in time approaches infinity. At a shut-in time of infinity the difference in pressure between the infinite-acting reservoir pressure and the bounded reservoir pressure would be zero and the curve would again be flat along the x-axis. This region of the curve shows the infinite portion of the reservoir dominating the pressure data.

Regions three and four of Figure 4.4.1 show the response of the infinite portion of the reservoir acting to equilibrate the pressure in the entire reservoir. The shape of the curve in this area is the direct result of the difference in pressures between the infinite-acting reservoir and the bounded reservoir. In these regions, the pressure in the infinite-acting reservoir is changing only slightly in magnitude, while by comparison, the pressure in the bounded reservoir is changing much more and at quite varying rates. It is this combination of effects that gives the  $d(BIDP)$  curve a characteristic shape.

Qualitatively the magnitude of the maximum value of the  $d(BIDP)$  curve and the steepness of the curve between the maximum and minimum values of the  $d(BIDP)$  curve give an

indication of recharge, or the transmissibility of the reservoir, and hence permeability.

The minimum value of the  $d(\text{BIDP})$  curve is indicative of the reservoir coming back to an equilibrium state having redistributed reservoir fluids in the area between the flowing well and the boundary. It is not indicative of a boundary.

The maximum value of the  $d(\text{BIDP})$  curve is indicative of the first boundary. Using the shut-in time corresponding to this point in the radius of investigation equation gives the distance to the boundary. Figure 4.4.2 illustrates this point. A sample calculation for the distance to the boundary using the radius of investigation equation is included in the Appendix.

In the case of multiple boundaries, the shut-in time corresponding to the initial maximum value of the  $d(\text{BIDP})$  curve in the radius of investigation equation gives the distance to the closest boundary.

For more than one boundary, the boundaries are indicated by additional flex points in the  $d(\text{BIDP})$  curve. Figure 4.4.3 illustrates an example  $d(\text{BIDP})$  curve for a well producing in a reservoir having two boundaries. The first boundary is indicated on the  $d(\text{BIDP})$  curve in the same way as in the case of a single boundary.

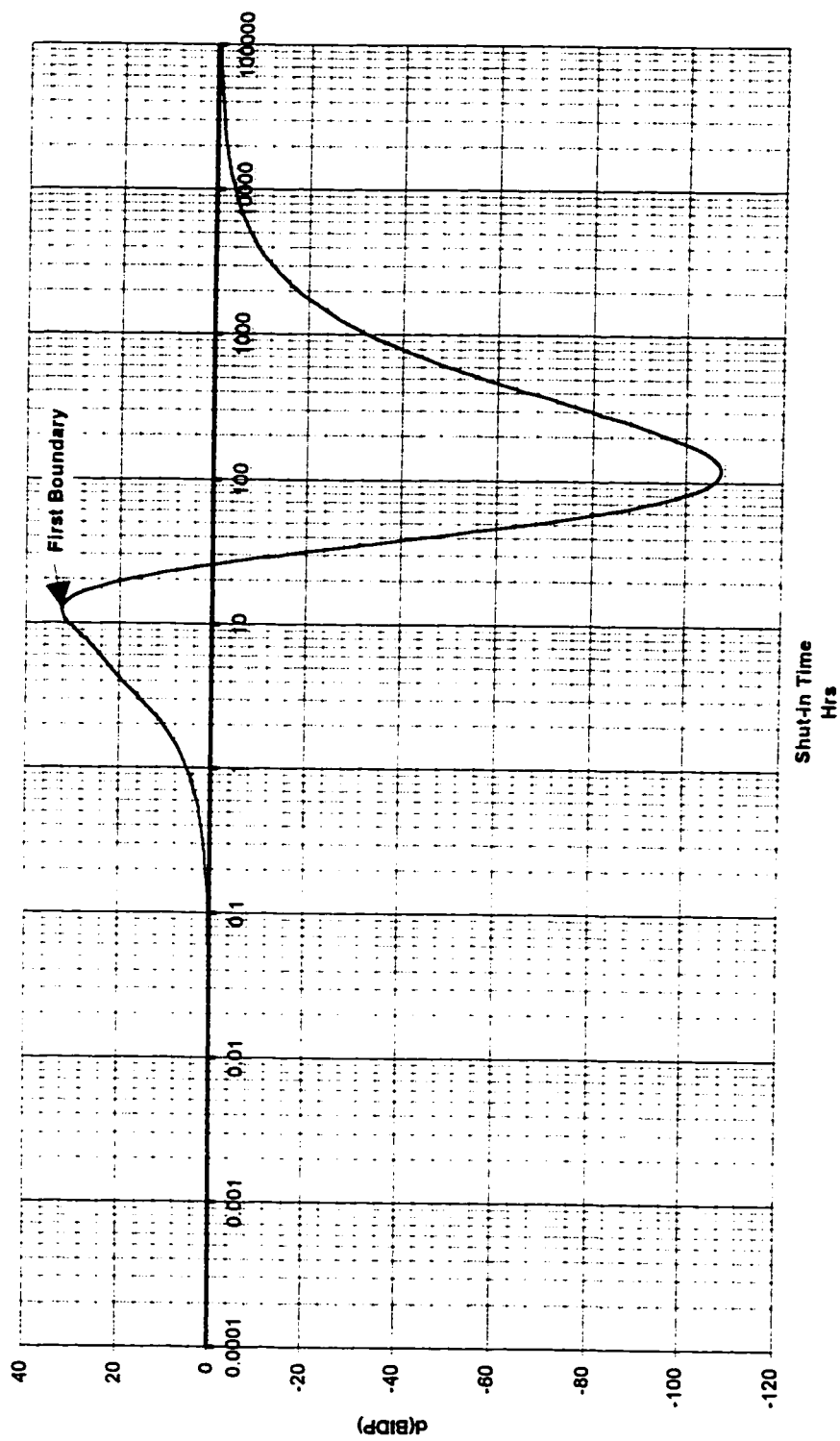


**Figure 4.4.2  $d(BIDP)$  Curve for a Reservoir with a Single No-Flow Boundary**

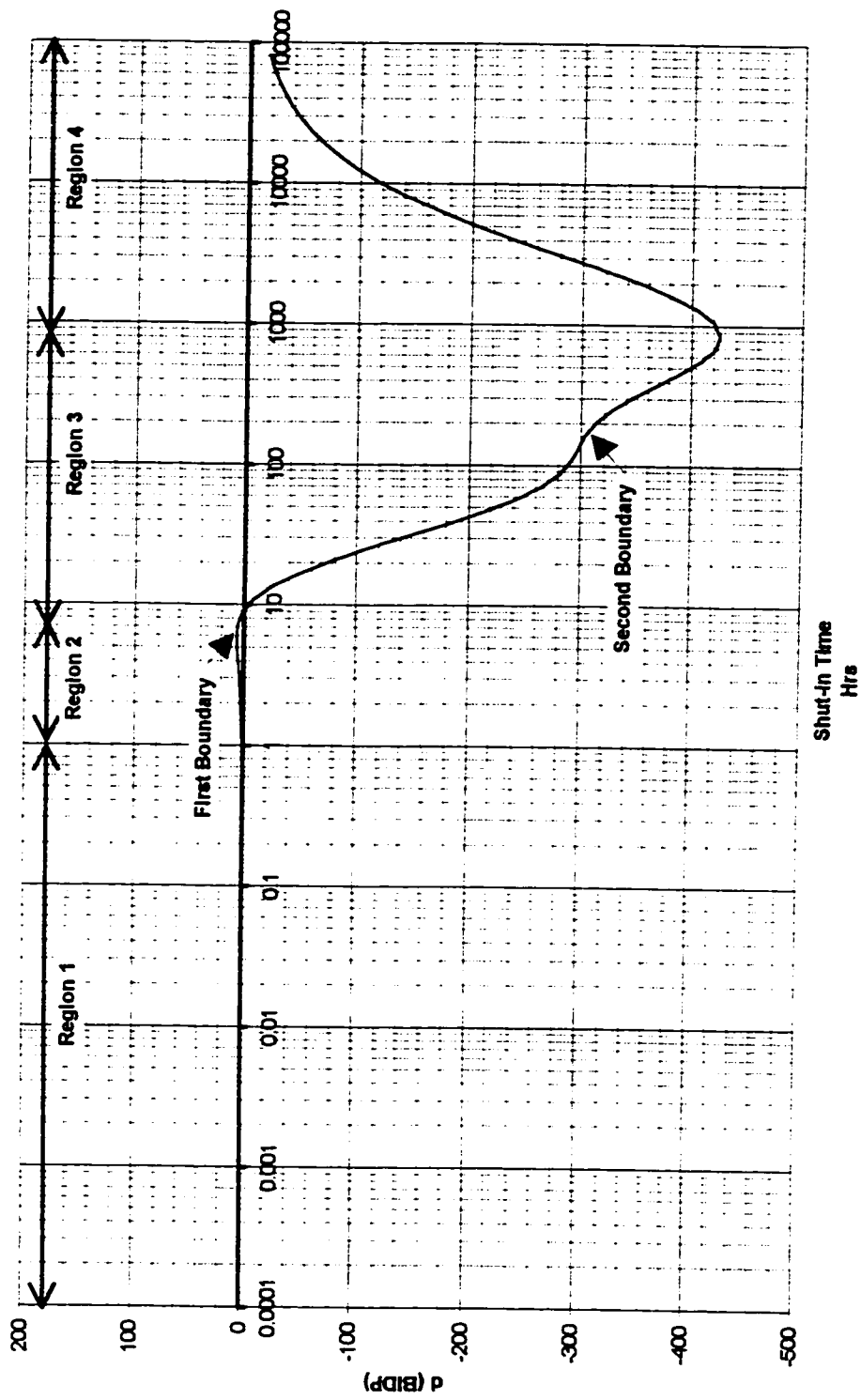


**Figure 4.4.3  $d(BIDP)$  Curve for a Reservoir with Two No-Flow Boundaries**

The region of the curve in Figure 4.4.3 denoted as Region 3 has a definite flex point. Unlike Region 3 in Figure 4.4.1, which has a constant rate of change from the maximum to the minimum values of the  $d(\text{BIDP})$  curve in Region 3, Region 3 of Figure 4.4.3 has a change in the rate of change from the maximum value to the minimum value of the  $d(\text{BIDP})$  curve. This flex point is indicative of the second boundary. In the first case, Figure 4.4.1, the reservoir is recharging one region of depletion from the unbounded portion. This leads to the constant rate of change illustrated in Figure 4.4.1. In the second case, Figure 4.4.3, the reservoir is initially recharging the depleted portion of the reservoir between the well and the first boundary; this is illustrated by the first slope. The reservoir then begins the recharge of the region to the second boundary, resulting in the second slope. Thus the flex point is indicative of the second boundary. Using the value of the shut-in time  $\Delta t$  at this flex point in the radius of investigation equation gives the distance to the second boundary.

Figure 4.4.4 shows the  $d(\text{BIDP})$  curve for a well in a reservoir having three boundaries. The first boundary is indicated in the same manner as the single boundary case. The second and third boundaries are indicated by flex points in the  $d(\text{BIDP})$  curve. These points are noted on Figure 4.4.4. The distances to the no-flow boundaries are calculated by using the values of shut-in time  $\Delta t$  corresponding to the flex points, in the radius of investigation equation.



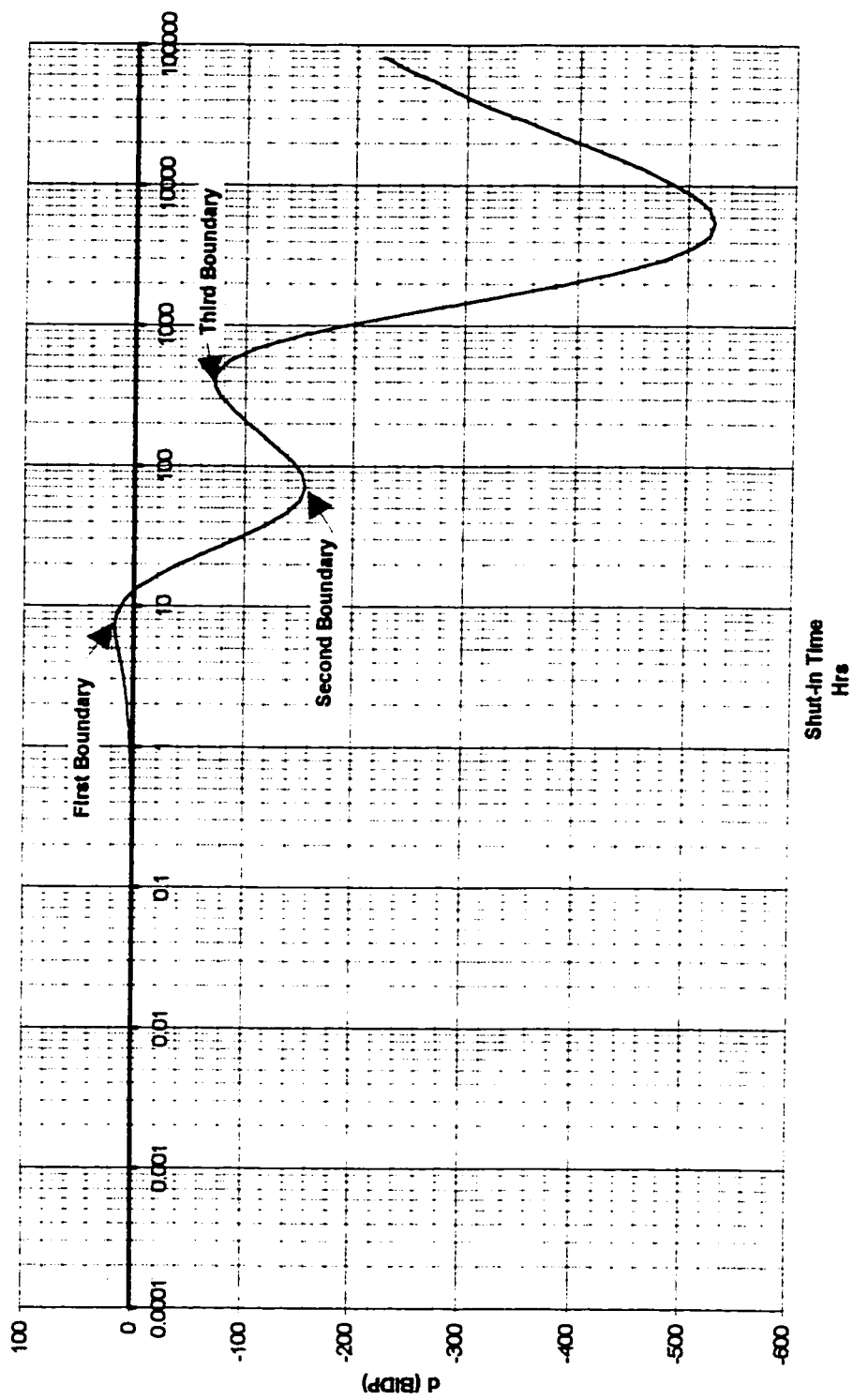


**Figure 4.4.4 d(BIDP) Curve for a Reservoir with Three No-Flow Boundaries**

The analysis of boundaries in a fully bounded, or finite, reservoir proceeds in the same manner as for a reservoir that is semi-infinite. Figure 4.4.5 illustrates the  $d(\text{BDIP})$  curve for a well producing in a finite reservoir. While Figure 4.4.5 exhibits similar characteristics to the previous cases, one notable exception is that, as  $\Delta t$  approaches infinity, the  $d(\text{BDIP})$  curve asymptotically approaches the x-axis from the positive  $d(\text{BDIP})$  range rather than from the negative  $d(\text{BDIP})$  range. This is a distinguishing feature of a finite reservoir, and is indicative of pressure depletion. Unlike the semi-infinite reservoirs, which will regain their original pressure as shut-in time,  $\Delta t$ , reaches infinity, finite reservoirs, once produced, will not regain their initial pressures, but will stabilize at a pressure lower than the original pressure as the shut-in time,  $\Delta t$ , approaches infinity.

The second peak, which indicates the maximum value of the  $d(\text{BDIP})$  curve, is a qualitative indication of depletion in the reservoir. It does not indicate a boundary.

The boundaries for the finite reservoir are indicated on Figure 4.4.5. The distance to the boundaries is calculated as in the previous cases by using the shut-in times,  $\Delta t$ , corresponding to the noted flex points in the radius of investigation equation.

In all boundary configurations the first boundary is very obvious. It is denoted by the first maximum. All other boundaries are present, but depending on the reservoir characteristics and

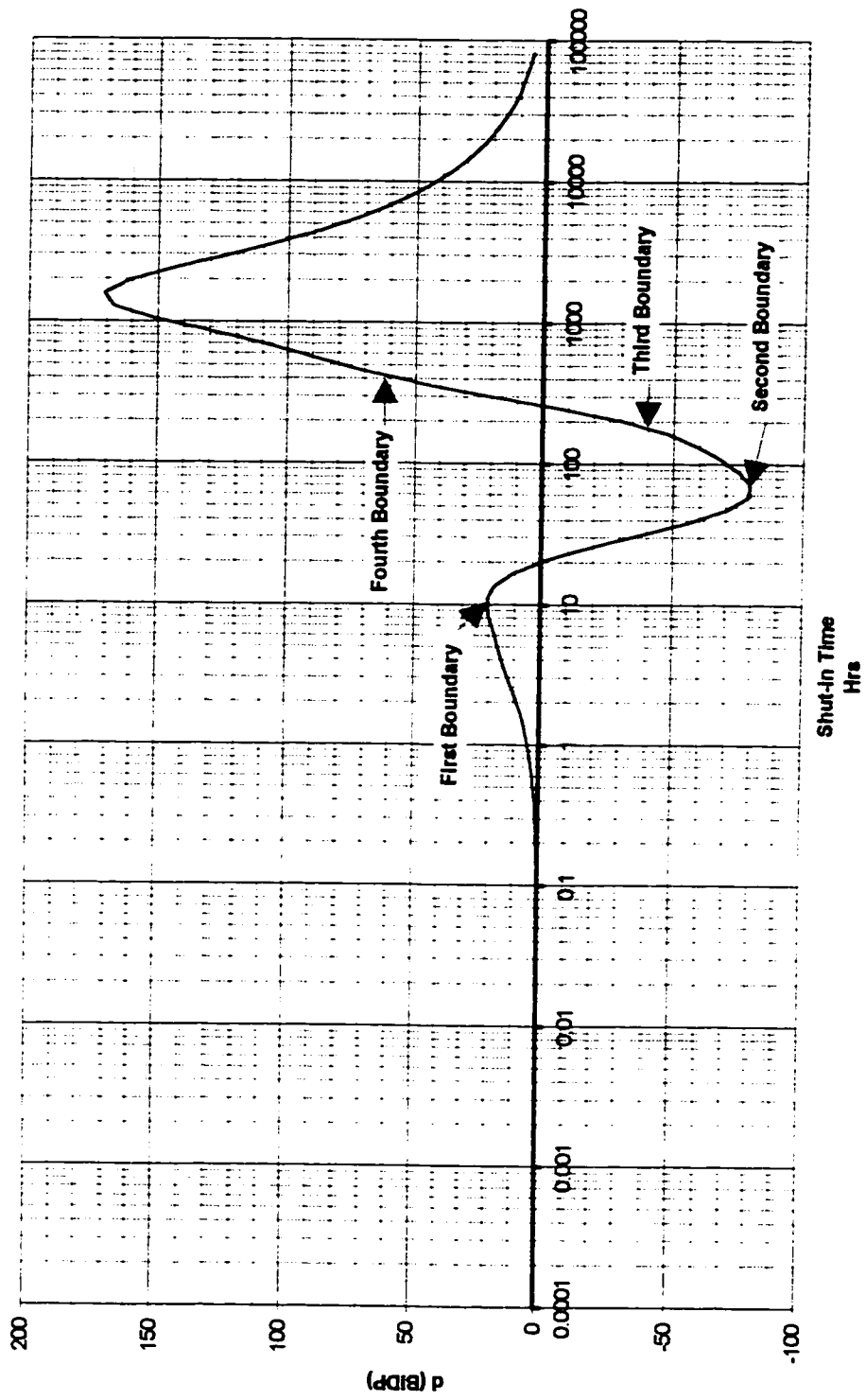


**Figure 4.4.5  $d(BIDP)$  Curve for a Reservoir with Four No-Flow Boundaries**

boundary configuration, their presence on the  $d(\text{BIDP})$  curve can range from very obvious to quite subtle. In many cases, expanding the vertical scale, which causes the data to “shrink”, makes the flex points more obvious. For example, compare Figure 4.4.5 with Figure 4.4.6; these figures represent exactly the same reservoir configuration. In Figure 4.4.6 the scale for  $d(\text{BIDP})$  has been expanded. Also, the labels for the boundaries have been removed so as not to distract the reader from the shape of the curve.

During the analysis of the  $d(\text{BIDP})$  versus  $\log \Delta t$  plots as a tool for the detection of no-flow boundaries, the inflection points found on the curves were investigated as potential indications of these boundaries. It was found that by substituting the value of the shut-in time  $\Delta t$  at which the inflections occurred, into the radius of investigation equation (Equation 4.2.3.1), the distance so calculated could be correlated to the distance to the boundary. In other words, the inflection points were first investigated, not the time which corresponded to the boundaries in the synthetic data.

In all boundary configurations, after all boundaries have been felt, the  $d(\text{BIDP})$  curve becomes smooth, regardless of whether it is increasing or decreasing.

The use of the derivative of the  $d(\text{BIDP})$  curve was considered to assist in the determination of subtle boundary responses. It was found that while this second derivative had a response at the

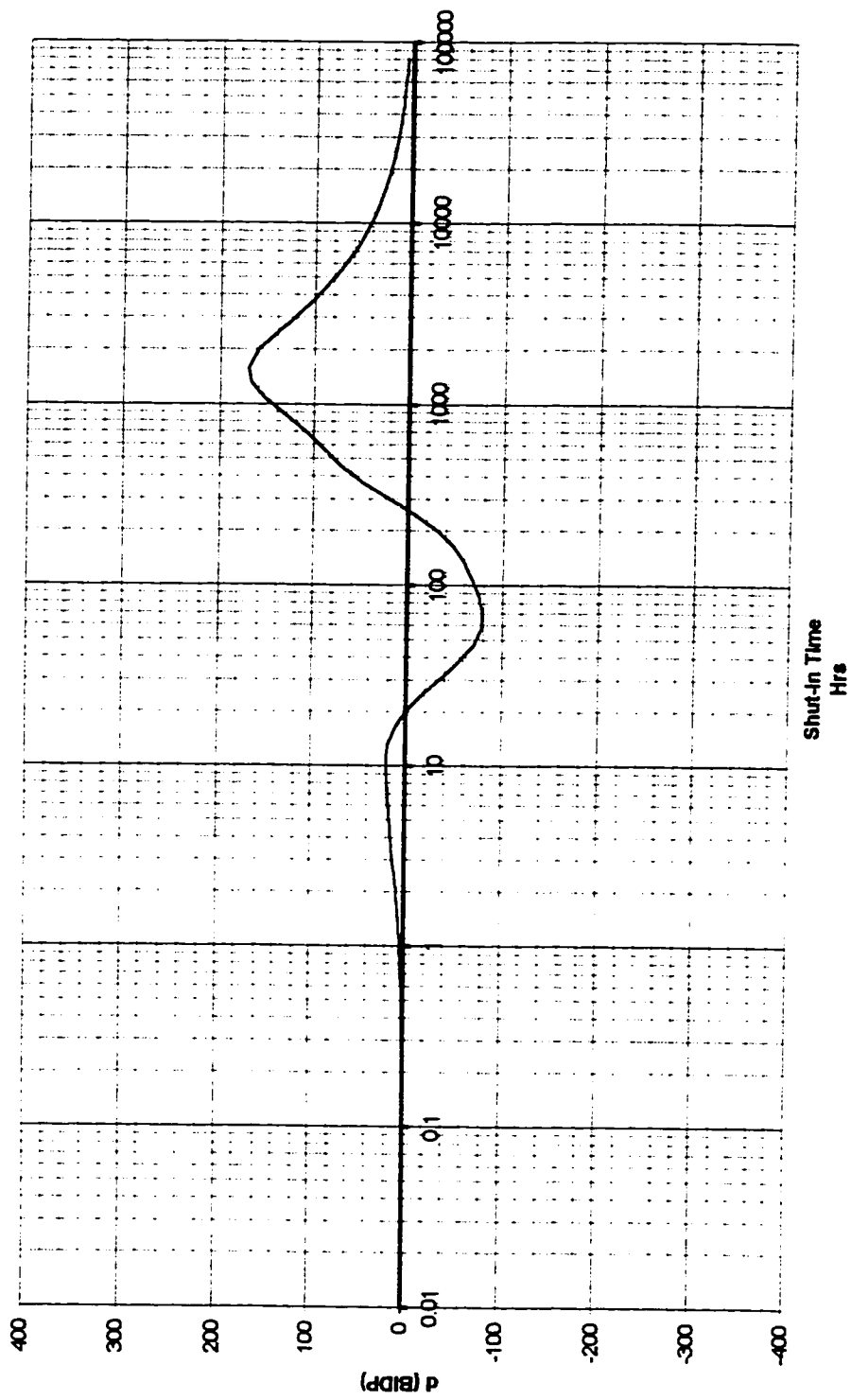


**Figure 4.4.6  $d(BIDP)$  Curve for a Reservoir with Four No-Flow Boundaries - expanded scale**

appropriate time, the response was not unique. Additionally, there were responses in the second derivative that were not apparent in the  $d(\text{BIDP})$  curve. Therefore, at this time, the second derivative is not considered to be useful in identifying boundaries in the  $d(\text{BIDP})$  method.

The following sections give an analytical derivation of the Boundary Influenced Difference of Pressure and the  $d(\text{BIDP})$  for the cases of a single boundary, two intersecting boundaries, two parallel boundaries, three boundaries, and four boundaries. While these models were used to test for accuracy in the examples presented herein, the actual plots presented were generated by calculating the buildup pressure data for each case, then subtracting it from the infinite-acting case giving the BIDP, and then calculating the  $d(\text{BIDP})$ . This is indicative of how the method would be used with real data.

## 4.5 Single No-Flow Boundary

Using the Principle of Superposition, a single no-flow boundary located at a distance “ $d$ ” from a well can be represented by two wells a distance of  $2d$  apart with both wells having identical flow characteristics and production histories. The second well is considered to be the “image” well. Mathematically, it can be shown that a line equidistant between two wells with identical flow characteristics will be a no flow boundary. By adding the solutions of the radial diffusivity equation for the two wells using the actual well as the reference location one obtains a solution for a single no-flow boundary (Lee 1982). See Figure 4.5.1.

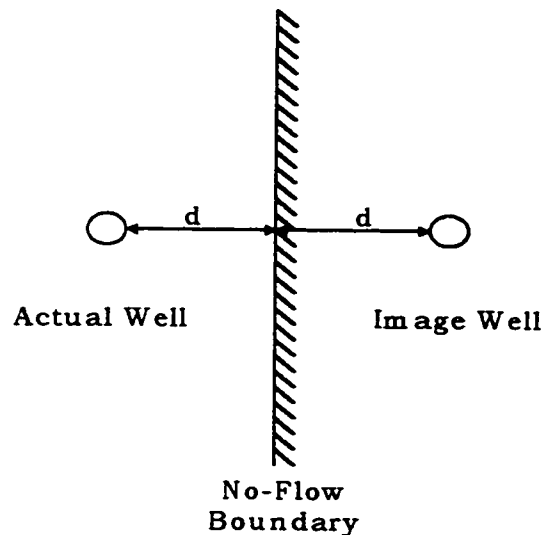


**Figure 4.5.1 Method of Images for Single No-Flow Boundary**

The solution of the radial diffusivity equation for a well flowing in an infinite reservoir is given above. For the same well that has been shut-in after a period of flow the solution is:

$$p_i - p_{ws\infty} = \frac{qB\mu}{4\pi kh} \left[ -Ei\left(-\frac{\phi\mu c_t r_w^2}{4k(t_p + \Delta t)}\right) + Ei\left(-\frac{\phi\mu c_t r_w^2}{4k\Delta t}\right) \right] \dots\dots(4.5.1)$$

Similarly, for a well in a reservoir with a single no-flow boundary that is shut-in after a period of flow, the bottom hole pressure can be determined from the expression:

$$p_i - p_{wsb} = \frac{qB\mu}{4\pi kh} \left[ -Ei\left(-\frac{\phi\mu c_t r_w^2}{4k(t_p + \Delta t)}\right) + Ei\left(-\frac{\phi\mu c_t r_w^2}{4k(\Delta t)}\right) \right. \\ \left. - Ei\left(-\frac{\phi\mu c_t (2d)^2}{4k(t_p + \Delta t)}\right) + Ei\left(-\frac{\phi\mu c_t (2d)^2}{4k(\Delta t)}\right) \right] \dots\dots(4.5.2)$$

Subtracting these two quantities gives the Boundary Influenced Difference of Pressure, BIDP:

$$BIDP = p_{ws\infty} - p_{wsb} = \frac{qB\mu}{4\pi kh} \left[ -Ei\left(-\frac{\phi\mu c_t (2d)^2}{4k(t_p + \Delta t)}\right) + Ei\left(-\frac{\phi\mu c_t (2d)^2}{4k(\Delta t)}\right) \right] \dots\dots(4.5.3)$$



As was discussed earlier, a plot of BIDP versus  $\log \Delta t$  does not give a unique characteristic boundary signature.

Bourdet et al. (1983) proposed an interpretation method based on the analysis of the derivative of pressure with respect to a time function. These authors found that the derivative response was more sensitive to the small phenomena of interest in pressure transient analysis. Using the derivative curve, a distinct signature for a given flow condition could be identified.

Following this method, a plot of the semi-log derivative of BIDP versus  $\log \Delta t$  results in a curve that displays a unique signature for each set of boundary conditions applied. Figure 4.5.2 illustrates this for a single boundary.

The semi-log derivative is defined as follows:

$$\frac{d(\text{BIDP})}{d(\log(\Delta t))} = \Delta t \left( \frac{d(\text{BIDP})}{d(\Delta t)} \right) \quad \text{.....(4.5.4)}$$

For example, the semi-log derivative, for a well in a reservoir with a single boundary, is:

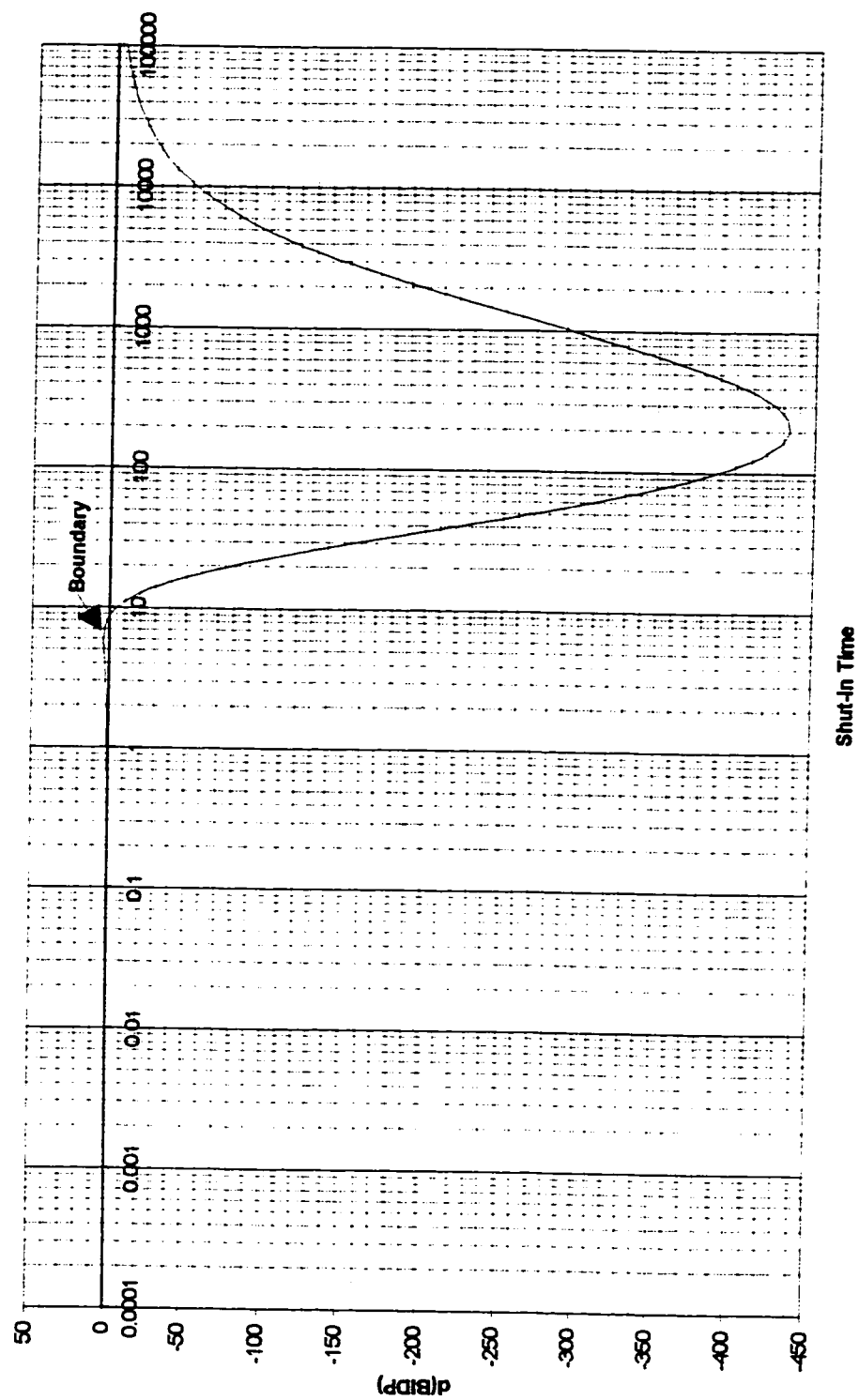


**Figure 4.5.2  $d(BIDP)$  Curve for Single Boundary**

$$\frac{d(\text{BIDP})}{d(\log(\Delta t))} = \Delta t \frac{qB\mu}{4\pi kh} \left[ \frac{\exp\left(-\frac{\phi\mu c_t (2d)^2}{4k(t_p + \Delta t)}\right)}{\frac{\phi\mu c_t (2d)^2}{4k(t_p + \Delta t)}} - \frac{\exp\left(-\frac{\phi\mu c_t (2d)^2}{4k(\Delta t)}\right)}{\frac{\phi\mu c_t (2d)^2}{4k(\Delta t)}} \right] \dots(4.5.5)$$

For the examples presented in this work a central difference formulation was used to evaluate the derivative of BIDP with respect to  $\Delta t$ . It was found that while forward, central, and backward differences gave very similarly shaped curves, a time shift occurred along the  $\Delta t$  axis for the backward and forward difference methods. This was rather insignificant at low values of  $\Delta t$ ; however, the time shift compounded itself as  $\Delta t$  increased. See Figure 4.5.3.

The time shift with forward or backward differences was further compounded by the use of a logarithmic scale for  $\Delta t$ . At large values of  $\Delta t$ , the time between data points increases and the shift is magnified. The logarithmic time scale was chosen to give a reasonable distribution of data across the time interval.

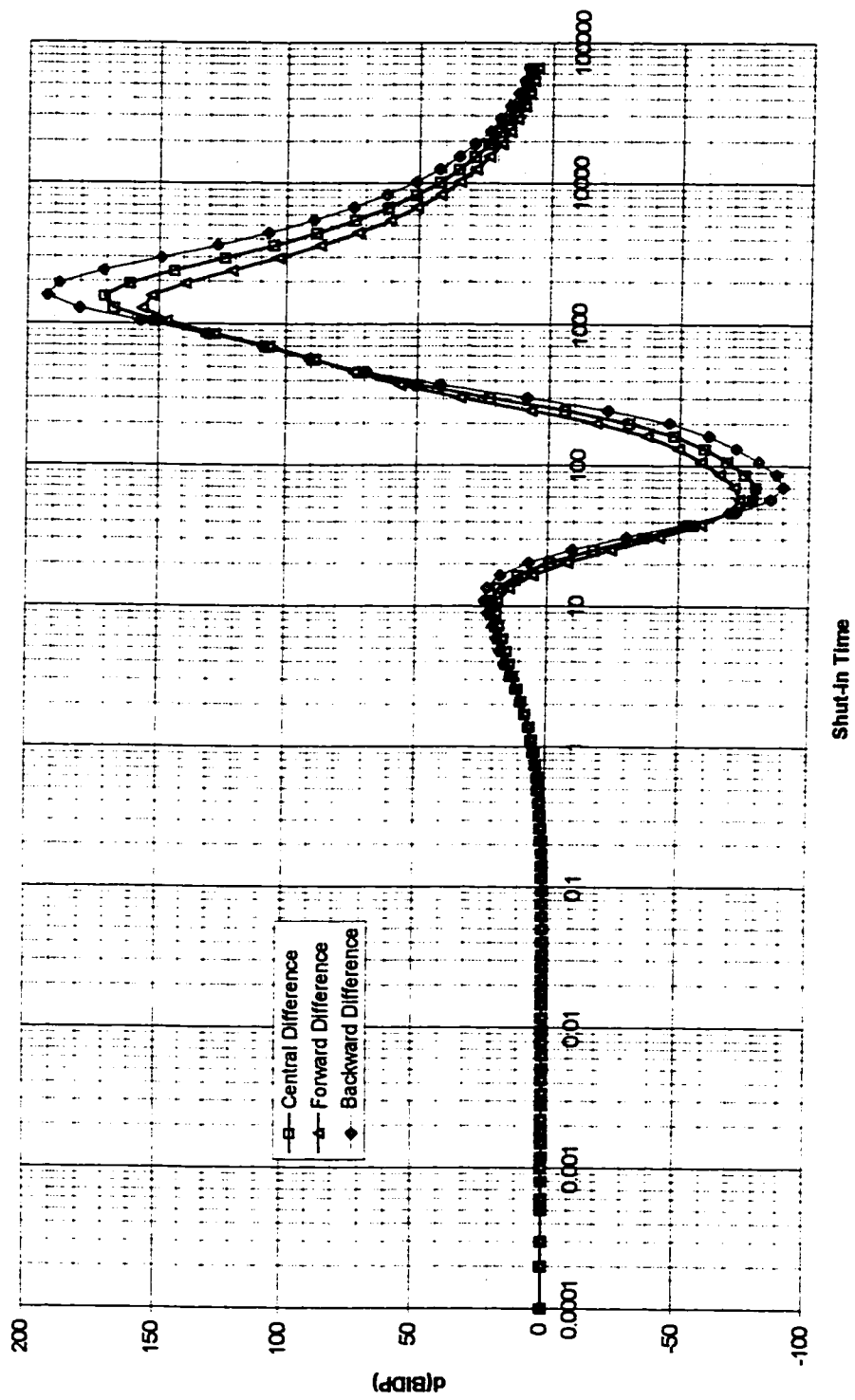


**Figure 4.5.3 Comparison of Difference Techniques**

## 4.6 Two Intersecting No-Flow Boundaries

Using the Method of Images, two intersecting no-flow boundaries can be represented as shown in Figure 4.6.1. This is similar to the case of a single no-flow boundary; however, in this case there are three image wells.

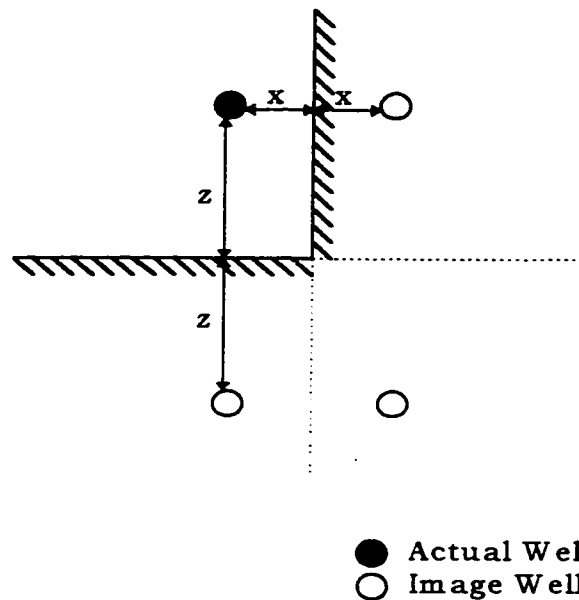


**Figure 4.6.1 Method of Images Two Intersecting Boundaries**

For a well in a reservoir bounded by two intersecting no-flow boundaries, the bottomhole pressure after shut-in can be

determined from the following expression. This expression is developed using the Principle of Superposition.

$$\begin{aligned}
p_{ws} = p_i + \frac{qB\mu}{4\pi kh} & \left[ Ei\left(-\frac{\phi\mu c_t r_w^2}{4k(t_p + \Delta t)}\right) - Ei\left(-\frac{\phi\mu c_t r_w^2}{4k(\Delta t)}\right) \right. \\
& + Ei\left(-\frac{\phi\mu c_t (2x)^2}{4k(t_p + \Delta t)}\right) - Ei\left(-\frac{\phi\mu c_t (2x)^2}{4k(\Delta t)}\right) \\
& + Ei\left(-\frac{\phi\mu c_t (2z)^2}{4k(t_p + \Delta t)}\right) - Ei\left(-\frac{\phi\mu c_t (2z)^2}{4k(\Delta t)}\right) \\
& \left. + Ei\left(-\frac{\phi\mu c_t (4x^2 + 4z^2)}{4k(t_p + \Delta t)}\right) - Ei\left(-\frac{\phi\mu c_t (4x^2 + 4z^2)}{4k(\Delta t)}\right) \right] \quad \dots(4.6.1)
\end{aligned}$$

Subtracting the above solution from the solution for a well in an infinite reservoir gives the Boundary Influenced Difference of Pressure, BIDP, for two intersecting no-flow boundaries.

$$\begin{aligned}
BIDP = p_{w\infty} - p_{wsb} = \frac{qB\mu}{4\pi kh} & \left[ -Ei\left(-\frac{\phi\mu c_t (2x)^2}{4k(t_p + \Delta t)}\right) + Ei\left(-\frac{\phi\mu c_t (2x)^2}{4k(\Delta t)}\right) \right. \\
& \left. - Ei\left(-\frac{\phi\mu c_t (2z)^2}{4k(t_p + \Delta t)}\right) + Ei\left(-\frac{\phi\mu c_t (2z)^2}{4k(\Delta t)}\right) \right]
\end{aligned}$$

$$- \text{Ei} \left( - \frac{\phi \mu c_i (4x^2 + 4z^2)}{4k(t_p + \Delta t)} \right) + \text{Ei} \left( - \frac{\phi \mu c_i (4x^2 + 4z^2)}{4k(\Delta t)} \right) \Bigg] \quad \text{.....(4.6.2)}$$

A plot of the d(BIDP) versus log  $\Delta t$  is shown in Figure 4.6.2. It can be seen that the magnitude of the initial deviation is greater than for the case of a single boundary. Also the “infinite acting” data is shifted to a later time. Further, the smooth curve evident in the single boundary case is no longer smooth. The additional flex point indicates a second boundary, and allows for the calculation of the distance to the second boundary. The distance to the first boundary is found in the same way as in the single boundary case.

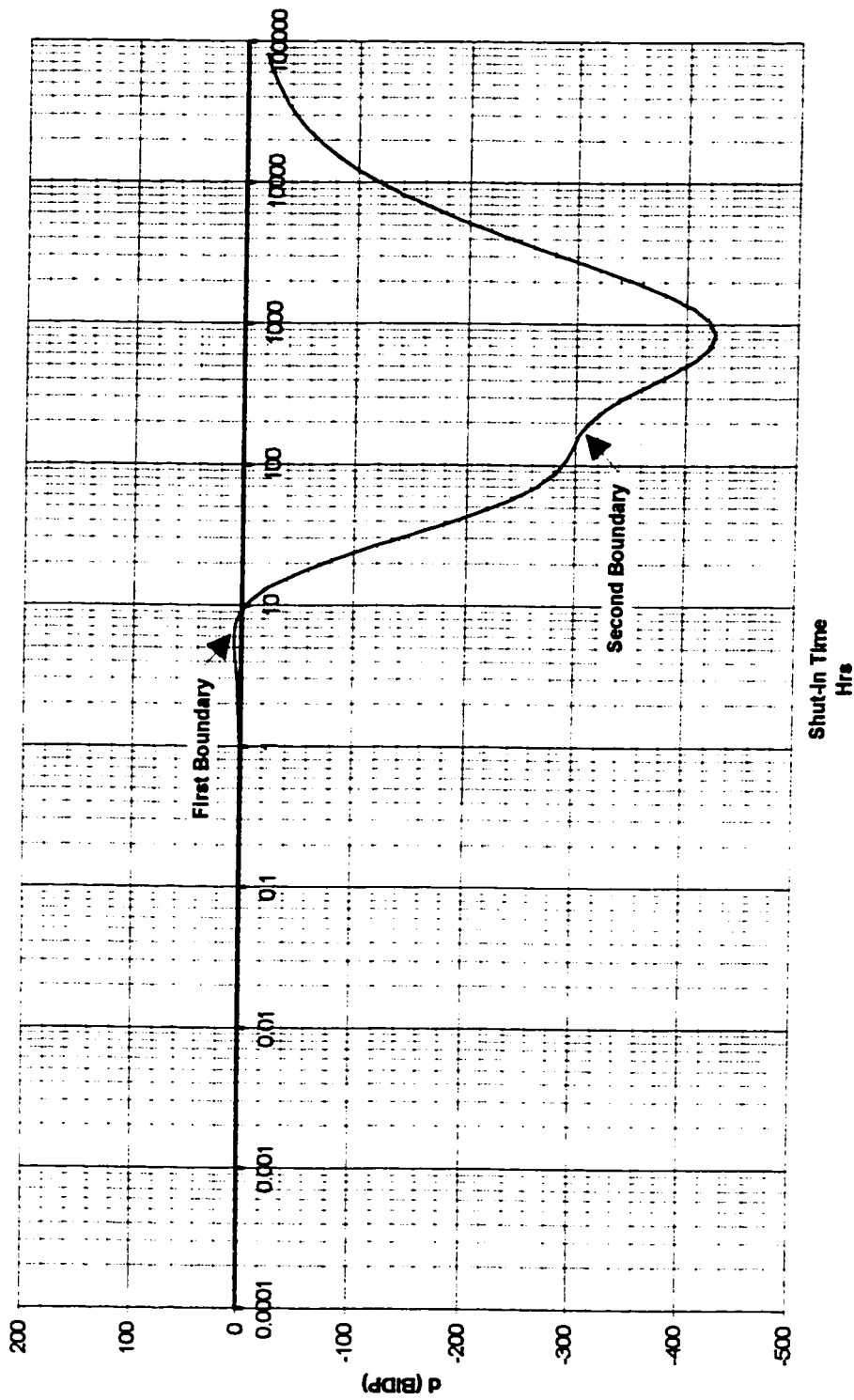


**Figure 4.6.2  $d(BIDP)$  Curve for Reservoir With Two Intersecting Boundaries**



## 4.7 Two Parallel No-Flow Boundaries

Using the Method of Images, two parallel no-flow boundaries can be represented as shown in Figure 4.7.1. For parallel boundaries, the method of images results in an infinite array of image wells extending from each boundary.

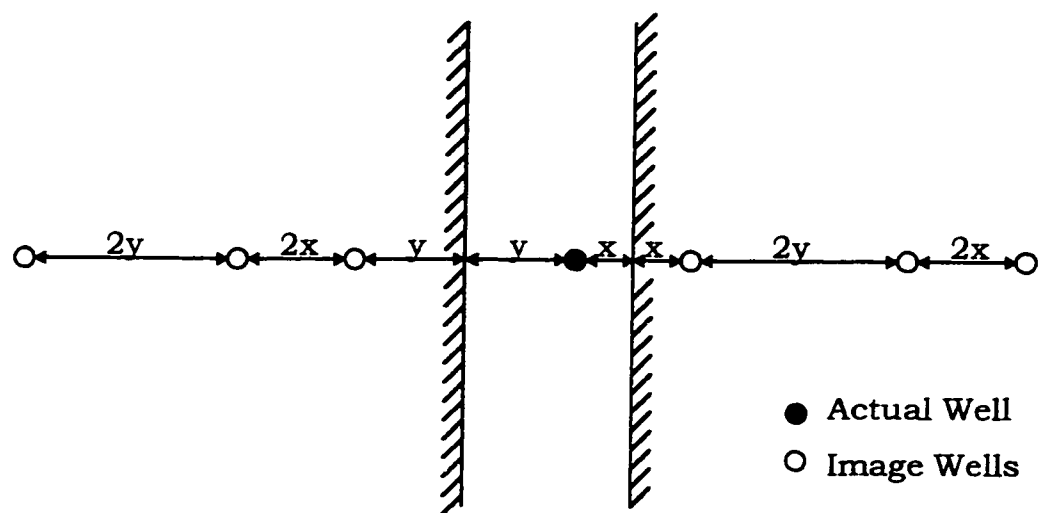


**Figure 4.7.1 Method of Images for Two Parallel Boundaries**

For a well in a reservoir bounded by two parallel no-flow boundaries, the bottomhole pressure after shut-in can be determined from the following expression. This expression is developed using the Principle of Superposition.

$$\begin{aligned}
p_{ws} = p_i + \frac{qB\mu}{4\pi kh} & \left[ Ei\left(-\frac{\phi\mu c_t r_w^2}{4k(t_p + \Delta t)}\right) - Ei\left(-\frac{\phi\mu c_t r_w^2}{4k(\Delta t)}\right) \right. \\
& + \sum_{l=1}^{\infty} \left[ Ei\left(-\frac{\phi\mu c_t (2lx + 2(l-1)y)^2}{4k(t_p + \Delta t)}\right) - Ei\left(-\frac{\phi\mu c_t (2lx + 2(l-1)y)^2}{4k(\Delta t)}\right) \right. \\
& + Ei\left(-\frac{\phi\mu c_t (2(l-1)x + 2ly)^2}{4k(t_p + \Delta t)}\right) - Ei\left(-\frac{\phi\mu c_t (2(l-1)x + 2ly)^2}{4k(\Delta t)}\right) \\
& \left. \left. + 2Ei\left(-\frac{\phi\mu c_t (2lx + 2ly)^2}{4k(t_p + \Delta t)}\right) - 2Ei\left(-\frac{\phi\mu c_t (2lx + 2ly)^2}{4k(\Delta t)}\right) \right] \right] \dots (4.7.1)
\end{aligned}$$

Subtracting the above solution from the solution for a well in an infinite reservoir gives the Boundary Influenced Difference of Pressure, BIDP, for two parallel no-flow boundaries.

$$\begin{aligned}
BIDP = p_{w\infty} - p_{wsb} = \\
= \frac{qB\mu}{4\pi kh} \sum_{l=1}^{\infty} & \left[ -Ei\left(-\frac{\phi\mu c_t (2lx + 2(l-1)y)^2}{4k(t_p + \Delta t)}\right) + Ei\left(-\frac{\phi\mu c_t (2lx + 2(l-1)y)^2}{4k(\Delta t)}\right) \right. \\
& \left. - Ei\left(-\frac{\phi\mu c_t (2(l-1)x + 2ly)^2}{4k(t_p + \Delta t)}\right) + Ei\left(-\frac{\phi\mu c_t (2(l-1)x + 2ly)^2}{4k(\Delta t)}\right) \right]
\end{aligned}$$

$$-2\text{Ei}\left(-\frac{\phi\mu c_t(2I_x + 2I_y)^2}{4k(t_p + \Delta t)}\right) + 2\text{Ei}\left(-\frac{\phi\mu c_t(2I_x + 2I_y)^2}{4k(\Delta t)}\right) \dots\dots(4.7.2)$$

A plot of the d(BIDP) versus log  $\Delta t$  is shown in Figure 4.7.2. There is a definite change of slope on the plot between times of 100 and 1000. This is indicative of a second boundary. The distance to the first boundary is calculated as for a single no-flow boundary. To calculate the distance to the second boundary note the time  $\Delta t$  where the curve “flexes”. Using this time  $\Delta t$ , in Equation (4.2.3.2) for distance to the boundary given in Section 4.2.3, calculate the distance to the boundary.

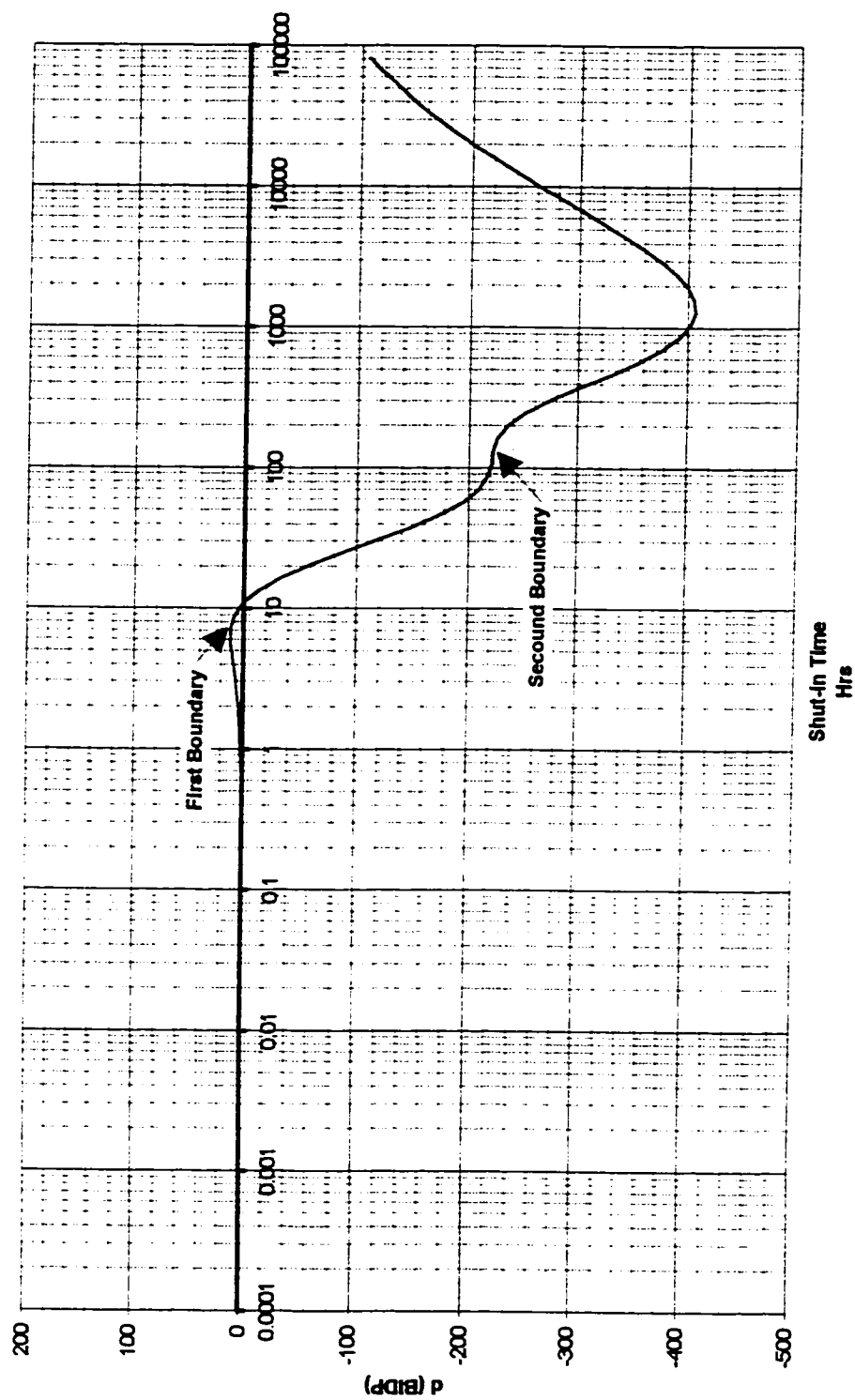


**Figure 4.7.2  $d(BIDP)$  Curve for Two Parallel No-Flow Boundaries**

## 4.8 Three Intersecting No-Flow Boundaries

Using the Method of Images, three intersecting no-flow boundaries can be represented as shown in Figure 4.8.1. For parallel boundaries, the method of images results in an infinite array of image wells extending from each boundary. Adding a third boundary results in two rows of an infinite number of wells.

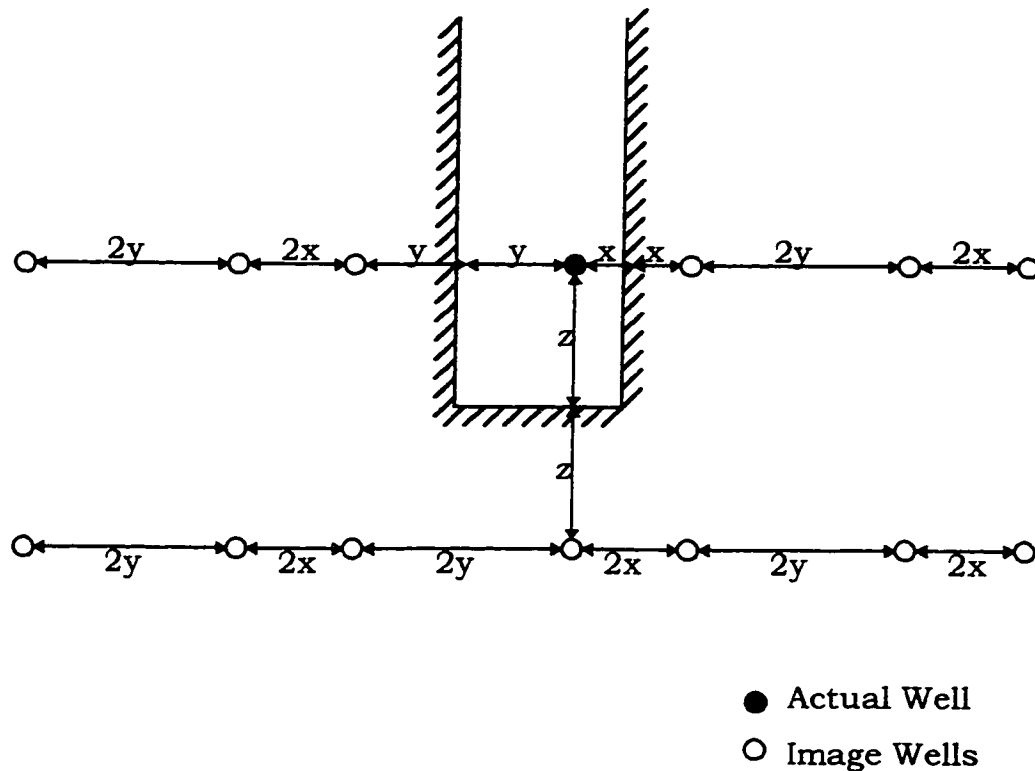


**Figure 4.8.1 Method of Images for Three No-Flow Boundaries**

For a well in a reservoir bounded by three intersecting no-flow boundaries, the bottomhole pressure after shut-in can be determined from the following expression. This expression is developed using the Principle of Superposition.

From the case of two parallel boundaries the solution is:

$$\begin{aligned}
 p_{ws} = p_i + \frac{qB\mu}{4\pi kh} & \left[ Ei\left(-\frac{\phi\mu c_t r_w^2}{4k(t_p + \Delta t)}\right) - Ei\left(-\frac{\phi\mu c_t r_w^2}{4k(\Delta t)}\right) \right. \\
 & + \sum_{l=1}^{\infty} \left[ Ei\left(-\frac{\phi\mu c_t (2lx + 2(l-1)y)^2}{4k(t_p + \Delta t)}\right) - Ei\left(-\frac{\phi\mu c_t (2lx + 2(l-1)y)^2}{4k(\Delta t)}\right) \right. \\
 & + Ei\left(-\frac{\phi\mu c_t (2(l-1)x + 2ly)^2}{4k(t_p + \Delta t)}\right) - Ei\left(-\frac{\phi\mu c_t (2(l-1)x + 2ly)^2}{4k(\Delta t)}\right) \\
 & \left. \left. + 2Ei\left(-\frac{\phi\mu c_t (2lx + 2ly)^2}{4k(t_p + \Delta t)}\right) - 2Ei\left(-\frac{\phi\mu c_t (2lx + 2ly)^2}{4k(\Delta t)}\right) \right] \right] \dots\dots(4.8.1)
 \end{aligned}$$

For the second infinite row of image wells, the contribution to pressure drop is:

$$p_{ws} = p_i + \frac{qB\mu}{4\pi kh} \left[ Ei\left(-\frac{\phi\mu c_t (2z)^2}{4k(t_p + \Delta t)}\right) - Ei\left(-\frac{\phi\mu c_t (2z)^2}{4k(\Delta t)}\right) \right]$$

$$\begin{aligned}
& +\text{Ei}\left(-\frac{\phi\mu c_t((2x)^2+(2z)^2)}{4k(t_p+\Delta t)}\right)-\text{Ei}\left(-\frac{\phi\mu c_t((2x)^2+(2z)^2)}{4k(\Delta t)}\right) \\
& +\text{Ei}\left(-\frac{\phi\mu c_t((2y)^2+(2z)^2)}{4k(t_p+\Delta t)}\right)-\text{Ei}\left(-\frac{\phi\mu c_t((2y)^2+(2z)^2)}{4k(\Delta t)}\right) \\
& +2\text{Ei}\left(-\frac{\phi\mu c_t((2x+2y)^2+(2z)^2)}{4k(t_p+\Delta t)}\right)-2\text{Ei}\left(-\frac{\phi\mu c_t((2x+2y)^2+(2z)^2)}{4k(\Delta t)}\right) \\
& +\text{Ei}\left(-\frac{\phi\mu c_t((4x+2y)^2+(2z)^2)}{4k(t_p+\Delta t)}\right)-\text{Ei}\left(-\frac{\phi\mu c_t((4x+2y)^2+(2z)^2)}{4k(\Delta t)}\right) \\
& +\text{Ei}\left(-\frac{\phi\mu c_t((4y+2x)^2+(2z)^2)}{4k(t_p+\Delta t)}\right)-\text{Ei}\left(-\frac{\phi\mu c_t((4y+2x)^2+(2z)^2)}{4k(\Delta t)}\right) \\
& +2\text{Ei}\left(-\frac{\phi\mu c_t((4x+4y)^2+(2z)^2)}{4k(t_p+\Delta t)}\right)-2\text{Ei}\left(-\frac{\phi\mu c_t((4x+4y)^2+(2z)^2)}{4k(\Delta t)}\right)+\dots \\
& \dots\dots(4.8.2)
\end{aligned}$$

Combining these two results gives:

$$p_{ws} = p_i + \frac{qB\mu}{4\pi kh} \left[ \text{Ei}\left(-\frac{\phi\mu c_t r_w^2}{4k(t_p+\Delta t)}\right) - \text{Ei}\left(-\frac{\phi\mu c_t r_w^2}{4k(\Delta t)}\right) \right]$$

$$\begin{aligned}
& +\text{Ei}\left(-\frac{\phi\mu c_t(2z)^2}{4k(t_p + \Delta t)}\right) - \text{Ei}\left(-\frac{\phi\mu c_t(2z)^2}{4k(\Delta t)}\right) \\
& +\sum_{l=1}^{\infty}\left[\text{Ei}\left(-\frac{\phi\mu c_t(2lx + 2(I-1)y)^2}{4k(t_p + \Delta t)}\right) - \text{Ei}\left(-\frac{\phi\mu c_t(2lx + 2(I-1)y)^2}{4k(\Delta t)}\right)\right. \\
& \left.+\text{Ei}\left(-\frac{\phi\mu c_t(2ly + 2(I-1)x)^2}{4k(t_p + \Delta t)}\right) - \text{Ei}\left(-\frac{\phi\mu c_t(2ly + 2(I-1)x)^2}{4k(\Delta t)}\right)\right. \\
& \left.+\text{Ei}\left(-\frac{\phi\mu c_t(2lx + 2ly)^2}{4k(t_p + \Delta t)}\right) - 2\text{Ei}\left(-\frac{\phi\mu c_t(2lx + 2ly)^2}{4k(\Delta t)}\right)\right. \\
& \left.+\text{Ei}\left(-\frac{\phi\mu c_t\left((2lx + 2(I-1)y)^2 + (2z)^2\right)}{4k(t_p + \Delta t)}\right)\right. \\
& \left.-\text{Ei}\left(-\frac{\phi\mu c_t\left((2lx + 2(I-1)y)^2 + (2z)^2\right)}{4k(\Delta t)}\right)\right. \\
& \left.+\text{Ei}\left(-\frac{\phi\mu c_t\left((2ly + 2(I-1)x)^2 + (2z)^2\right)}{4k(t_p + \Delta t)}\right)\right)
\end{aligned}$$



$$\begin{aligned}
& -\text{Ei}\left(-\frac{\phi\mu c_t\left((2Iy + 2(I-1)x)^2 + (2z)^2\right)}{4k(\Delta t)}\right) \\
& + \text{Ei}\left(-\frac{\phi\mu c_t\left((2Ix + 2Iy)^2 + (2z)^2\right)}{4k(t_p + \Delta t)}\right) - \text{Ei}\left(-\frac{\phi\mu c_t\left((2Ix + 2Iy)^2 + (2z)^2\right)}{4k(\Delta t)}\right) \Bigg] \Bigg] \\
& \dots\dots(4.8.3)
\end{aligned}$$

Subtracting from the infinite system result gives the BIDP for a system with three no-flow boundaries:

$$\begin{aligned}
\text{BIDP} = p_{w\infty} - p_{wsb} &= \frac{qB\mu}{4\pi kh} \left[ -\text{Ei}\left(-\frac{\phi\mu c_t(2z)^2}{4k(t_p + \Delta t)}\right) + \text{Ei}\left(-\frac{\phi\mu c_t(2z)^2}{4k(\Delta t)}\right) \right. \\
& + \sum_{l=1}^{\infty} \left[ -\text{Ei}\left(-\frac{\phi\mu c_t(2Ix + 2(I-1)y)^2}{4k(t_p + \Delta t)}\right) + \text{Ei}\left(-\frac{\phi\mu c_t(2Ix + 2(I-1)y)^2}{4k(\Delta t)}\right) \right. \\
& \left. -\text{Ei}\left(-\frac{\phi\mu c_t(2Iy + 2(I-1)x)^2}{4k(t_p + \Delta t)}\right) + \text{Ei}\left(-\frac{\phi\mu c_t(2Iy + 2(I-1)x)^2}{4k(\Delta t)}\right) \right. \\
& \left. -2\text{Ei}\left(-\frac{\phi\mu c_t(2Ix + 2Iy)^2}{4k(t_p + \Delta t)}\right) + 2\text{Ei}\left(-\frac{\phi\mu c_t(2Ix + 2Iy)^2}{4k(\Delta t)}\right) \right]
\end{aligned}$$

$$\begin{aligned}
& -Ei\left(-\frac{\phi\mu c_t\left((2Ix + 2(I-1)y)^2 + (2z)^2\right)}{4k(t_p + \Delta t)}\right) \\
& +Ei\left(-\frac{\phi\mu c_t\left((2Ix + 2(I-1)y)^2 + (2z)^2\right)}{4k(\Delta t)}\right) \\
& -Ei\left(-\frac{\phi\mu c_t\left((2Iy + 2(I-1)x)^2 + (2z)^2\right)}{4k(t_p + \Delta t)}\right) \\
& +Ei\left(-\frac{\phi\mu c_t\left((2Iy + 2(I-1)x)^2 + (2z)^2\right)}{4k(\Delta t)}\right) \\
& -Ei\left(-\frac{\phi\mu c_t\left((2Ix + 2Iy)^2 + (2z)^2\right)}{4k(t_p + \Delta t)}\right) + Ei\left(-\frac{\phi\mu c_t\left((2Ix + 2Iy)^2 + (2z)^2\right)}{4k(\Delta t)}\right)\Bigg] \\
& \dots\dots(4.8.4)
\end{aligned}$$

A plot of the d(BIDP) versus log  $\Delta t$  is shown in Figure 4.8.2. There is a definite flex point on the plot between times of 10 and 100. This is indicative of a second boundary. There is another flex point between times of 100 and 1000. This is indicative of the third boundary.

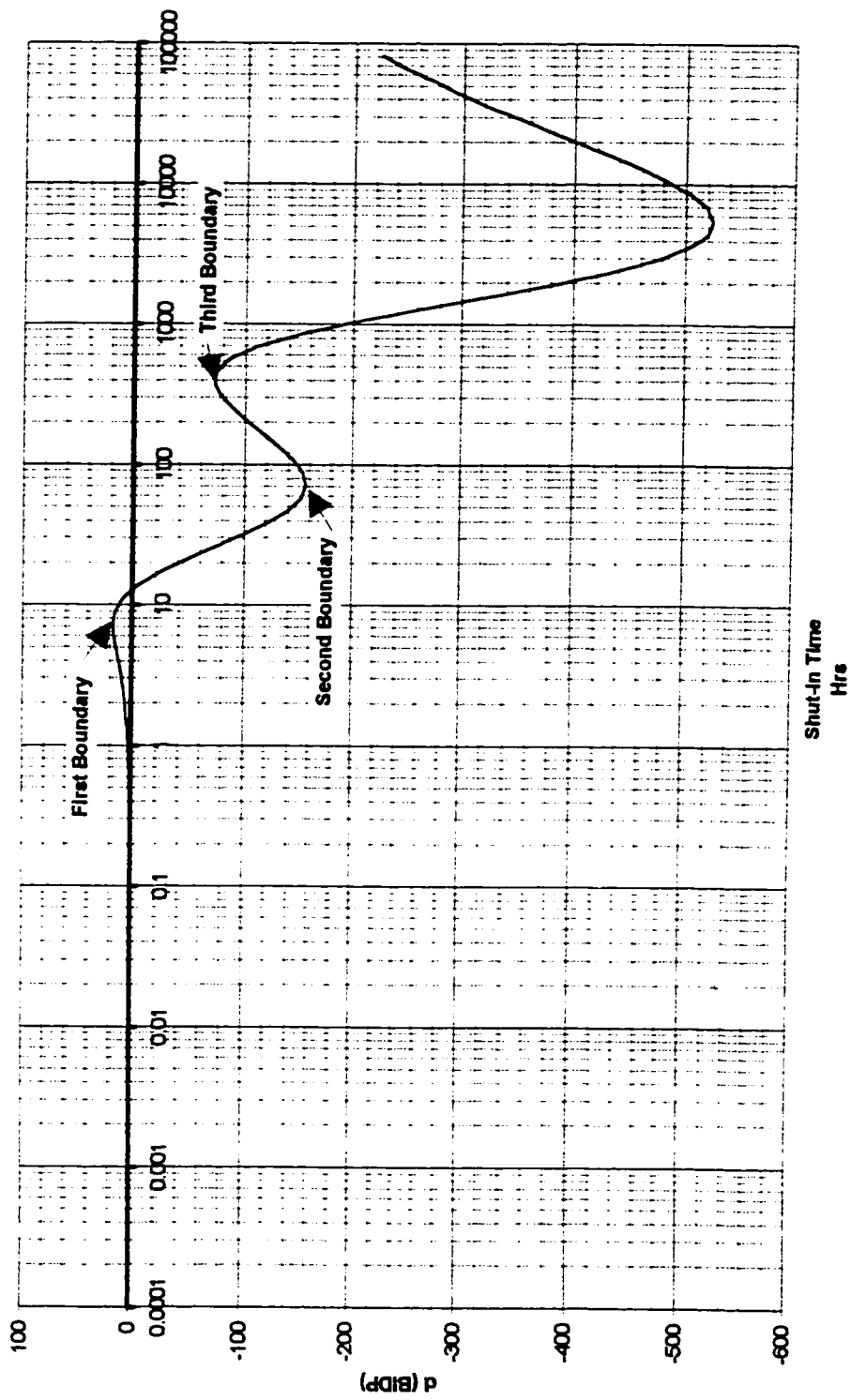


**Figure 4.8.2  $d(BIDP)$  Curve for Three No-Flow Boundaries**

The distance to the first boundary is calculated as for a single no-flow boundary. To calculate the distance to the second and third boundaries note the flex points on the curve. Using the time  $\Delta t$ , where the curve flexes, and using those values in Equation (4.2.3.2), the distance to the boundary, given in Section 4.2.3, calculate the distance to each boundary. On this graph, the flex points are quite evident. This is due as much to the distance between each of the boundaries as it is to the method.

## 4.9 Four Intersecting No-Flow Boundaries

Using the Method of Images, four intersecting no-flow boundaries can be represented as shown in Figure 4.9.1. For

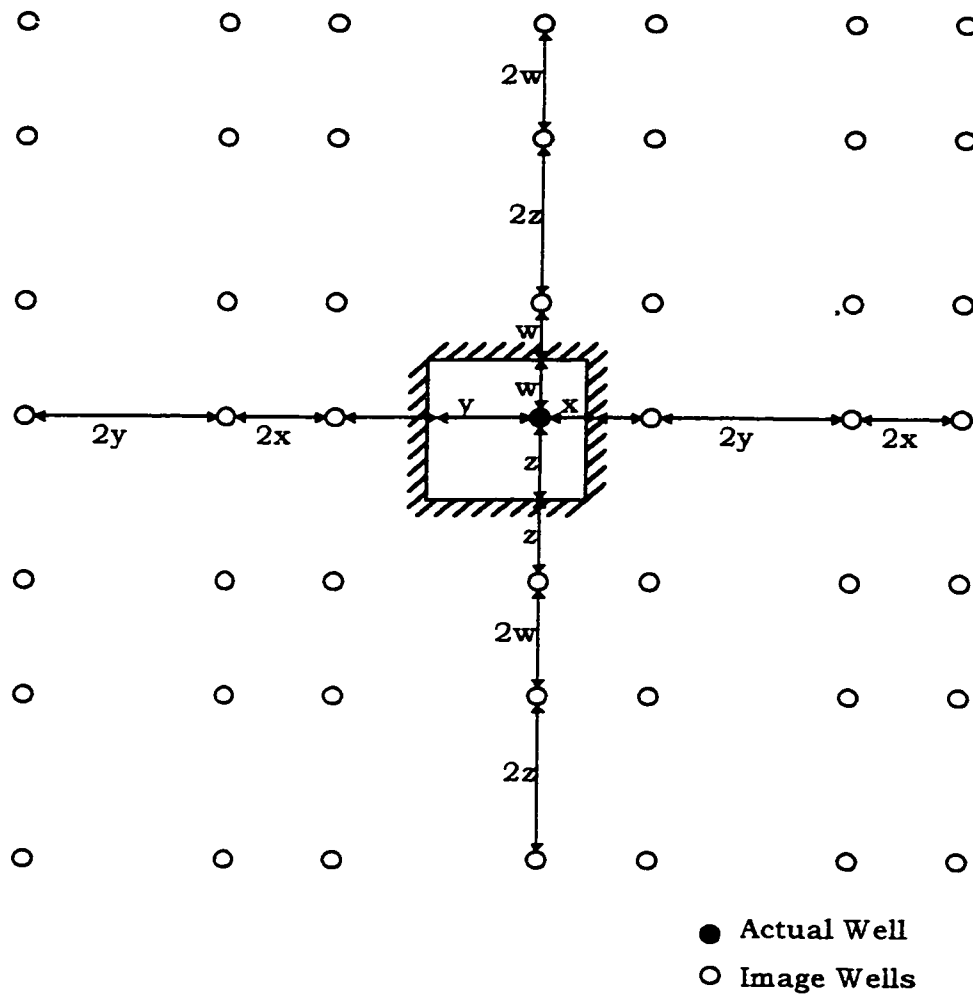


**Figure 4.9.1 Method of Images for Four No-Flow Boundaries**

parallel boundaries, the method of images results in an infinite array of image wells extending from each boundary. For four boundaries, there are infinite arrays of image wells extending in all directions. These wells are spaced as shown in Figure 4.9.1

Using the Principle of Superposition, an expression for bottomhole pressure after shut-in was developed for a system having four intersecting no-flow boundaries. The equation is an extension of the case for three no-flow boundaries; however, the infinite arrays of image wells extend in both directions. This leads to a double series of terms, summing in the “north-south” and “east-west” directions. Each quadrant of the arrays of wells has four terms in the summation. The two single summations are the wells that lie along the “axis”. To assist in reviewing this derivation, the common groups of variables are defined as follows:

$$\alpha = -\frac{\phi\mu c_t}{4k(t_p + \Delta t)}, \text{ and } \beta = -\frac{\phi\mu c_t}{4k(\Delta t)}.$$

$$\begin{aligned} p_{ws} = p_i + \frac{qB\mu}{4\pi kh} & \left[ Ei\left(-\frac{\phi\mu c_t r_w^2}{4k(t_p + \Delta t)}\right) - Ei\left(-\frac{\phi\mu c_t r_w^2}{4k(\Delta t)}\right) \right. \\ & + \sum_{l=1}^{\infty} \left[ Ei\left(\alpha(2lx + 2(l-1)y)^2\right) - Ei\left(\beta(2lx + 2(l-1)y)^2\right) \right. \\ & \left. + Ei\left(\alpha(2(l-1)x + 2ly)^2\right) - Ei\left(\beta(2(l-1)x + 2ly)^2\right) + 2Ei\left(\alpha(2lx + 2ly)^2\right) \right] \end{aligned}$$

$$\begin{aligned}
& -2\text{Ei}\left(\beta(2\text{I}\mathbf{x} + 2\text{I}\mathbf{y})^2\right) + \text{Ei}\left(\alpha(2\text{I}\mathbf{z} + 2(\text{I} - 1)\mathbf{w})^2\right) - \text{Ei}\left(\left(\beta(2\text{I}\mathbf{z} + 2(\text{I} - 1)\mathbf{w})^2\right)\right) \\
& + \text{Ei}\left(\alpha(2(\text{I} - 1)\mathbf{z} + 2\text{I}\mathbf{w})^2\right) - \text{Ei}\left(\beta(2(\text{I} - 1)\mathbf{z} + 2\text{I}\mathbf{w})^2\right) \\
& + 2\text{Ei}\left(\alpha(2\text{I}\mathbf{z} + 2\text{I}\mathbf{w})^2\right) - 2\text{Ei}\left(\beta(2\text{I}\mathbf{z} + 2\text{I}\mathbf{w})^2\right) \Big] \\
& + \sum_{\mathbf{J}=1}^{\infty} \sum_{\mathbf{I}=1}^{\infty} \Big[ \text{Ei}\left(\alpha\left((2\text{I}\mathbf{y} + 2(\mathbf{i} - 1)\mathbf{x})^2 + (2\mathbf{J}\mathbf{w} + 2(\mathbf{J} - 1)\mathbf{z})^2\right)\right) \\
& - \text{Ei}\left(\beta\left((2\text{I}\mathbf{y} + 2(\mathbf{I} - 1)\mathbf{x})^2 + (2\mathbf{J}\mathbf{w} + 2(\mathbf{J} - 1)\mathbf{z})^2\right)\right) \\
& + \text{Ei}\left(\alpha\left((2\text{I}\mathbf{y} + 2\text{I}\mathbf{x})^2 + (2\mathbf{J}\mathbf{w} + 2(\mathbf{J} - 1)\mathbf{z})^2\right)\right) \\
& - \text{Ei}\left(\beta\left((2\text{I}\mathbf{y} + 2\text{I}\mathbf{x})^2 + (2\mathbf{J}\mathbf{w} + 2(\mathbf{J} - 1)\mathbf{z})^2\right)\right) \\
& + \text{Ei}\left(\alpha\left((2\text{I}\mathbf{y} + 2(\mathbf{I} - 1)\mathbf{x})^2 + (2\mathbf{J}\mathbf{w} + 2\mathbf{J}\mathbf{z})^2\right)\right) \\
& - \text{Ei}\left(\beta\left((2\text{I}\mathbf{y} + 2(\mathbf{I} - 1)\mathbf{x})^2 + (2\mathbf{J}\mathbf{w} + 2\mathbf{J}\mathbf{z})^2\right)\right) \\
& + \text{Ei}\left(\alpha\left((2\text{I}\mathbf{y} + 2\text{I}\mathbf{x})^2 + (2\mathbf{J}\mathbf{w} + 2\mathbf{J}\mathbf{z})^2\right)\right) - \text{Ei}\left(\beta\left((2\text{I}\mathbf{y} + 2\text{I}\mathbf{x})^2 + (2\mathbf{J}\mathbf{w} + 2\mathbf{J}\mathbf{z})^2\right)\right) \Big]
\end{aligned}$$

$$+\text{Ei}\left(\alpha\left((2\text{Iy}+2(\text{I}-1)\mathbf{x})^2+(2\text{Jz}+2(\text{J}-1)\mathbf{w})^2\right)\right)$$

$$-\text{Ei}\left(\beta\left((2\text{Iy}+2(\text{I}-1)\mathbf{x})^2+(2\text{Jz}+2(\text{J}-1)\mathbf{w})^2\right)\right)$$

$$+\text{Ei}\left(\alpha\left((2\text{Iy}+2\text{Ix})^2+(2\text{Jz}+2(\text{J}-1)\mathbf{w})^2\right)\right)$$

$$-\text{Ei}\left(\beta\left((2\text{Iy}+2\text{Ix})^2+(2\text{Jz}+2(\text{J}-1)\mathbf{w})^2\right)\right)$$

$$+\text{Ei}\left(\alpha\left((2\text{Iy}+2(\text{I}-1)\mathbf{x})^2+(2\text{Jz}+2\text{Jw})^2\right)\right)$$

$$-\text{Ei}\left(\beta\left((2\text{Iy}+2(\text{I}-1)\mathbf{x})^2+(2\text{Jz}+2\text{Jw})^2\right)\right)$$

$$+\text{Ei}\left(\alpha\left((2\text{Iy}+2\text{Ix})^2+(2\text{Jz}+2\text{Jw})^2\right)\right)-\text{Ei}\left(\beta\left((2\text{Iy}+2\text{Ix})^2+(2\text{Jz}+2\text{Jw})^2\right)\right)$$

$$+\text{Ei}\left(\alpha\left((2\text{Ix}+2(\text{I}-1)\mathbf{y})^2+(2\text{Jw}+2(\text{J}-1)\mathbf{z})^2\right)\right)$$

$$-\text{Ei}\left(\beta\left((2\text{Ix}+2(\text{I}-1)\mathbf{y})^2+(2\text{Jw}+2(\text{J}-1)\mathbf{z})^2\right)\right)$$

$$+\text{Ei}\left(\alpha\left((2\text{Ix}+2\text{Iy})^2+(2\text{Jw}+2(\text{J}-1)\mathbf{z})^2\right)\right)$$



$$\begin{aligned}
& -\text{Ei}\left(\beta\left((2\text{I}\mathbf{x} + 2\text{I}\mathbf{y})^2 + (2\text{J}\mathbf{w} + 2(\text{J} - 1)\mathbf{z})^2\right)\right) \\
& +\text{Ei}\left(\alpha\left((2\text{I}\mathbf{x} + 2(\text{I} - 1)\mathbf{y})^2 + (2\text{J}\mathbf{w} + 2\text{J}\mathbf{z})^2\right)\right) \\
& -\text{Ei}\left(\beta\left((2\text{I}\mathbf{x} + 2(\text{I} - 1)\mathbf{y})^2 + (2\text{J}\mathbf{w} + 2\text{J}\mathbf{z})^2\right)\right) \\
& +\text{Ei}\left(\alpha\left((2\text{I}\mathbf{x} + 2\text{I}\mathbf{y})^2 + (2\text{J}\mathbf{w} + 2\text{J}\mathbf{z})^2\right)\right) - \text{Ei}\left(\beta\left((2\text{I}\mathbf{x} + 2\text{I}\mathbf{y})^2 + (2\text{J}\mathbf{w} + 2\text{J}\mathbf{z})^2\right)\right) \\
& +\text{Ei}\left(\alpha\left((2\text{I}\mathbf{x} + 2(\text{I} - 1)\mathbf{y})^2 + (2\text{J}\mathbf{z} + 2(\text{J} - 1)\mathbf{w})^2\right)\right) \\
& -\text{Ei}\left(\beta\left((2\text{I}\mathbf{x} + 2(\text{I} - 1)\mathbf{y})^2 + (2\text{J}\mathbf{z} + 2(\text{J} - 1)\mathbf{w})^2\right)\right) \\
& +\text{Ei}\left(\alpha\left((2\text{I}\mathbf{x} + 2\text{I}\mathbf{y})^2 + (2\text{J}\mathbf{z} + 2(\text{J} - 1)\mathbf{w})^2\right)\right) \\
& -\text{Ei}\left(\beta\left((2\text{I}\mathbf{x} + 2\text{I}\mathbf{y})^2 + (2\text{J}\mathbf{z} + 2(\text{J} - 1)\mathbf{w})^2\right)\right) \\
& +\text{Ei}\left(\alpha\left((2\text{I}\mathbf{x} + 2(\text{I} - 1)\mathbf{y})^2 + (2\text{J}\mathbf{z} + 2\text{J}\mathbf{w})^2\right)\right) \\
& -\text{Ei}\left(\beta\left((2\text{I}\mathbf{x} + 2(\text{I} - 1)\mathbf{y})^2 + (2\text{J}\mathbf{z} + 2\text{J}\mathbf{w})^2\right)\right) \\
& \vdots
\end{aligned}$$

$$+ \text{Ei}\left(\alpha\left((2I_x + 2I_y)^2 + (2J_z + 2J_w)^2\right)\right) - \text{Ei}\left(\beta\left((2I_x + 2I_y)^2 + (2J_z + 2J_w)^2\right)\right)\right]\right] \\ \text{.....(4.9.1)}$$

If Equation 4.9.1 is then subtracted from the solution for an infinite reservoir, Equation 4.2.1.5, the terms containing  $r_w$  drop out and the signs in the summations change. The BIDP for a finite reservoir is given by:

$$\begin{aligned} \text{BIDP} = \frac{qB\mu}{4\pi kh} & \left[ \sum_{i=1}^{\infty} \left[ -\text{Ei}\left(\alpha(2I_x + 2(I-1)y)^2\right) + \text{Ei}\left(\beta(2I_x + 2(I-1)y)^2\right) \right. \right. \\ & - \text{Ei}\left(\alpha(2(I-1)x + 2I_y)^2\right) + \text{Ei}\left(\beta(2(I-1)x + 2I_y)^2\right) - 2\text{Ei}\left(\alpha(2I_x + 2I_y)^2\right) \\ & + 2\text{Ei}\left(\beta(2I_x + 2I_y)^2\right) - \text{Ei}\left(\alpha(2I_z + 2(I-1)w)^2\right) + \text{Ei}\left(\beta(2I_z + 2(I-1)w)^2\right) \\ & - \text{Ei}\left(\alpha(2(I-1)z + 2I_w)^2\right) + \text{Ei}\left(\beta(2(I-1)z + 2I_w)^2\right) \\ & \left. \left. - 2\text{Ei}\left(\alpha(2I_z + 2I_w)^2\right) + 2\text{Ei}\left(\beta(2I_z + 2I_w)^2\right) \right] \right. \\ & \left. + \sum_{J=1}^{\infty} \sum_{i=1}^{\infty} \left[ -\text{Ei}\left(\alpha\left((2I_y + 2(i-1)x)^2 + (2J_w + 2(J-1)z)^2\right)\right) \right. \right. \end{aligned}$$

$$+ \text{Ei} \left( \beta \left( (2Iy + 2(I-1)x)^2 + (2Jw + 2(J-1)z)^2 \right) \right)$$

$$- \text{Ei} \left( \alpha \left( (2Iy + 2Ix)^2 + (2Jw + 2(J-1)z)^2 \right) \right)$$

$$+ \text{Ei} \left( \beta \left( (2Iy + 2Ix)^2 + (2Jw + 2(J-1)z)^2 \right) \right)$$

$$- \text{Ei} \left( \alpha \left( (2Iy + 2(I-1)x)^2 + (2Jw + 2Jz)^2 \right) \right)$$

$$+ \text{Ei} \left( \beta \left( (2Iy + 2(I-1)x)^2 + (2Jw + 2Jz)^2 \right) \right)$$

$$- \text{Ei} \left( \alpha \left( (2Iy + 2Ix)^2 + (2Jw + 2Jz)^2 \right) \right) + \text{Ei} \left( \beta \left( (2Iy + 2Ix)^2 + (2Jw + 2Jz)^2 \right) \right)$$

$$- \text{Ei} \left( \alpha \left( (2Iy + 2(I-1)x)^2 + (2Jz + 2(J-1)w)^2 \right) \right)$$

$$+ \text{Ei} \left( \beta \left( (2Iy + 2(I-1)x)^2 + (2Jz + 2(J-1)w)^2 \right) \right)$$

$$- \text{Ei} \left( \alpha \left( (2Iy + 2Ix)^2 + (2Jz + 2(J-1)w)^2 \right) \right)$$

$$+ \text{Ei} \left( \beta \left( (2Iy + 2Ix)^2 + (2Jz + 2(J-1)w)^2 \right) \right)$$

$$-\text{Ei}\left(\alpha\left((2Iy + 2(I - 1)x)^2 + (2Jz + 2Jw)^2\right)\right)$$

$$+\text{Ei}\left(\beta\left((2Iy + 2(I - 1)x)^2 + (2Jz + 2Jw)^2\right)\right)$$

$$-\text{Ei}\left(\alpha\left((2Iy + 2Ix)^2 + (2Jz + 2Jw)^2\right)\right) + \text{Ei}\left(\beta\left((2Iy + 2Ix)^2 + (2Jz + 2Jw)^2\right)\right)$$

$$-\text{Ei}\left(\alpha\left((2Ix + 2(I - 1)y)^2 + (2Jw + 2(J - 1)z)^2\right)\right)$$

$$+\text{Ei}\left(\beta\left((2Ix + 2(I - 1)y)^2 + (2Jw + 2(J - 1)z)^2\right)\right)$$

$$-\text{Ei}\left(\alpha\left((2Ix + 2Iy)^2 + (2Jw + 2(J - 1)z)^2\right)\right)$$

$$+\text{Ei}\left(\beta\left((2Ix + 2Iy)^2 + (2Jw + 2(J - 1)z)^2\right)\right)$$

$$-\text{Ei}\left(\alpha\left((2Ix + 2(I - 1)y)^2 + (2Jw + 2Jz)^2\right)\right)$$

$$+\text{Ei}\left(\beta\left((2Ix + 2(I - 1)y)^2 + (2Jw + 2Jz)^2\right)\right)$$

$$-\text{Ei}\left(\alpha\left((2Ix + 2Iy)^2 + (2Jw + 2Jz)^2\right)\right) + \text{Ei}\left(\beta\left((2Ix + 2Iy)^2 + (2Jw + 2Jz)^2\right)\right)$$

$$\begin{aligned}
& -\text{Ei}\left(\alpha\left((2I_x + 2(I-1)y)^2 + (2J_z + 2(J-1)w)^2\right)\right) \\
& +\text{Ei}\left(\beta\left((2I_x + 2(I-1)y)^2 + (2J_z + 2(J-1)w)^2\right)\right) \\
& -\text{Ei}\left(\alpha\left((2I_x + 2I_y)^2 + (2J_z + 2(J-1)w)^2\right)\right) \\
& +\text{Ei}\left(\beta\left((2I_x + 2I_y)^2 + (2J_z + 2(J-1)w)^2\right)\right) \\
& -\text{Ei}\left(\alpha\left((2I_x + 2(I-1)y)^2 + (2J_z + 2J_w)^2\right)\right) \\
& +\text{Ei}\left(\beta\left((2I_x + 2(I-1)y)^2 + (2J_z + 2J_w)^2\right)\right) \\
& -\text{Ei}\left(\alpha\left((2I_x + 2I_y)^2 + (2J_z + 2J_w)^2\right)\right) + \text{Ei}\left(\beta\left((2I_x + 2I_y)^2 + (2J_z + 2J_w)^2\right)\right) \Big] \\
& \dots(4.9.2)
\end{aligned}$$

A plot of the d(BIDP) versus  $\log \Delta t$  for a system of four intersecting no-flow boundaries is shown in Figure 4.9.2. There is a definite flex point on the plot around the time  $\Delta t=10$ . This is indicative of the first boundary. The second flex point occurs around  $\Delta t=60$ . This would be the second boundary. The third flex point occurs around  $\Delta t=180$ . This is the third boundary, and the final flex point occurs around  $\Delta t=420$ . This is the fourth boundary.

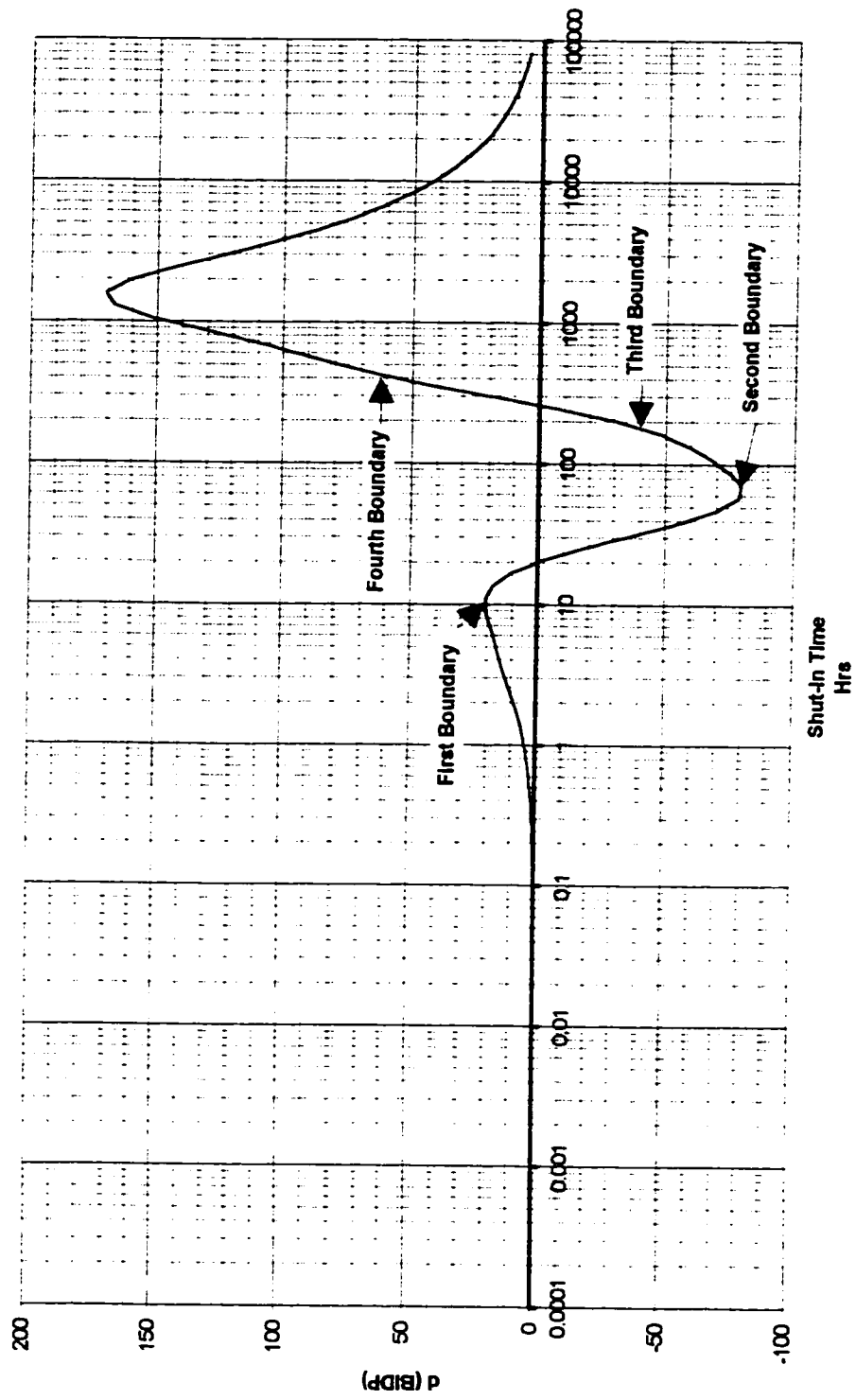


**Figure 4.9.2  $d(BIDP)$  Curve for Four No-Flow Boundaries**

Substituting the times  $\Delta t$  for each flex point, in Equation 4.2.3.2, distance to the boundary, given in Section 4.2.3, calculate the distance to each of the boundaries. On Figure 4.9.2 the flex points are illustrated.

#### **4.10 Summary of Method of Boundary Determination**

Following traditional procedures, analyze the measured pressure data to determine the parameters of permeability, wellbore storage, and skin. Using these calculated parameters, generate the buildup data for an identical well in an infinite-acting reservoir.

Subtract the measured buildup data from the infinite-acting data. This gives the BIDP.

Plot the semi-log derivative of BIDP versus log of shut-in time. This gives the  $d(\text{BIDP})$  curve that was described in the previous section. From this curve, boundaries may be identified, and the distance to those boundaries calculated.

Boundaries are identified by points of inflection in the curve. The first boundary is represented by a maximum in the positive  $d(\text{BIDP})$  domain. Additional boundaries are noted by points of inflection along the curve.

It should be noted that the minimum value of the  $d(\text{BIDP})$  curve does not represent a boundary. It is the consequence of the recharging of the reservoir from the infinite source.



#### **4.11 Discussion of Computer Programs**

To generate the synthetic data used in this work a FORTRAN computer program was written for each of the five boundary cases discussed.

The programs follow the equation development as outlined in the previous sections. Rather than compute the BIDP within each FORTRAN program, the programs produce the bottom hole pressures for buildup in each boundary case. The BIDP and its semi- log derivative was then calculated in an additional program.

This technique was used to simulate the actual "field" experience. In practice, one would have downhole pressure data gathered from a test. This data would be compared with an ideal infinite-acting homogeneous reservoir response, and the semi-log derivatives calculated.

To check the accuracy of the finite difference equations, the analytically derived derivative was used to calculate the semi-log derivative of BIDP using the synthetic data. Comparison with the above technique resulted in good agreement with variations of less than  $\pm 0.00001$  in the value of the derivative.

To calculate the exponential integral function, an IBM subroutine was used (Ramey et al. (1977)). Further, it was decided that rather than using a logarithmic approximation for the  $Ei$

function, the Ei function would be calculated for all terms. This decision resulted from early trials where the data became “noisy” around the times where the Ei function began to be represented by the logarithmic approximation. This noise was eliminated when the Ei function was used for all times.

For the formulations that have infinite summations, the summations were programmed to have 10,000 terms. However, there was a summation termination condition applied. That condition was that once each of the arguments of the Ei function was greater than 10, the summation was terminated. The value of the Ei function is zero when the argument is greater than ten. A counter in the DO loop indicated that less than 200 terms were needed to satisfy this Ei termination condition.

A copy of FORTRAN programs is included in the Appendix.

This method was also tested using FAST Well Test™. FAST™ is a computer based pressure transient analysis tool developed by Fekete Associates. FAST™ uses a Green’s function formulation to solve the diffusivity equation. Comparisons of the value of the  $d(BIDP)$  calculated by the two methods showed differences of less than  $\pm 0.0001$  kPa.

The figures used to illustrate the three and four boundary cases in this work were generated using FAST™.

## **5.0 Results and Discussion**

This method of boundary identification, the  $d(\text{BIDP})$  method, gives directly an indication of the reservoir-well model. It allows for the direct observation of the number of boundaries, and direct calculation of the distance to those boundaries.

This section provides a discussion of the application of the  $d(\text{BIDP})$  method to boundary detection and reservoir classification. A discussion of the effect of each of the variables in the defining equation is given. Also discussed is the application of the  $d(\text{BIDP})$  method to noisy data.

## 5.1 Semi-Infinite Reservoir d(BIDP) Curves

Figure 5.1.1 shows the d(BIDP) curve for a reservoir with a single boundary. It can be observed on that plot that the value of the d(BIDP) asymptotically approaches zero from the negative region. This suggests that the difference in pressure between the infinite case and the semi-bounded case is continually decreasing until it asymptotically approaches a constant value. In fact, the constant value is zero at infinite time.

Consider the definition of the semi-log derivative of BIDP:

$$\frac{d(\text{BIDP})}{d(\log(\Delta t))} = \Delta t \left( \frac{d(\text{BIDP})}{d(\Delta t)} \right) = \Delta t \left( \lim_{\Delta(\Delta t) \rightarrow 0} \frac{\Delta \text{BIDP}}{\Delta(\Delta t)} \right)$$

It is known that  $\Delta t$  is positive as its range is zero to infinity. Also,  $\Delta(\Delta t)$  is a positive quantity. This means that the value of  $\Delta \text{BIDP}$  is a negative quantity. For the value of  $\Delta \text{BIDP}$  to be a negative the value of BIDP decreases as shut-in time increases.

$$\text{BIDP}_2 - \text{BIDP}_1 < 0$$

$$\text{BIDP}_2 < \text{BIDP}_1$$

$$(p_{\text{ws}\infty})_2 - (p_{\text{wsb}})_2 < (p_{\text{ws}\infty})_1 - (p_{\text{wsb}})_1$$

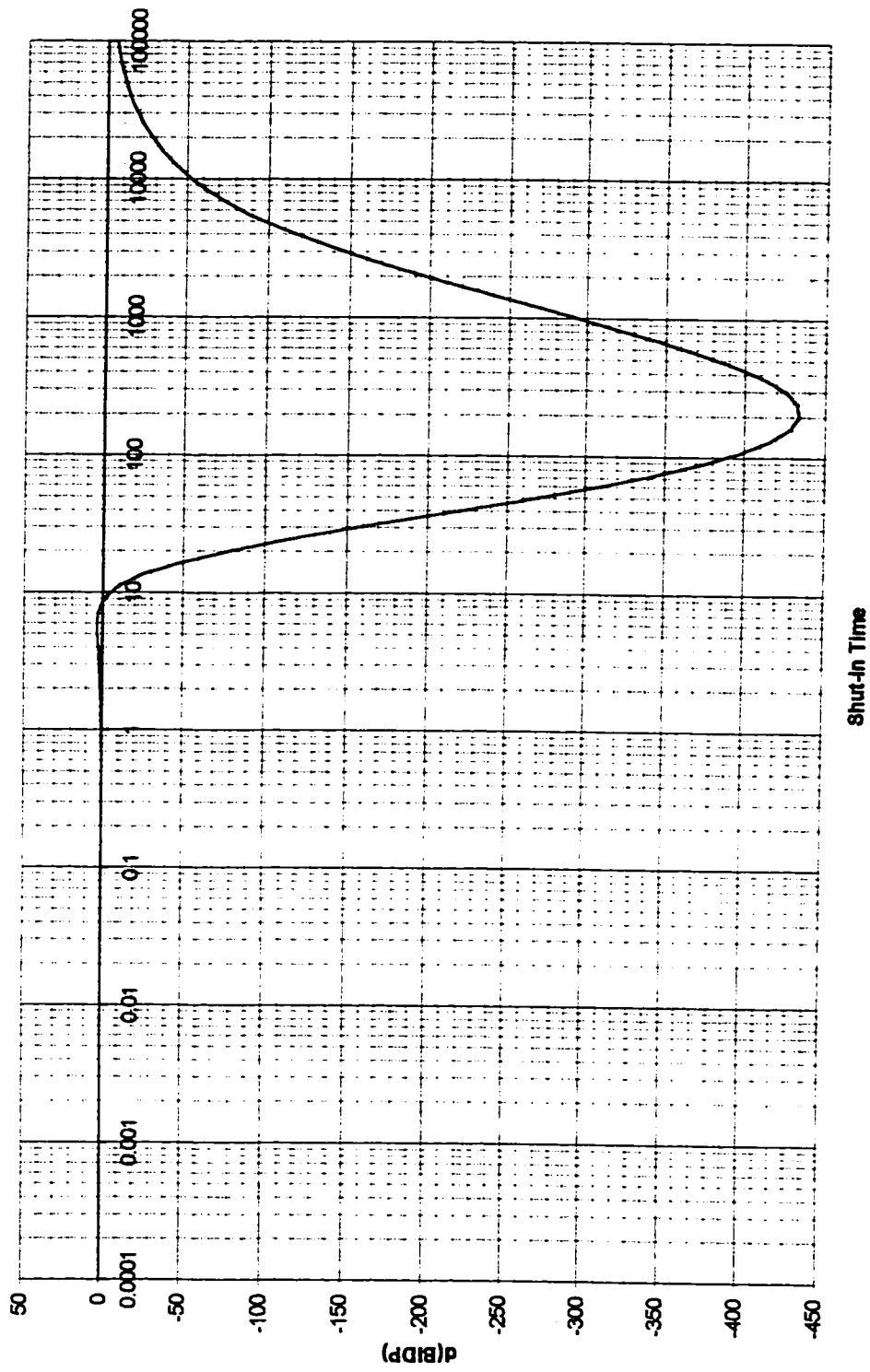


**Figure 5.1.1.1 Single Boundary Reservoir**

In fact if the buildup data in both cases were allowed to reach infinite time, the value of the BIDP would be zero. It has been shown that in a semi-infinite reservoir, if the well is allowed an infinite amount of shut-in time, the measured wellbore pressure will return to  $p_i$ . Hence, the value of the BIDP will be zero, and the semi-log derivative of the BIDP will be zero also.

The early time data also indicate a value of zero for the semi-log derivative of the BIDP. This is due to the early time phenomena where the pressure difference between the infinite case and the semi-infinite case is constant; that is, the plots of bottom hole pressure in the two cases are parallel.

The asymptotic approach to zero of the value of the  $d(\text{BIDP})$  from the negative region is a characteristic of these plots unique to semi-infinite reservoirs. For all cases tested where the reservoir was semi-infinite (that is, the reservoir is infinite in at least one direction) the semi-log derivative of the BIDP approached zero asymptotically from the negative direction.

## 5.2 Finite Reservoir d(BIDP) Curves

Figure 5.2.1 shows a d(BIDP) curve for a finite reservoir. A finite reservoir is one that is completely bounded. It can be observed on that plot that the value of d(BIDP) asymptotically approaches zero from the positive region. This suggests that the difference in pressure between the infinite case and the finite case after the pressure transient has reached all four boundaries is continuously decreasing with increasing shut-in time. At an infinite shut-in time the difference will be a constant value greater than zero.

Again consider the definition of the semi-log derivative of the BIDP:

$$\frac{d(\text{BIDP})}{d(\log(\Delta t))} = \Delta t \left( \frac{d(\text{BIDP})}{d(\Delta t)} \right) = \Delta t \left( \lim_{\Delta(\Delta t) \rightarrow 0} \frac{\Delta \text{BIDP}}{\Delta(\Delta t)} \right)$$

It is known that  $\Delta t$  is a positive quantity. Also,  $\Delta(\Delta t)$  is a positive quantity. For the semi-log derivative of the BIDP to be positive then the value of  $\Delta \text{BIDP}$  must also be positive.

$$\text{BIDP}_2 - \text{BIDP}_1 > 0$$

$$\text{BIDP}_2 > \text{BIDP}_1$$

$$(p_{ws\infty})_2 - (p_{wsb})_2 > (p_{ws\infty})_1 - (p_{wsb})_1$$

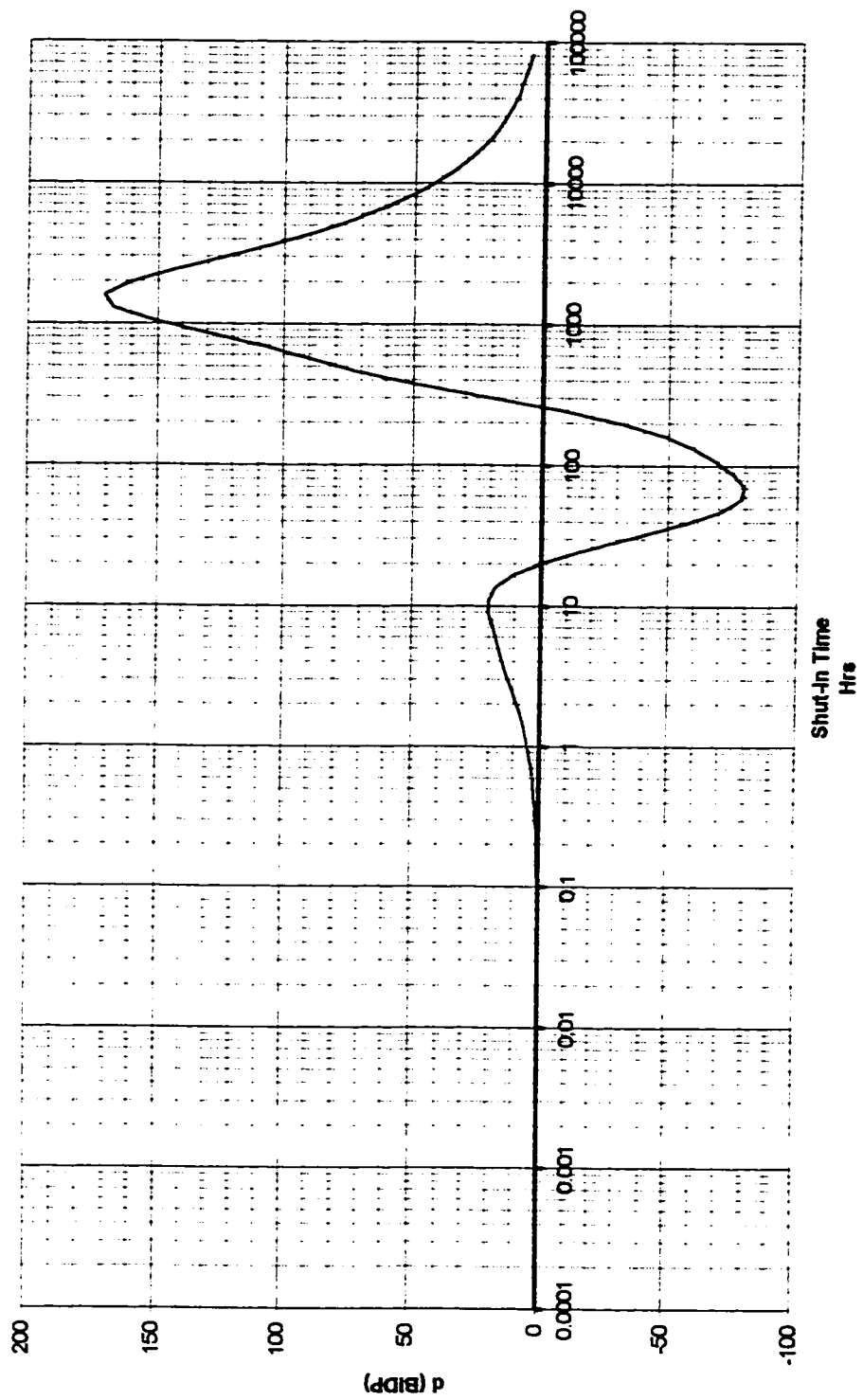


**Figure 5.2.1 Finite Reservoir**



Once the four boundaries have been impacted by the pressure transient, the difference in pressure between the infinite case and the bounded case asymptotically approaches a constant value greater than zero as  $\Delta t$  approaches infinity.

This asymptotic difference illustrates pressure depletion in a finite reservoir. A finite reservoir once produced will never return to the value of  $p_i$ . Instead, at infinite shut-in time it will reach a constant value of pressure that will be less than  $p_i$ . This pressure difference is indicative of depletion of the reservoir and hence a finite reservoir.

Similar to the semi-infinite reservoir case, the early time data has a semi-log derivative of the BIDP of zero. This is due to the difference in pressure between the infinite case and the bounded case being constant. Again, this is the time region where the pressure signal acts as if the reservoir is infinite. No boundaries are yet seen by the shut-in pressure signal.

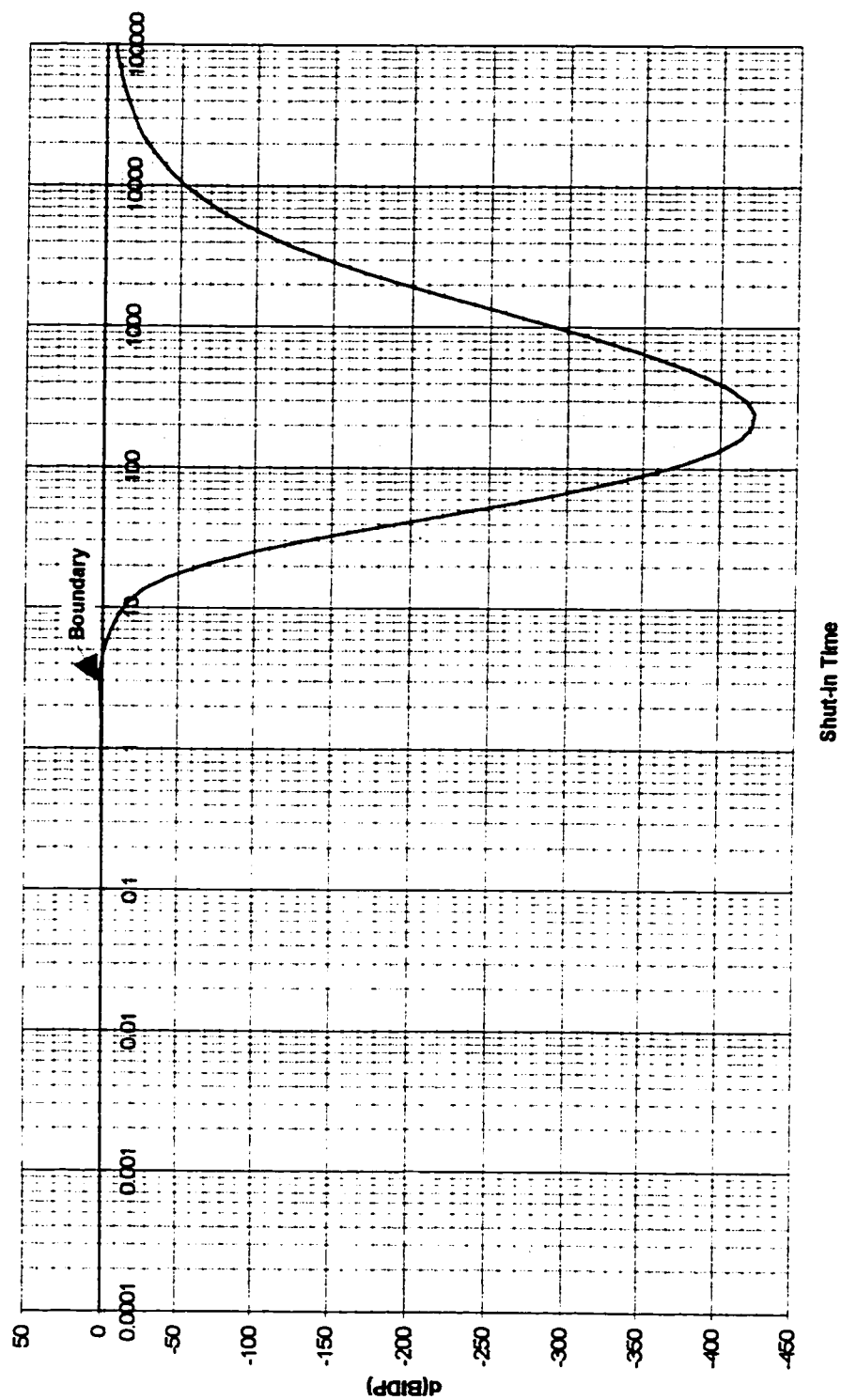
### **5.3 Effects of Wellbore Storage and Skin**

This method was developed initially without including the effects of wellbore storage and skin. When included, it was found that wellbore storage and skin effects had no influence on the results of this method. The effect of both phenomena cancelled out in the calculation of the BIDP and the method of boundary detection was unaffected by these phenomena.

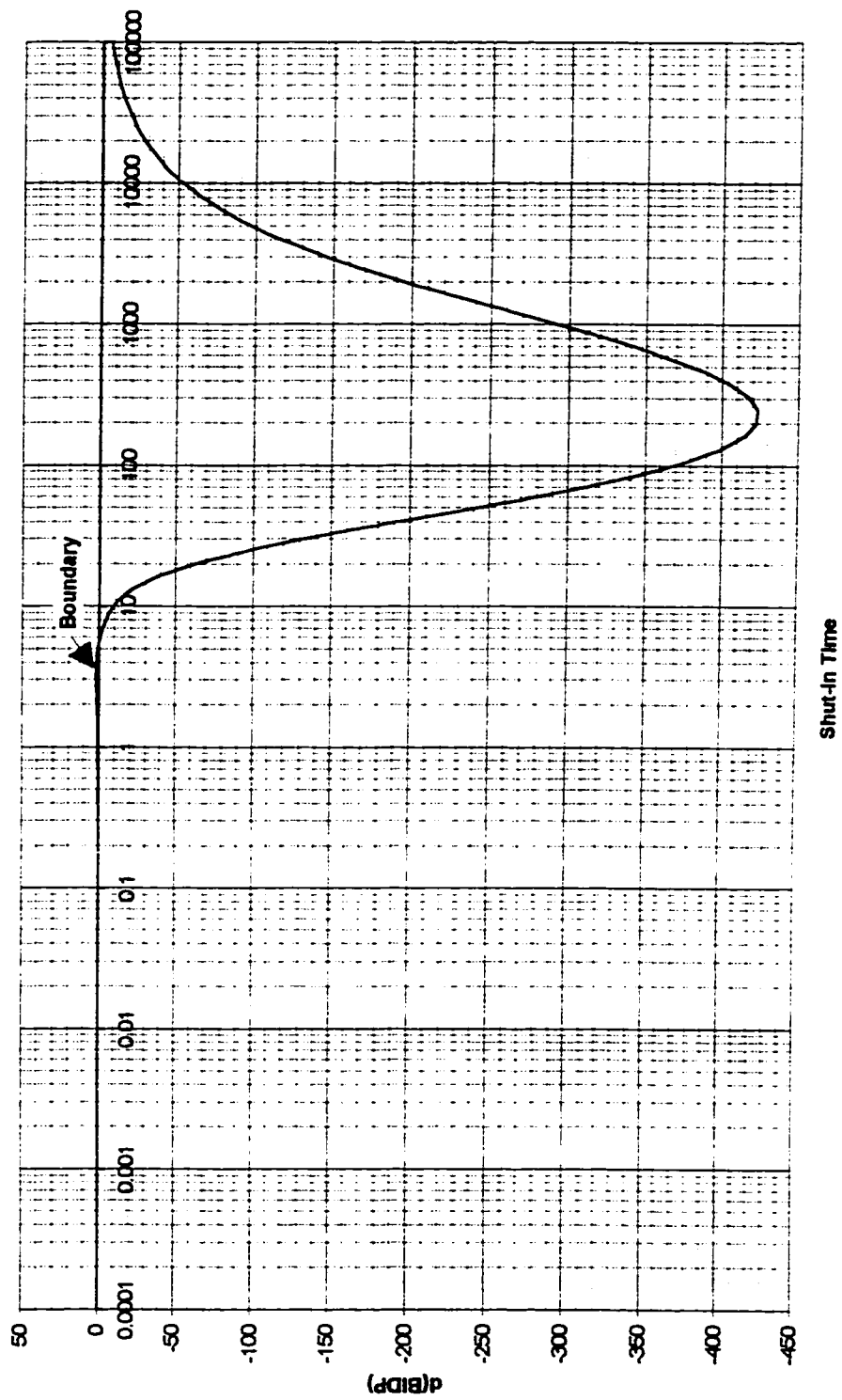
There is a decided advantage in this new method in that early time data can now be used for boundary detection. Boundaries that were previously masked in the wellbore storage portion of the data can now be detected.

Figure 5.3.1 shows a plot of semi-log derivative of BIDP that indicates a boundary at early time. Figure 5.3.2 shows the same system with dimensionless wellbore storage of 100 and skin of 3. The boundary is very much apparent. In traditional analysis, this boundary would be masked in the wellbore storage region of the data.

One advantage of using buildup data for analysis is that skin does not enter the equations. This is illustrated using the model for a single boundary. The general expression for the solution of the radial diffusivity equation for buildup for an infinite system which includes skin is:



**Figure 5.3.1 Single Boundary Reservoir without Wellbore Storage or Skin**



**Figure 5.3.2 Single Boundary Reservoir with Wellbore Storage and Skin**

$$p_i - p_{wso} = \frac{qB\mu}{4\pi kh} \left[ -Ei\left(-\frac{\phi\mu c_t r_w^2}{4k(t_p + \Delta t)}\right) - 2s + Ei\left(-\frac{\phi\mu c_t r_w^2}{4k\Delta t}\right) + 2s \right] \dots\dots 5.3.1$$

For a well in a reservoir with a single boundary and skin the solution is:

$$p_i - p_{wsb} = \frac{qB\mu}{4\pi kh} \left[ -Ei\left(-\frac{\phi\mu c_t r_w^2}{4k(t_p + \Delta t)}\right) - 2s + Ei\left(-\frac{\phi\mu c_t r_w^2}{4k(\Delta t)}\right) + 2s \right. \\ \left. - Ei\left(-\frac{\phi\mu c_t (2d)^2}{4k(t_p + \Delta t)}\right) + Ei\left(-\frac{\phi\mu c_t (2d)^2}{4k(\Delta t)}\right) \right] \dots\dots 5.3.2$$

In both equations the skin effect cancels itself out. Similarly, skin does not affect the calculation of the BIDP. The expression for the BIDP remains:

$$BIDP = p_{wso} - p_{wsb} = \frac{qB\mu}{4\pi kh} \left[ -Ei\left(-\frac{\phi\mu c_t (2d)^2}{4k(t_p + \Delta t)}\right) + Ei\left(-\frac{\phi\mu c_t (2d)^2}{4k(\Delta t)}\right) \right] \dots\dots 5.3.3$$

Wellbore storage is a term that describes “wellbore unloading” in a flowing well, and “after production” in a shut-in well. This phenomenon can last for a significant period of time depending on the flow characteristics of the reservoir.

Wellbore storage is usually described as a dimensionless constant for a given reservoir and flow conditions. It relates the properties of the reservoir fluid(s) and the volume of the wellbore. As a constant in the equation it, too, drops out in the calculation of the BIDP.

Instead of being an additional pressure drop, as is skin, wellbore storage is a boundary condition of the radial diffusivity equation. It has the effect of masking the commencement of radial flow.

## 5.4 Effect of Changing Permeability $k$

Changing the permeability affects both the shape of the semi-log derivative of the BIDP versus  $\log \Delta t$  curve, and where the flex points occur with respect to time. Figures 5.4.1 through 5.4.4 show values of permeability increasing by orders of magnitude, starting at  $k=1$ . The reservoir model used in these figures is for a single no-flow boundary.

It can be seen that the smaller the value of permeability, the longer the shut-in time that is required to see the signature of the boundary. This follows directly from the theory of pressure moving through the reservoir.

Consider the equation for the distance to the no-flow boundary:  $d = \sqrt{\frac{4k(\Delta t)}{\gamma\phi\mu c_t}}$ . Assuming that the distance to the boundary in all examples is constant, and that  $\phi$ ,  $\mu$ , and  $c_t$  are constant, then it can be seen that  $k$  and  $\Delta t$  vary inversely. As  $k$  increases  $\Delta t$  decreases. This is graphically illustrated in Figures 5.4.1 through 5.4.4.

The magnitude of the peak of the semi-log BIDP decreases as the value of permeability increases. The peak is a qualitative measure of the depletion the well experiences. In reservoirs with large values of permeability the rate of recharge is much higher,

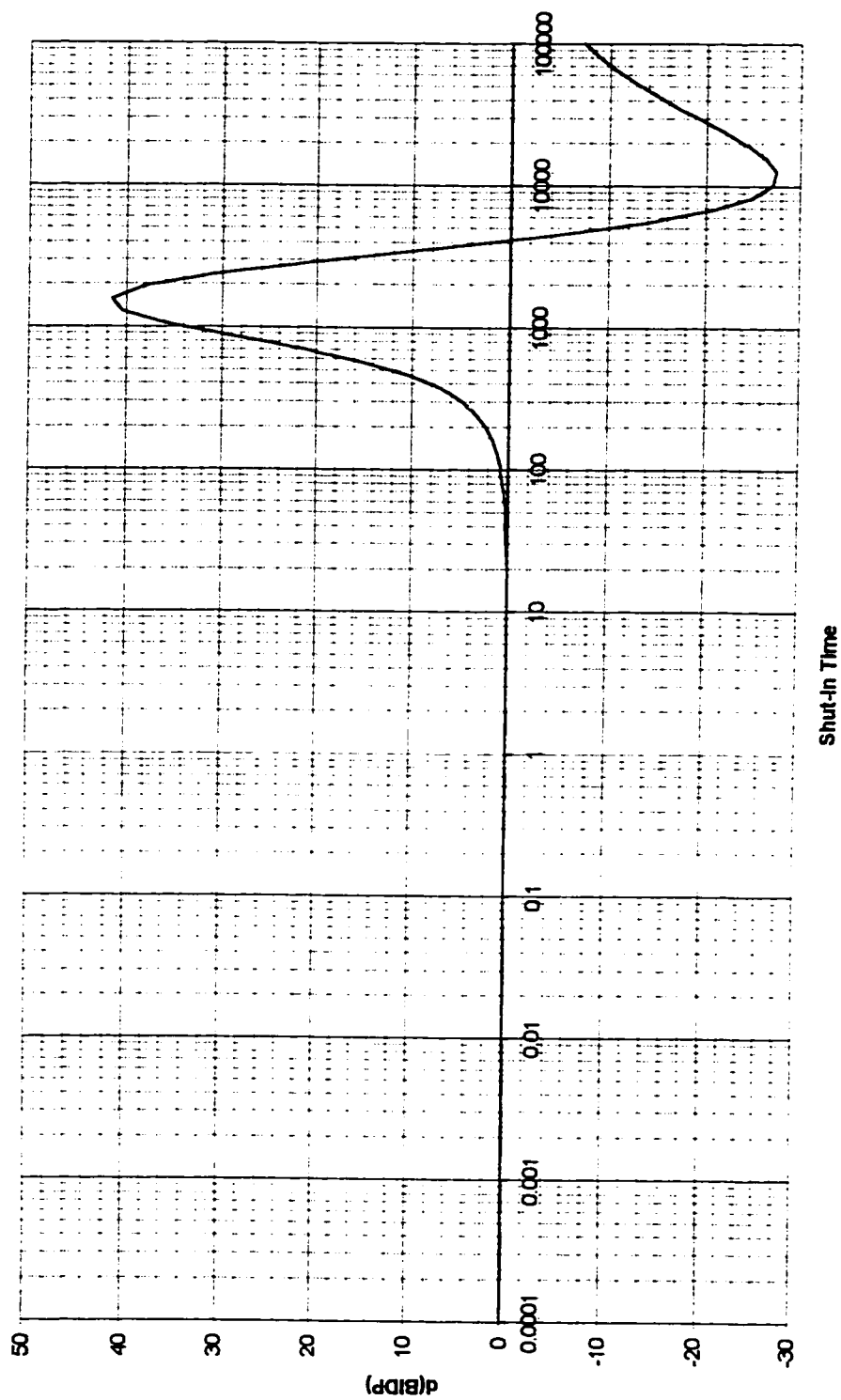


**Figure 5.4.1 Single Boundary Reservoir with Permeability of 1 md**



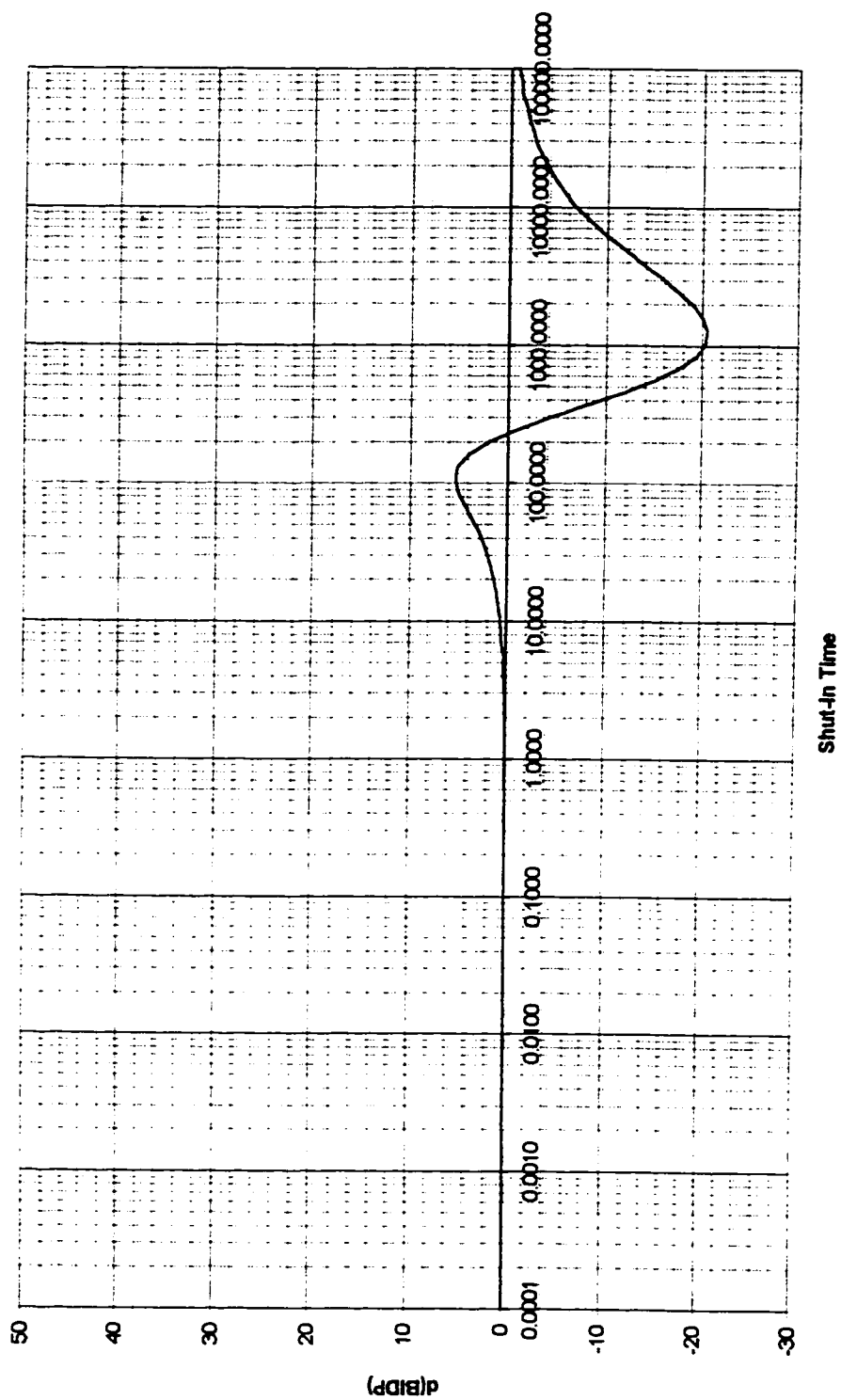


**Figure 5.4.2 Single Boundary Reservoir with Permeability of 10md**

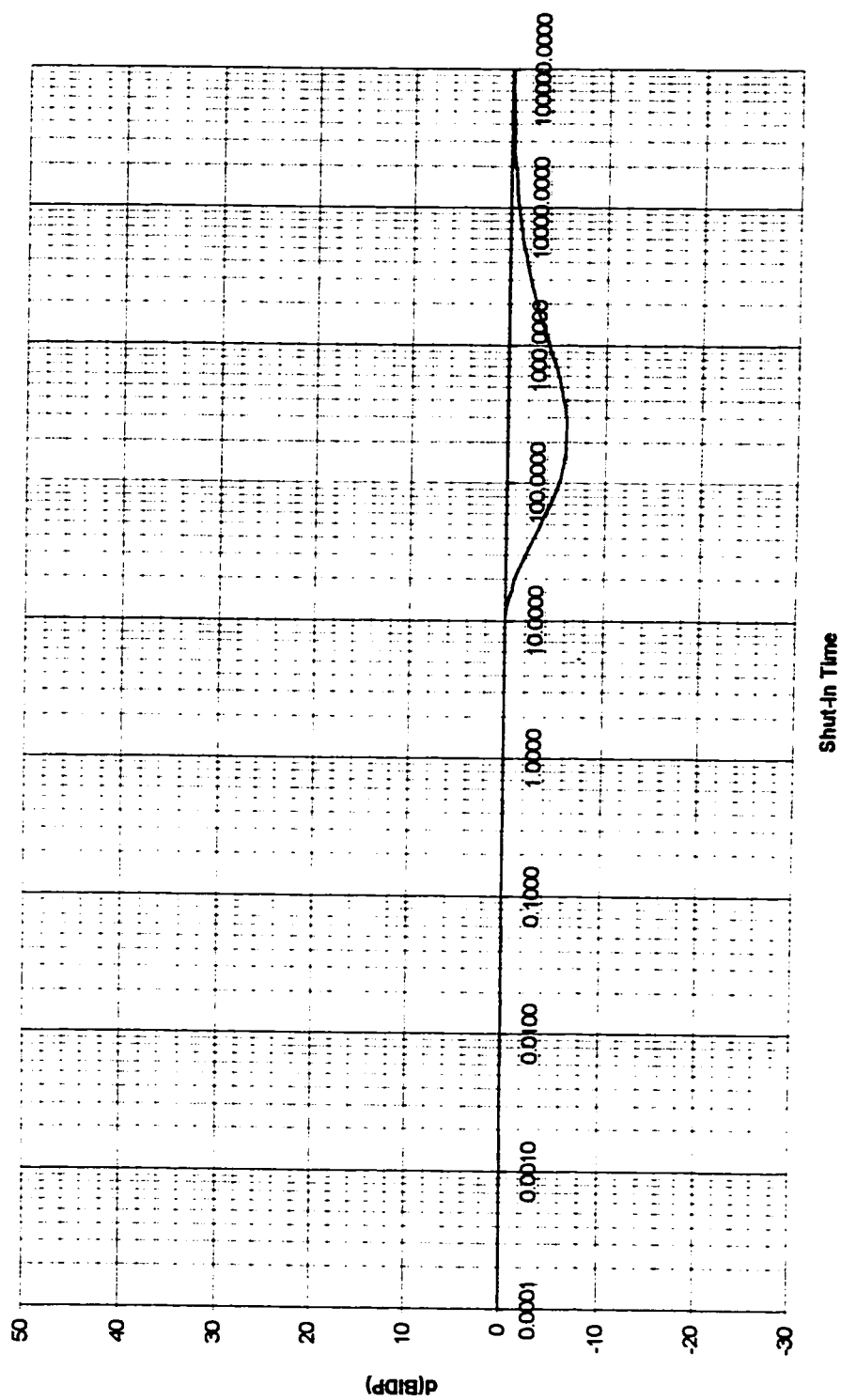


**Figure 5.4.3 Single Boundary Reservoir with Permeability of 100md**

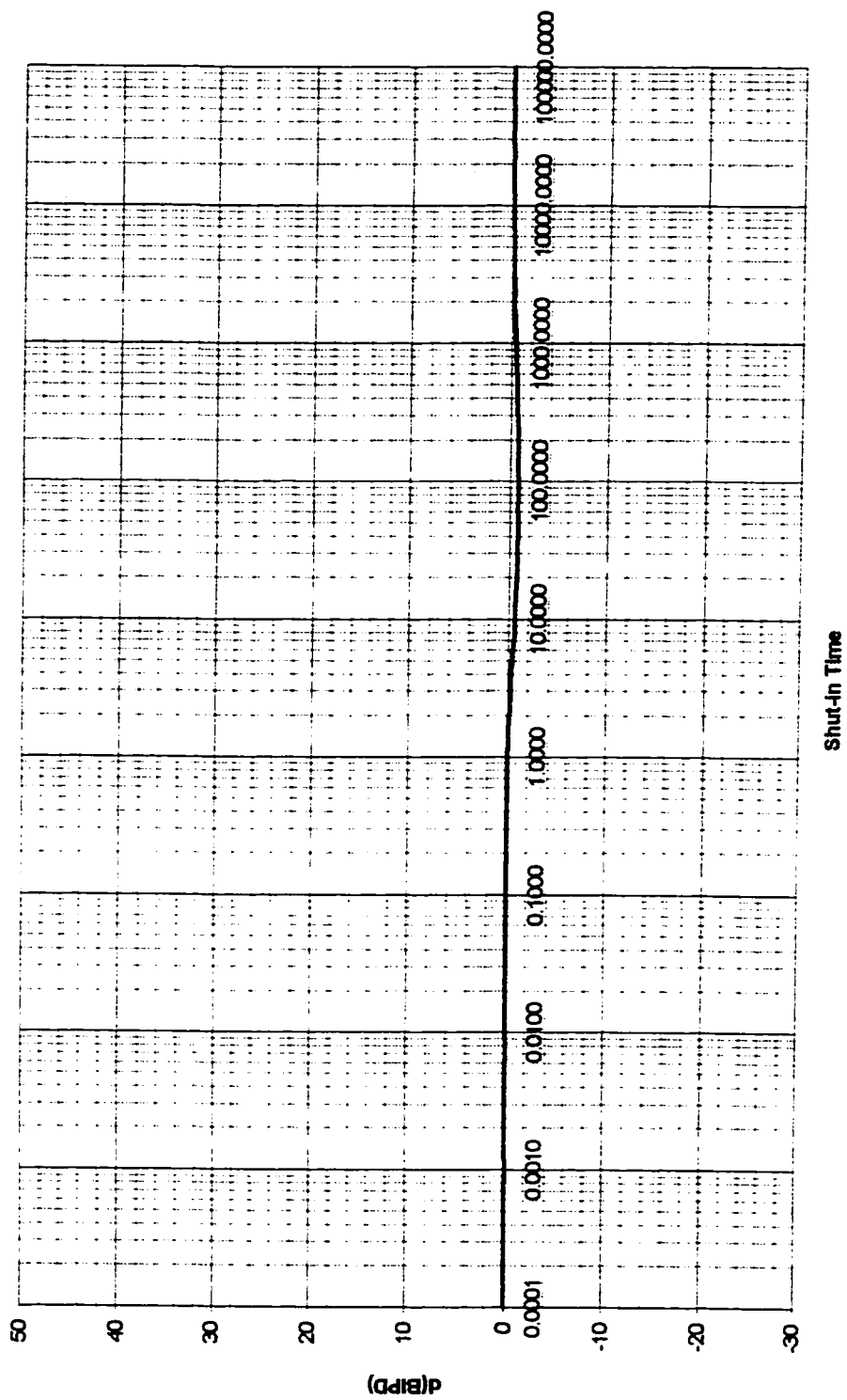


**Figure 5.4.4 Single Boundary Reservoir with Permeability of 1000md**

and thus the amount of depletion a well experiences is less, compared to a reservoir system of lower permeability.

Figures 5.4.1 through 5.4.4 further illustrate a qualitative relationship between permeability and the effect of a boundary in a semi-infinite reservoir. As permeability increases the response of a reservoir to the depletion between a well and a boundary is much faster, and the pressure drop in the area of the reservoir between the well and the boundary is much less. That is, the reservoir is capable of recharging itself very quickly.

McKinley and Streltsova (1988) indicated on Horner plots that before the plot turned up indicating a no-flow boundary, the curve actually turned down slightly. McKinley and Streltsova theorized that this was due to a recharging of the fluid in the area of the reservoir between the well and the no-flow boundary. Interestingly, this effect was more evident in lower permeability reservoirs.

## **5.5 Effect of Changing Flow Rate $q$**

In the equation defining the BIDP, the flow rate,  $q$ , is a multiplier to the terms containing the exponential integral function. As might be expected, the flow rate affects the magnitude of the value of the semi-log derivative of the BIDP.

There is a direct proportionality between different rates. If one flow rate is twice another, the magnitude of the maximum value of semi-log derivative of the BIDP will be twice that of the lower flow rate.

The shut-in time,  $\Delta t$ , at which the maximum value of the semi-log derivative of the BIDP curve occurs is independent of flow rate,  $q$ . That is, the flow rate does not affect the time it takes the pressure transient to reach the boundary. This is expected. Equation 4.2.3.2 describes the relationship between distance a pressure transient travels and shut-in time. Flow rate,  $q$ , is not a variable in this equation.

These points are illustrated in Figures 5.5.1 and 5.5.2. The flow rate used to generate Figure 5.5.2 is 2.5 times larger than the flow rate used to generate Figure 5.5.1.

Utilization of these concepts is useful in interpreting raw data. It can also be used to fine tune the reservoir model to a more precise answer.

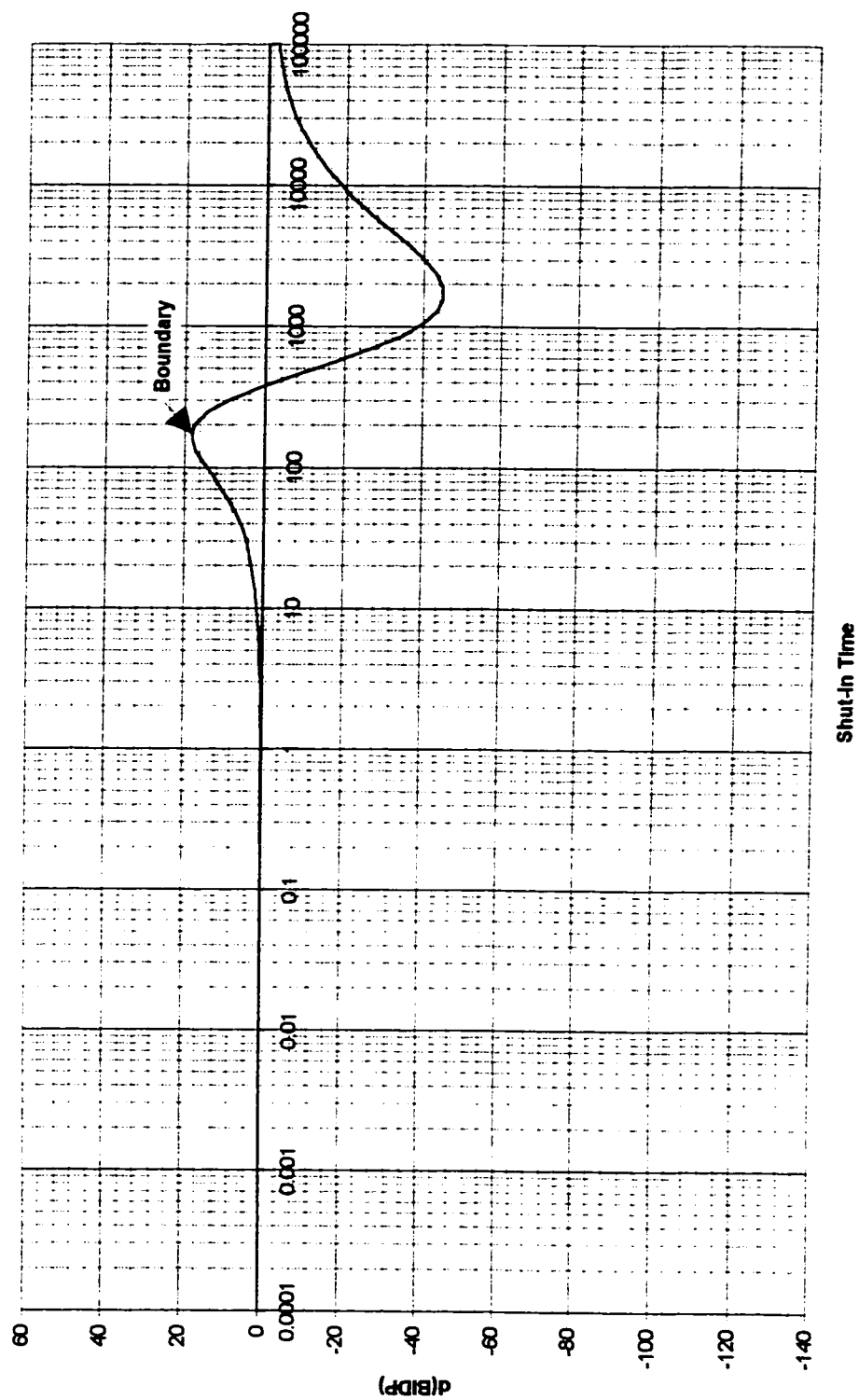


**Figure 5.5.1 Single Boundary Reservoir - Flow Rate of 10m<sup>3</sup>/d**

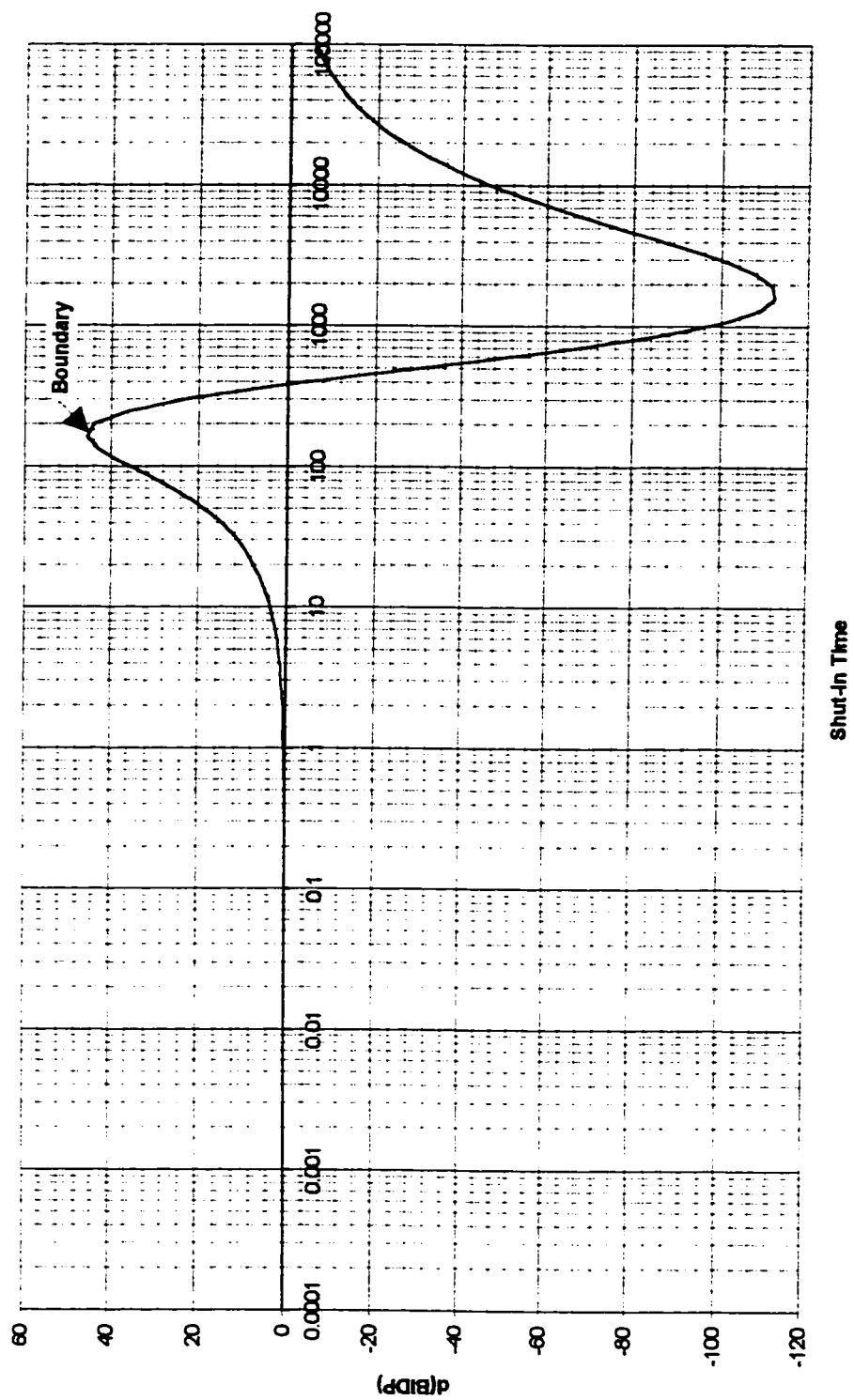


**Figure 5.5.2 Single Boundary Reservoir - Flow Rate of 25m<sup>3</sup>/d**

## **5.6 Multiple Equidistant Boundaries**

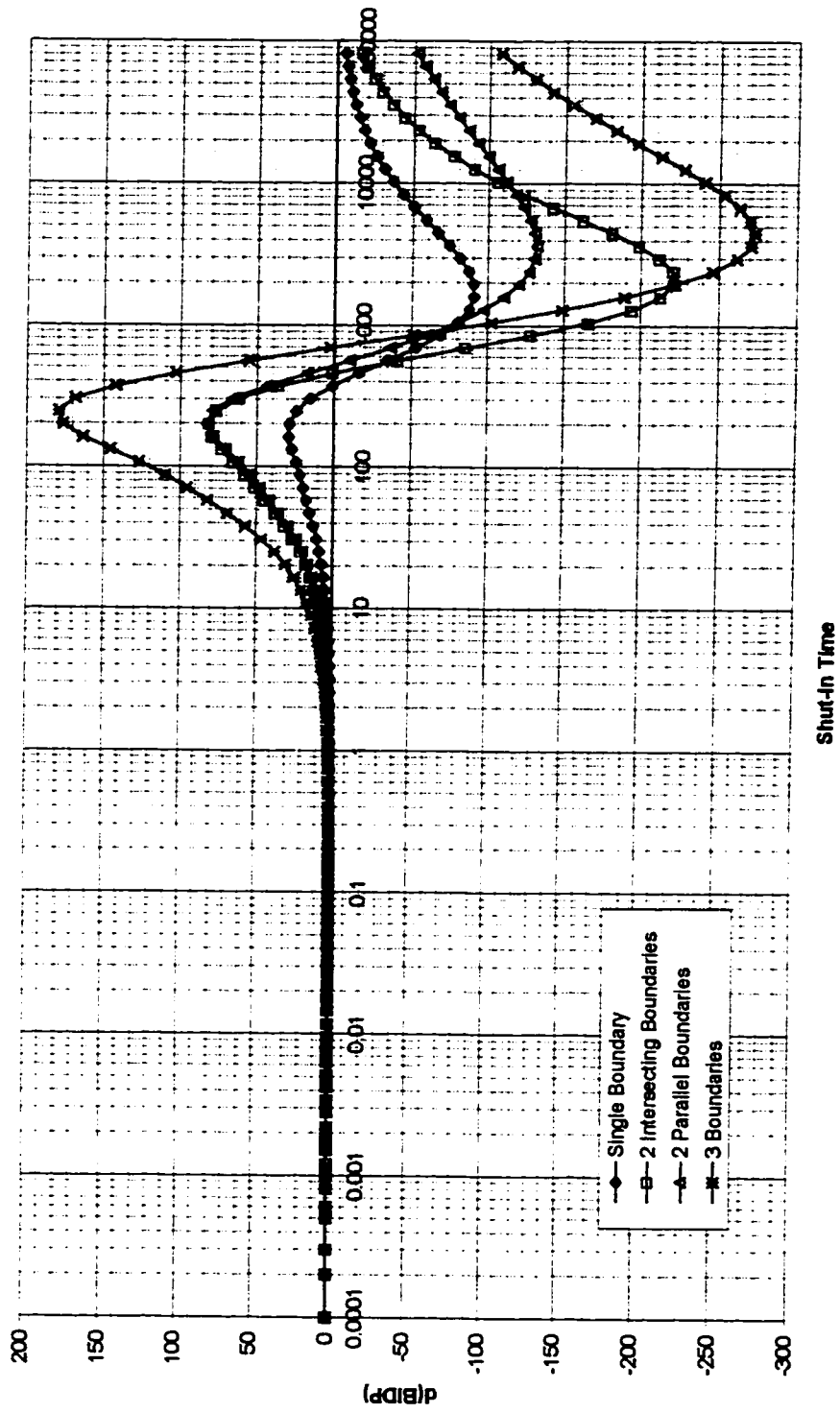
To this point in the discussion, it has been assumed that the well is located in such a way that the distance to each boundary is different. From that it has been possible to identify flex points in the semi-log derivative of the BIDP curve. When multiple boundaries are equidistant from the well, the  $d(\text{BIDP})$  curve has an interesting response.

Figure 5.6.1 illustrates the responses for systems where the boundaries are equidistant from the well. As is shown in the figure, all cases have a response that would indicate a single boundary. The difference in the response is the magnitude of the semi-log derivative of the BIDP.

The magnitude of depletion in the reservoir depends on the number of boundaries in the reservoir. The greater the number of boundaries, the greater the rate of depletion. Hence, the larger the magnitude of the response of the semi-log derivative of the BIDP, the larger the number of boundaries.

Unfortunately, there is no unique correlation between the values of the magnitudes of the semi-log derivative of the BIDP that would allow for easy determination of the number of boundaries. That is, the value of the semi-log derivative of the BIDP for three boundaries is not five or seven or eleven times the magnitude of





**Figure 5.6.1 Multiple Equidistant Boundaries**

the value of the semi-log derivative of BIDP for a single boundary. To determine the number of boundaries, generate synthetic data for a single boundary case using the boundary distance indicated, and compare to the raw data. De-superposition may also be used in determining the number of boundaries.

De-superposition in this context means exactly the opposite of superposition. Instead of adding the responses of wells to determine the effect on the pressure at a given point, the responses are subtracted. The Method of Images is used and superposition is applied in reverse.

## 5.7 Effect of Producing Time $t_p$

In traditional analysis using the conventional frame of reference, there is a wide range of opinion as to how long a well must be flowed to have an observable response to a no-flow boundary. Lee(1982) suggests that the time required should be the time that would be required for the pressure signal to travel twice the distance to the boundary. Earlougher (1980) suggests that the time necessary is the time required for the pressure signal to travel four times the distance to the boundary. Others have suggested as much as sixteen times the distance to the boundary as the minimum time required to observe a boundary response.

There is another school of thought put forward by Mattar (1996) and others which suggests, based on the Principle of Conservation of Mass, that in theory, if only one molecule of hydrocarbon is removed from the reservoir, everything about that reservoir can be determined.

Figure 5.7.1 illustrates the effect of changing the producing time,  $t_p$ , for a given reservoir configuration. The reservoir configuration is a single boundary 25 meters from the producing well. The flex point should occur at 9.8 hours. The  $d(BIDP)$  curve in Figure 5.7.1 illustrates that for all producing times noted only a single boundary is indicated.

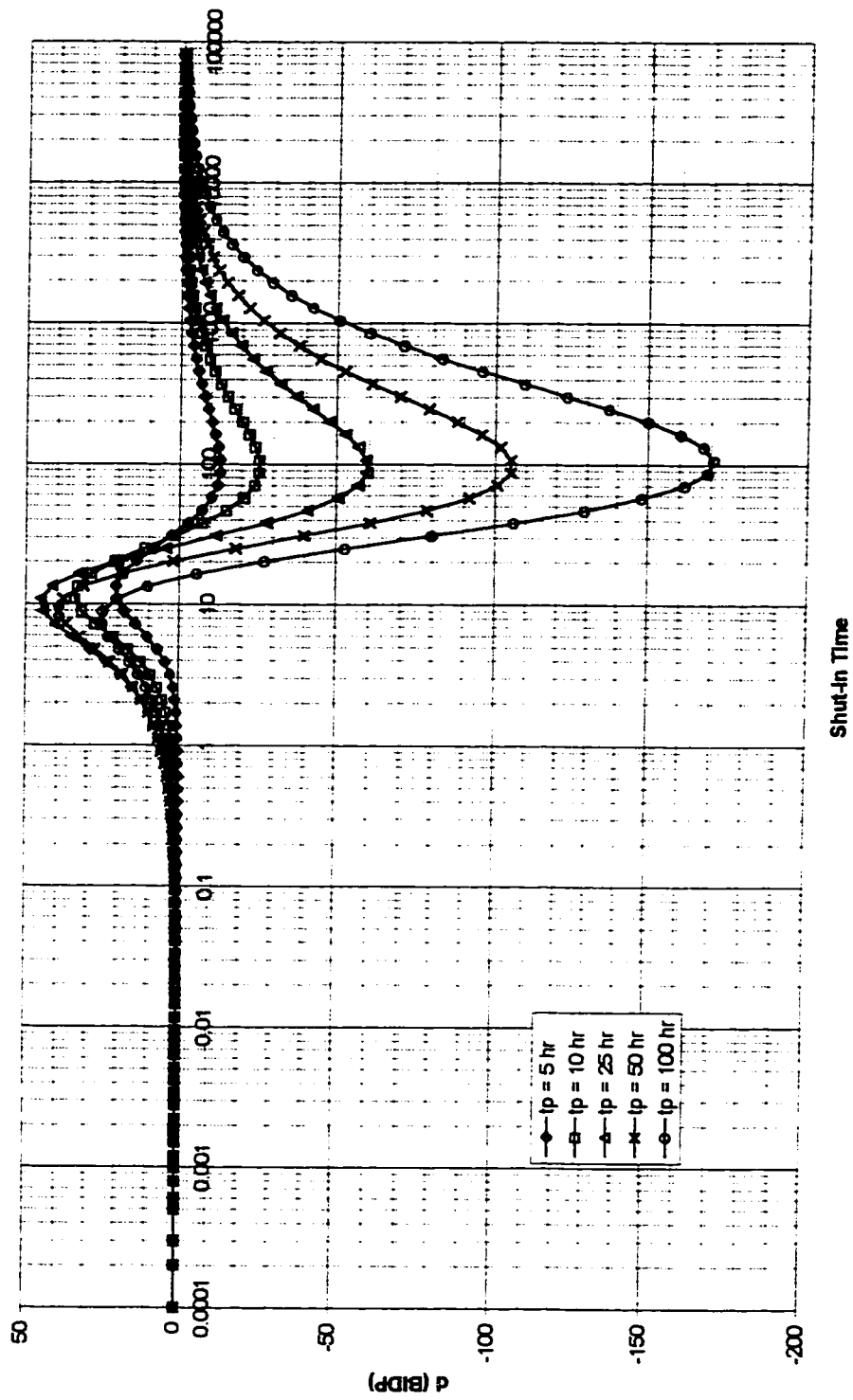


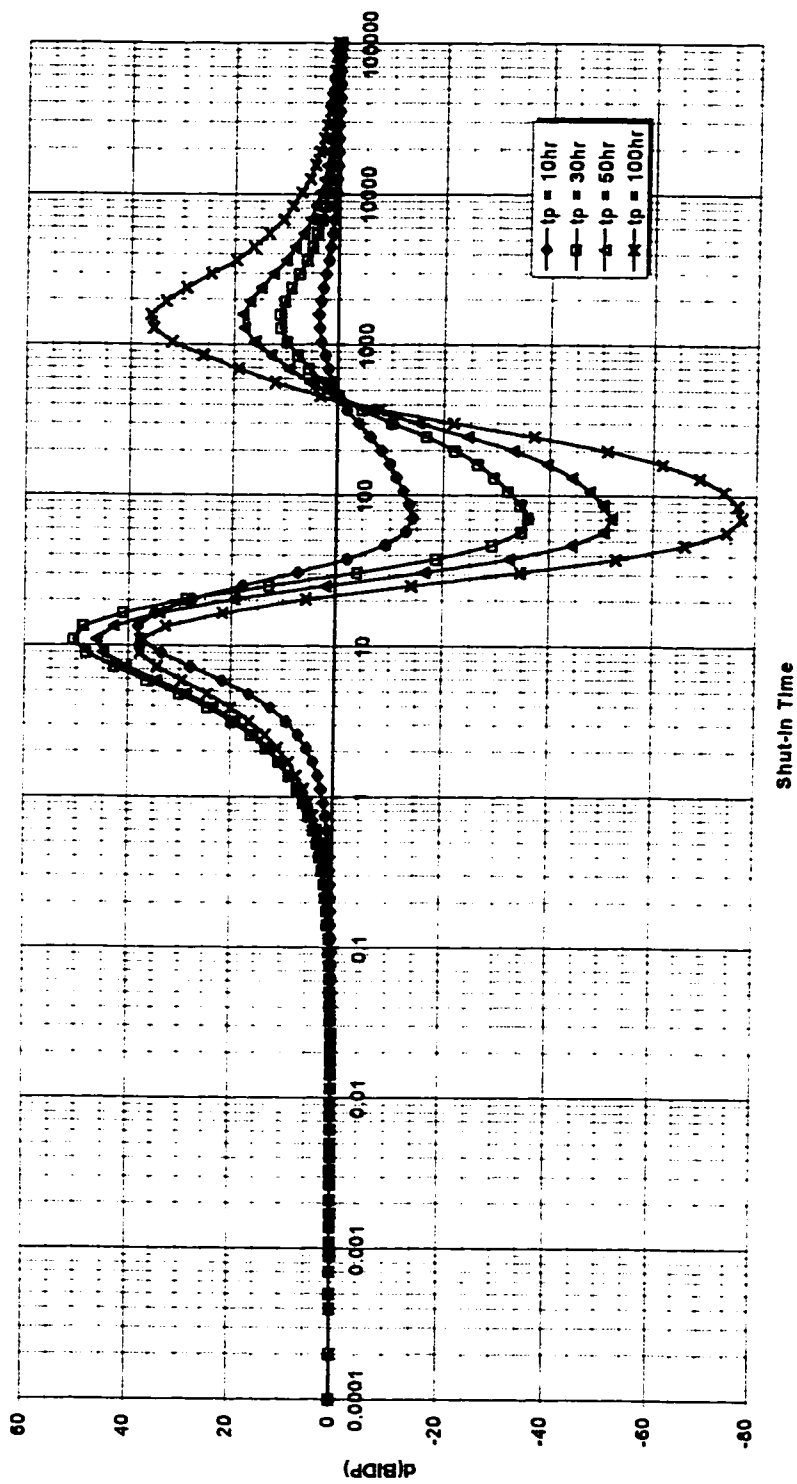
**Figure 5.7.1 Effect of Producing Time  $t_p$  - Single Boundary Reservoir**

For producing times of 5 hours and 10 hours, the boundary is indicated at a time of approximately 10.5 hours, slightly more than the actual time of 9.8 hours. For producing times of greater than 10 hours, the boundary is correctly predicted.

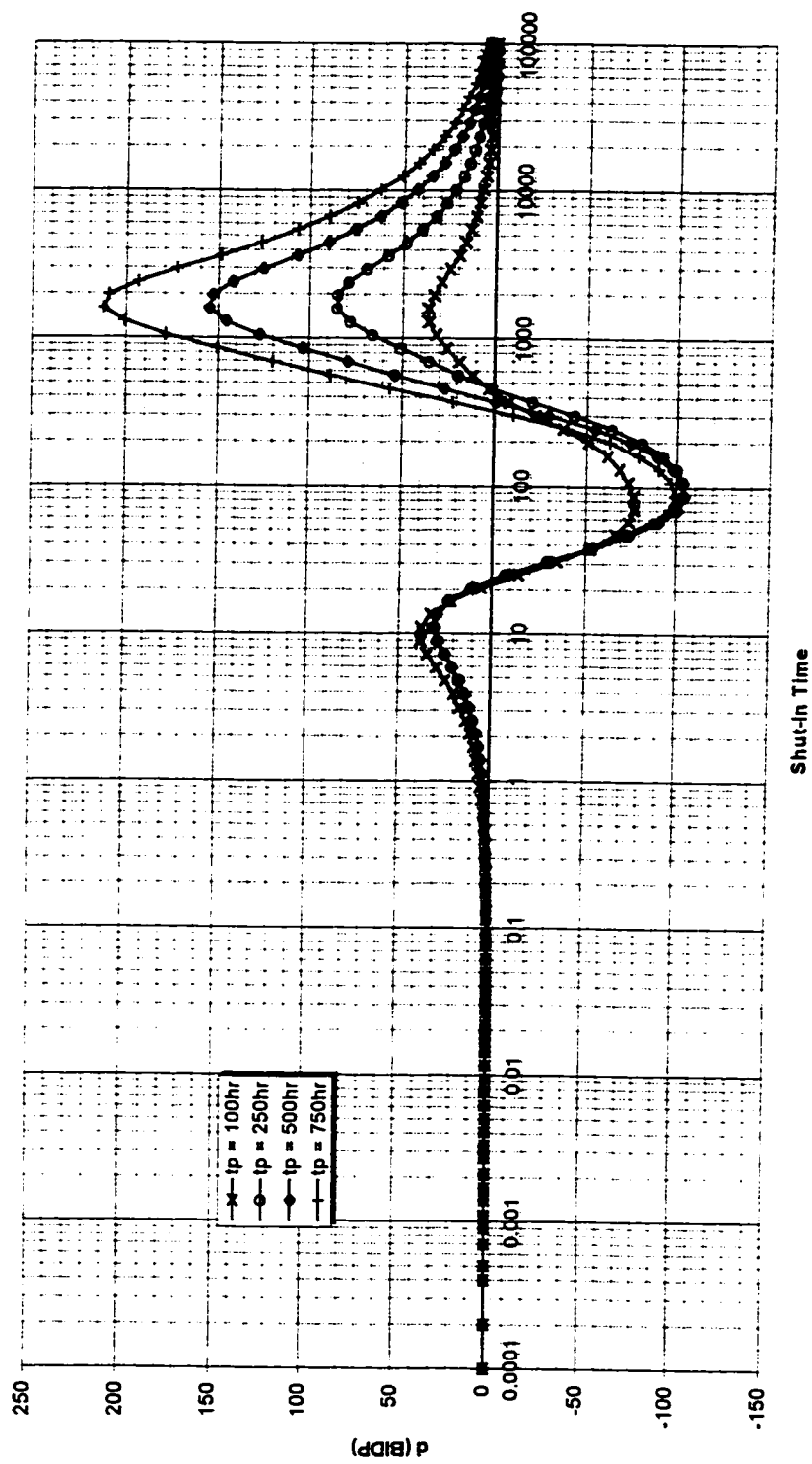
Figures 5.7.2 and 5.7.3 illustrate a finite system of four intersecting boundaries. First consider Figure 5.7.2. The boundaries occur at  $\Delta t = 10\text{hr}$ ,  $65\text{hr}$ ,  $150\text{hr}$ , and  $350\text{hr}$ . Following the method outlined in this document, even the short producing time of ten hours correctly predicts four boundaries.

Figure 5.7.3 is the identical system to that in the previous figure. It shows a wider range of producing times, and illustrates that the curves smooth with increasing producing time, and the maximum and minimum values of the semi-log derivative of BIDP change. However, the information gained does not increase with increasing production time.

The foregoing suggests that, when using the response of a well in an infinite system as the reference, *in theory* any small amount of production will yield all the information about a given reservoir. In practice, however, the well must be flowed sufficiently to be able to determine wellbore storage and skin effects and to determine the permeability. Given this consideration, it follows that the total time a well must be produced to determine the configuration of boundaries is significantly less than is currently the practice.



**Figure 5.7.2 Effect of Producing Time  $t_p$  - Four Boundary Case - Part 1**



**Figure 5.7.3 Effect of Producing Time  $t_p$  - Four Boundary Case - Part 2**

## 5.8 Effect of Shut-In Time $\Delta t$

When considering data in the current frames of reference,  $p_i$  for drawdown and  $p_{wfs}$  for buildup, a statement is often made to the effect that: "A short flow time cannot be compensated for by a long shut-in time." [Earlougher (1980)]. Certainly this is correct for those frames of reference.

When using the infinite response as the frame of reference, this is no longer a true statement. Lengthening or shortening  $\Delta t$  simply changes the amount of data one has to consider. A shorter shut-in time merely truncates the data. A longer shut-in time adds data to be considered.

The examples used in this work all have a shut-in time of 100,000 hours. This was used to ensure that all models were conforming to the trends discussed previously. It is highly unlikely in practice that any well would be shut-in for this period of time!

Shutting a well in for only 100, 500, or 1000 hours would truncate the data available. For example, consider Figure 5.7.3, if the well was shut-in for only 100 hours, it would be possible to determine only the presence of two boundaries, and one could not conclude that the reservoir was in fact finite.

If the well was shut-in for 500 hours, all four boundaries would be in evidence, and it would be possible to infer that the



reservoir was finite. The semi-log derivative of the BIDP has crossed the x-axis back to the positive domain. This occurs only when the reservoir is finite.

If the well was shut-in for 1000 hours, all four boundaries would be in evidence, and it can be concluded that the reservoir is finite. In this example, there is no additional information to be gained from the additional 500 hours of shut-in.

The above conclusions concerning the presence of boundaries determined at various shut-in times, are independent of the length of the producing time. This new method of boundary determination assumes that the producing time is of sufficient length to determine wellbore storage, permeability, and skin effects.

## **5.9 Use of the d(BIDP) Method with Noisy Data**

It is widely acknowledged that pressure data collected during well tests are noisy. That is to say, the real data does not necessarily form the smooth curves given by “synthetic” data. Rather, the data can be random and scattered. Figure 5.9.1 represents the d(BIDP) of such data. It is a four boundary case with all boundaries being a different distance from the well. It was generated using FAST™ software using the noise function in the generated data.

Employing the “preferred algorithm” presented by Bourdet et al. (1989) to smooth the derivative curve, gives a d(BIDP) curve which accurately predicts four boundaries. These boundaries are predicted to occur at the correct shut-in times. Figure 5.9.2 shows the data with the curve smoothed using the Bourdet method. The Bourdet method uses one point on either side of the point of interest, calculates the corresponding derivatives and places their weighted mean at the point of interest.

Figure 5.9.3 shows the noisy data, the smoothed d(BIDP) curve from that data, and the d(BIDP) curve of the same reservoir well configuration using pure synthetic data. It is observed that there is effectively no difference in the time, and hence distance, at which boundaries are evident in the smoothed curve as compared to the synthetic curve.

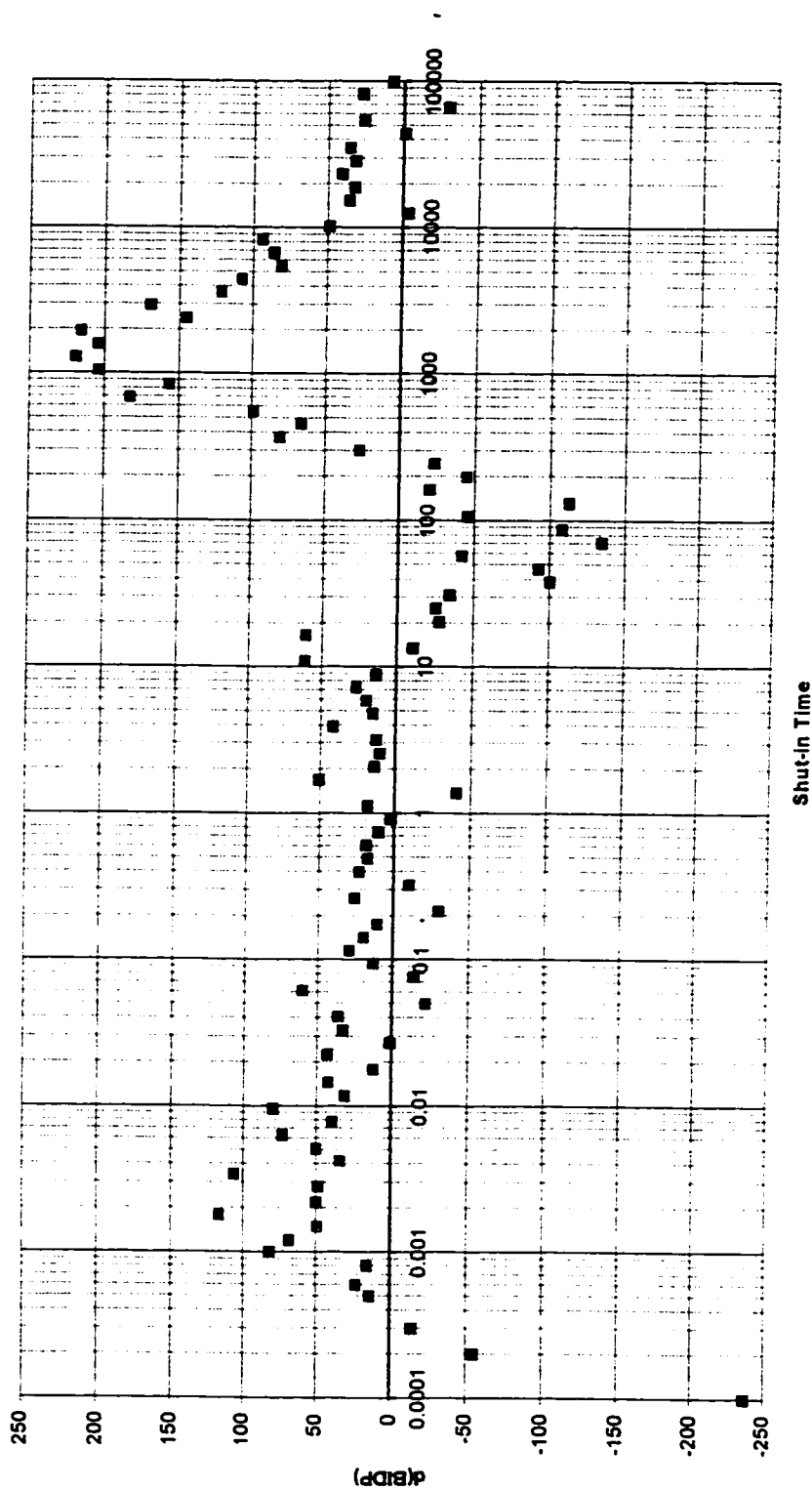


**Figure 5.9.1  $d(BIDP)$  Curve of “Noisy” Data**

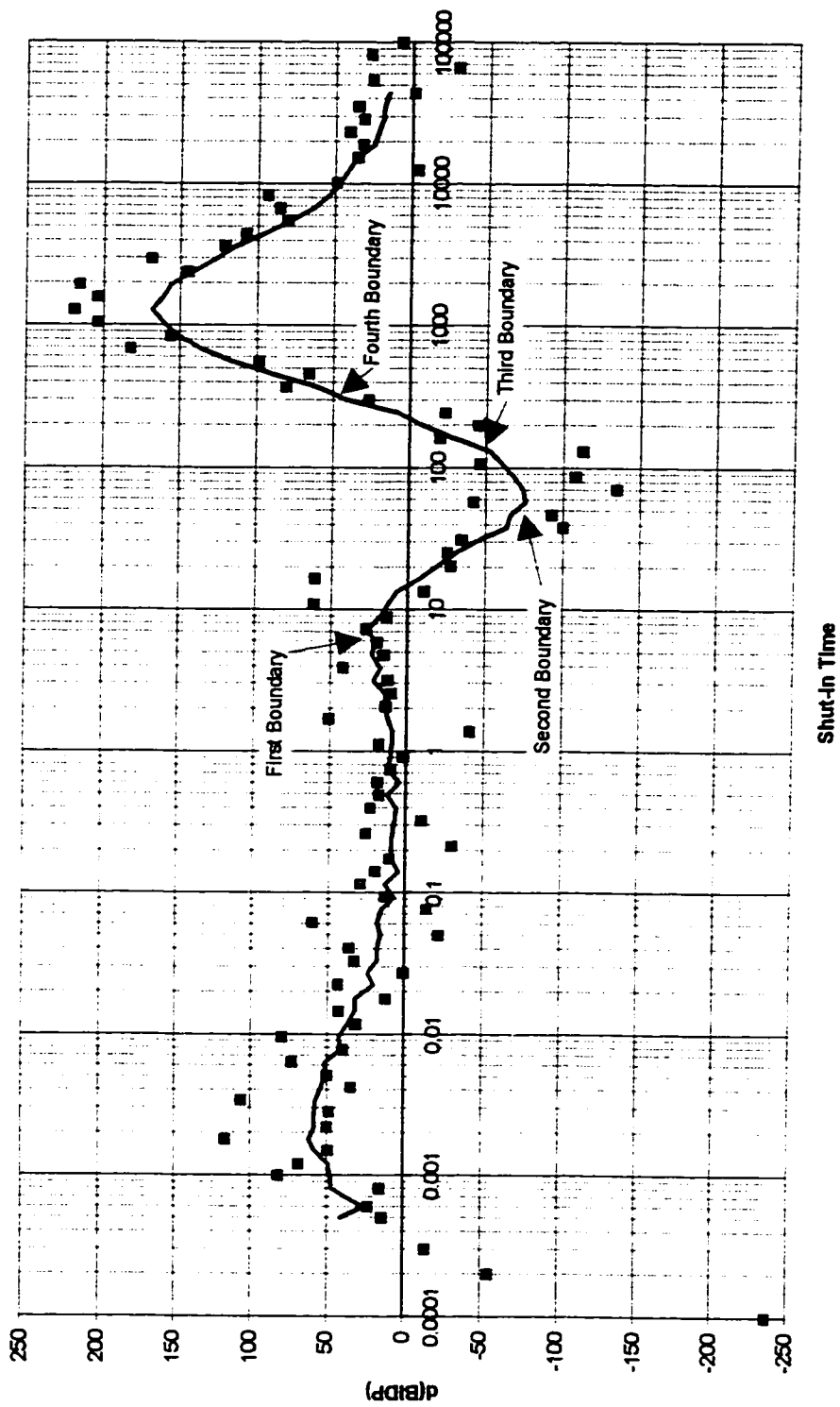


**Figure 5.9.2 Application of Bourdet Smoothing Algorithm**

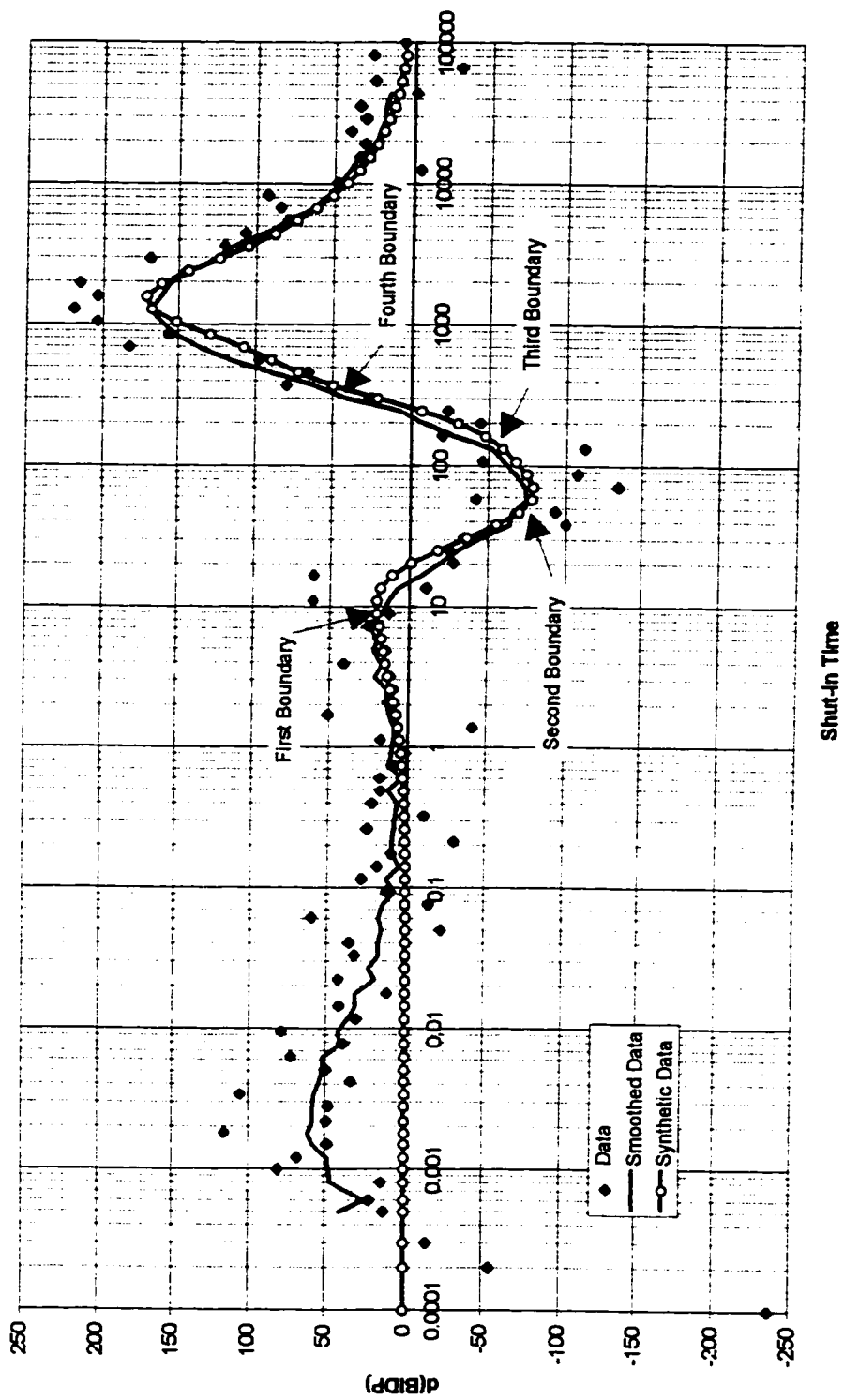


**Figure 5.9.3 Comparison of Smoothed and Synthetic Data**

## **6.0 Conclusions and Recommendations**

### **6.1 Conclusions**

A new method for the detection of no-flow boundaries in rectangular reservoirs using pressure buildup data has been outlined. This method is valid for both semi-infinite and finite reservoirs. It is equally applicable for oil and gas reservoirs.

This new method uses an infinite-acting reservoir response as the frame of reference. The pressure behaviour of a well produced in a specific reservoir is compared with an identical well producing in an infinite-acting homogeneous reservoir having the same characteristics. The semi-log derivative of this difference gives a unique signature curve from which no-flow boundaries may be determined directly.

The distance to the boundaries may be determined using the radius of investigation concept. The method does not mathematically manipulate the time variable, and thus the distance to a no flow boundary can be calculated directly using the radius of investigation equation.

Due to the mathematical structure of the model, all buildup data may be used in the analysis. Early time effects are not masked by wellbore phenomena or skin. This allows for

identification of boundaries very close to the well that would not be detectable with current techniques.

In this method, the length of shut-in time rather than the length of producing time is the significant variable. It was shown that, for very short flow periods, all the boundaries in a reservoir could be detected if the shut-in pressures were recorded for a sufficiently long period of time. This result has the potential for a significant change in the methodology currently used for testing wells.

## **6.2 Recommendations**

Future research on the  $d(BDIP)$  method of boundary detection should address the following issues:

1. An improved method for distinguishing between boundaries which occur very close together on the  $d(BDIP)$  curve. These reservoir configurations give very subtle boundary responses. Some investigation into using the second derivative was undertaken; however, the results were inconclusive.
2. The ability to distinguish how many boundaries there are in multiple equi-distant boundary configurations needs to be improved.
3. The potential to apply the  $d(BDIP)$  method to reservoirs which are not rectangular in shape. For example, reservoirs with oblique angles or that may be irregular in shape.
4. An investigation of the application of the  $d(BDIP)$  method to reservoirs with constant pressure boundaries.
5. An investigation of the application of the  $d(BDIP)$  method to composite reservoirs.



## **7.0 References**

Agarwal, R. G., Al-Hussainy, R., and Ramey, H. J., 1970: "An Investigation of Wellbore Storage and Skin Effect in Unsteady Liquid Flow: I, Analytical Treatment", Society of Petroleum Engineering Journal, (Sept. 1970), p279-290.

Agarwal, R. G., 1980: "A New Method to Account for Producing Time Effects when Drawdown Type Curves are used to Analyze Pressure Buildup and Other Test Data", SPE#9289, presented at the 55<sup>th</sup> Annual SPE Fall Technical Conference and Exhibition, Dallas Texas, September 21-24, 1980.

Ayestaran, L., Minhas, H. N., and Kuchuk, F. J., 1988: "The Use of Convolution Type Curves for the Analysis of Drawdown and Buildup Tests", SPE#18535, presented at the Eastern Regional Meeting of SPE, Charleston, WV, November 1-4, 1988.

Baygun, B., Kuchuk, F. J., and Arikan, O., 1994: "Deconvolution Under Normalized Autocorrelation Constraints", presented at the 69th annual Technical Conference and Exhibition of the SPE, New Orleans, LA, September 25-28, 1994.

Bourdet, D., Whittle, T. M., Douglas, A. A., and Pirard, Y. M., 1983: "A New Set of Type Curves Simplifies Well Test Analysis", World Oil, (May 1983).

Bourdet, D., Ayoub, J. A., and Pirard, Y. M., 1989: "Use of Pressure Derivative in Well-Test Interpretation", SPE#12777, SPE Formation Evaluation, (June 1989), p293-302.

Cobb, W. M. and Smith, J. T., 1975: "An Investigation of Pressure-Buildup Tests in Bounded Reservoirs", SPE#5133, Journal of Petroleum Technology, (August, 1975), p991-996.

Correa, A. C. and Ramey, H. J. Jr, 1986: "Combined Effects of Shut-In and Production: Solution with a New Inner Boundary Condition", SPE#15579, presented at the 61st Annual Technical Conference and Exhibition of SPE, New Orleans, LA, October 5-8, 1986.

Crank, J., 1975: "The Mathematics of Diffusion", Second Edition, Oxford University Press, London (1975).

Earlougher, R. C., 1977: "Advances in Well Test Analysis", SPE Monograph Series Volume 5, Society of Petroleum Engineers of AIME, Dallas, Texas (1977).

Earlougher, R. C., 1980: "Practicalities of Detecting Faults from Buildup Testing", Journal of Petroleum Technology, (January 1980), p18-20.

Gladfelter, R. E., Tracy, G. W., and Wilsey, L. E., 1955: "Selecting Wells which will Respond to Production-Stimulation Treatment", Drill. And Prod. Prac., API (1955) p117-119.

Horner, D.R., 1951: "Pressure Build-UP in Wells", Proceedings Third World Petroleum Congress, D. J. Brill, Leiden (1951) II., p503-521

Kuchuk, F. J., 1990-a: "Gladfelter Deconvolution", SPE#16377, SPE Formation Evaluation, (September 1990), p285-292.

Kuchuk, F. J., 1990-b: "Applications of Convolution and Deconvolution to Transient Well Tests", SPE#16394, SPE Formation Evaluation, (December 1990), p375-384.

Kuchuk, F. J., Carter, R. G., and Ayestaran, L., 1990: "Deconvolution of Wellbore Pressure and Flow Rate", SPE#1390, SPE Formation Evaluation, (March 1990), p53-59.

Lee, W. John, 1982: "Well Testing", Textbook Series Volume 1, SPE, Society of Petroleum Engineers of AIME , Dallas, Texas (1982)

Mattar, L. 1996: Personal communication, August 1996.

Matthews, C. S., Brons, F., and Hazebroek, P., 1954: "A Method for Determination of Average Reservoir Pressure in a Bounded Reservoir", Trans., AIME (1954) 201, p182-191.

Matthews, C. S., and Russell, D. G., 1967: "Pressure Buildup and Flow Tests in Wells", SPE Monograph Series Volume 1, Society of Petroleum Engineers of AIME, Dallas, Texas (1967).

McKinley, R. M., 1971: "Wellbore Transmissibility from Afterflow-Dominated Pressure Buildup Data", Journal of Petroleum Technology, (July 1971), p863-872.

McKinley, R. M. and Streltsova, T. D., 1988: "Nomograms for Analysis of Pressure Buildup Data Influenced by Heterogeneity", SPE#18121, presented at the 63<sup>rd</sup> Annual Technical Conference and Exhibition of the Society of Petroleum Engineers, Houston, Texas, October 2-5, 1988.

Meunier, D., Wittmann, M. J., and Stewart, G., 1983: "Interpretation of Pressure Buildup Test Using In-Situ measurement of Afterflow", SPE#11463, presented at the Middle East Oil Technical Conference of the SPE, Manama, Bahrain, March 14-17, 1983.

Miller, C. C., Dyes, A. B., and Hutchinson, C. A., 1950: "Estimation of Permeability and Reservoir Pressure from Bottom-Hole Pressure Build-up Characteristics", Trans. AIME (1950) 189, p91-104

Moser, H., 1983: "Late Time Pressure Analysis", SPE#12575, unsolicited manuscript provided to the Society of Petroleum Engineers for Distribution and possible publication in an SPE Journal, 1983.

Moser, H., 1985: "Practical Considerations When Reservoir Boundaries are Encountered During Well Testing", SPE#14313, presented at the 60th Annual Technical Conference and Exhibition of the SPE, Las Vegas, NV, September 22-25, 1985.

Moser, H., 1987: "An Alternative to Superposition for Monotonically Changing Flow Rates", SPE#16522, unsolicited manuscript provided to the Society of Petroleum Engineers for distribution and possible publication in an SPE Journal, 1987.

Raghavan, R., Meng, H-Z., and Reynolds, A. C., 1980: "Analysis of Pressure Buildup Data Following a Short Flow Period", SPE#9290, presented at the 55<sup>th</sup> Annual SPE Fall Technical Conference and Exhibition, Dallas Texas, September 21-24, 1980.

Ramey, H. J. Jr, 1976: "Practical Use of Modern Well Test Analysis", SPE#5878, presented at the 46th Annual California Regional Meeting of the SPE, Long Beach, California, April 8-9, 1976.

Ramey, H. J. and Cobb, W. M., 1971: "A General Pressure Buildup Theory for a Well in a Closed Drainage Area", SPE#3012, Journal of Petroleum Technology, (December 1971), p1493-1505.

Ramey, H. J., Kumar, A., and Gulati, M.S., 1977: "Gas Well Test Analysis Under Water-Drive Conditions", American Gas Association, Arlington, Virginia, (1977).

Slider, H. C., 1971: "A Simplified Method of Pressure Buildup Analysis for a Stabilized Well", SPE#3335, Journal of Petroleum Technology, (September 1971), p1155-1160.

Stewart, G., Wittmann, M. J., and Meunier, D., 1983: "Afterflow Measurement and Deconvolution in Well Test Analysis", SPE#12174, presented at the 58th Annual Technical Conference and Exhibition of the SPE, San Francisco, CA, October 5-8, 1983.

Thompson, L. G. and Reynolds, A. C., 1986: "Analysis of Variable-Rate Well-Test Pressure Data Using Duhamel's principle", SPE#13080, SPE Formation Evaluation, (October 1986), p453-469.

van Everdingen, A. F. and Hurst, W., 1949: "The Application of the Laplace Transformation to Flow Problems in Reservoirs", Trans. AIME (1949) 186, p305-324.

van Poolen, H. K., 1964: "Radius-of-Drainage and Stabilization-Time Equations", Oil and Gas Journal, (September 14, 1964) 138-146.

Wylie, C. Ray, 1975: "Advanced Engineering Mathematics", Fourth edition, McGraw-Hill Book Company, Toronto, 1975, p309-319.

*Few* are those who  
see with their own eyes and  
feel with their own hearts.

*Albert Einstein*

(1879 - 1955)



## Appendix

### Solution to the Radial Diffusivity Equation for Constant Flow Rate in an Infinite Medium

The mathematical problem is the solution of:

$$\frac{\partial^2 p}{\partial r^2} + \frac{1}{r} \frac{\partial p}{\partial r} = \frac{\phi \mu c_t}{k} \frac{\partial p}{\partial t} \quad \text{.....1}$$

with initial and boundary conditions of:

1)  $p = p_i$  at  $t=0$  for all  $r$

2)  $\left( r \frac{\partial p}{\partial r} \right)_{r_w} = \frac{q\mu}{2\pi kh}$  for all  $t > 0$

3)  $p \rightarrow p_i$  as  $r \rightarrow \infty$  for all  $t$ .

To facilitate a solution, the second condition is changed to the “line source” approximation:

$$\lim_{r \rightarrow 0} r \frac{\partial p}{\partial r} = \frac{q\mu}{2\pi kh} \quad \text{for } t > 0.$$

This boundary condition has been shown to yield identical results with those obtained from the solution of the problem with the original condition. (Matthews and Russell 1967)

To solve the equation, use the Boltzman transformation:

$$Y = \frac{\phi\mu c_t r^2}{4kt}.$$

Then  $\frac{dY}{dr} = \frac{\phi\mu c_t r}{2kt},$

$$\frac{d^2Y}{dr^2} = \frac{\phi\mu c_t}{2kt},$$

and  $\frac{dY}{dt} = -\frac{\phi\mu c_t r^2}{4kt^2}.$

Similarly,

$$\frac{\partial p}{\partial r} = \frac{dp}{dY} \frac{dY}{dr} = \frac{\phi\mu c_t r}{2kt} \frac{dp}{dY},$$

$$\frac{\partial^2 p}{\partial r^2} = \frac{\partial}{\partial r} \left( \frac{\partial p}{\partial r} \right) = \frac{\partial}{\partial r} \left( \frac{dp}{dY} \frac{dY}{dr} \right) = \frac{\partial}{\partial r} \left( \frac{\phi\mu c_t r}{2kt} \frac{dp}{dY} \right) = \frac{\phi\mu c_t}{2kt} \left[ \frac{dp}{dY} + \frac{\phi\mu c_t r^2}{2kt} \frac{d^2 p}{dY^2} \right]$$

and  $\frac{\partial p}{\partial t} = \frac{dp}{dY} \frac{dY}{dt} = -\frac{\phi\mu c_t r^2}{4kt^2} \frac{dY}{dt}.$

Substitute in equation 1:

$$\frac{\phi\mu c_t}{2kt} \left[ \frac{dp}{dY} + \frac{\phi\mu c_t r^2}{2kt} \frac{d^2p}{dY^2} \right] + \frac{\phi\mu c_t}{2kt} \frac{dp}{dY} = \frac{\phi\mu c_t}{k} \left( \frac{-\phi\mu c_t r^2}{4kt^2} \frac{dp}{dY} \right)$$

Collecting terms and simplifying gives:

$$2Y \frac{d^2p}{dY^2} + (2 + 2Y) \frac{dp}{dY} = 0, \text{ and finally}$$

$$\frac{d^2p}{dY^2} + \left(1 + \frac{1}{Y}\right) \frac{dp}{dY} = 0 \quad \text{.....2}$$

Applying this transformation to the boundary conditions gives

$$2) \lim_{Y \rightarrow 0} r \frac{dp}{dY} = \frac{q\mu}{2\pi kh} \quad \text{for } t > 0,$$

$$3) p \rightarrow p_i \text{ as } Y \rightarrow \infty \text{ for all } t.$$

$$\text{Let } W = \frac{dp}{dY} \text{ and then } \frac{dW}{dY} = \frac{d^2p}{dY^2}.$$

Substitute in equation 2.

$$\frac{dW}{dY} + \left(1 + \frac{1}{Y}\right)W = 0 \quad \text{.....3}$$

Separate variables

$$\frac{dW}{W} = -\left(1 + \frac{1}{Y}\right)dY$$

Integrating gives:

$$\ln(WY) = -Y + C_1 \quad \text{where } C_1 \text{ is a constant of integration.}$$

Then

$$WY = Ce^{-Y} \quad \text{where } C = e^{C_1}$$

$$W = \frac{Ce^{-Y}}{Y} = \frac{dp}{dY} \quad \text{and}$$

$$dp = \frac{Ce^{-Y}}{Y}dY \quad \text{.....4}$$

Applying boundary condition 2 gives

$$C = \frac{q\mu}{4\pi kh}$$

Integrating gives:

$$p = \frac{q\mu}{4\pi kh} (Ei(-Y)) + C_2 \quad \text{where } C_2 \text{ is a constant of integration.}$$

Substituting for Y gives:

$$p = \frac{q\mu}{4\pi kh} \left( Ei \left( -\frac{\phi\mu c_i r^2}{4kt} \right) \right) + C_2.$$

Applying boundary condition 3 gives

$$C_2 = p_i.$$

The solution to the Radial Diffusivity Equation for constant flow in an infinite reservoir is:

$$p = p_i + \frac{q\mu}{4\pi kh} \left( Ei \left( -\frac{\phi\mu c_i r^2}{4kt} \right) \right).$$

Or as it is more commonly written:

$$p_i - p = \frac{q\mu}{4\pi kh} \left( -Ei \left( -\frac{\phi\mu c_i r^2}{4kt} \right) \right).$$

## Key to Configurations Used in Figures

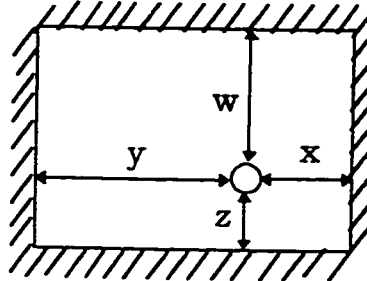


Figure Number	Page Number	x	y	z	w
4.3.2	40				
	2 Intersecting	25	$\infty$	100	$\infty$
	2 Parallel	25	100	$\infty$	$\infty$
	3 Intersecting	25	65	100	$\infty$
4.4.1	43	25	$\infty$	$\infty$	$\infty$
4.4.2	46	25	$\infty$	$\infty$	$\infty$
4.4.3	47	20	$\infty$	100	$\infty$
4.4.4	49	20	75	150	$\infty$
4.4.5	50	25	100	65	150
4.4.6	53	25	100	65	150
4.5.2	58	20	$\infty$	$\infty$	$\infty$
4.5.3	60	25	100	65	150
4.6.2	64	25	$\infty$	100	$\infty$
4.7.2	68	25	100	$\infty$	$\infty$
4.8.2	75	25	100	75	$\infty$
4.9.2	86	25	100	65	150
5.1.1	93	20	$\infty$	$\infty$	$\infty$

<b>Figure Number</b>	<b>Page Number</b>	<b>x</b>	<b>y</b>	<b>z</b>	<b>w</b>
5.2.1	96	25	100	65	150
5.3.1	99	10	$\infty$	$\infty$	$\infty$
5.3.2	100	10	$\infty$	$\infty$	$\infty$
5.4.1	104	100	$\infty$	$\infty$	$\infty$
5.4.2	105	100	$\infty$	$\infty$	$\infty$
5.4.3	106	100	$\infty$	$\infty$	$\infty$
5.4.4	107	100	$\infty$	$\infty$	$\infty$
5.5.1	110	100	$\infty$	$\infty$	$\infty$
5.5.2	111	100	$\infty$	$\infty$	$\infty$
5.6.1	113				
Single Boundary		100	$\infty$	$\infty$	$\infty$
2 Intersecting		100	$\infty$	100	$\infty$
2 Parallel		100	100	$\infty$	$\infty$
3 Boundaries		100	100	100	$\infty$
5.7.1	116	25	$\infty$	$\infty$	$\infty$
5.7.2	118	25	100	65	150
5.7.3	119	25	100	65	150
5.9.1	124	25	100	65	150
5.9.2	125	25	100	65	150
5.9.3	126	25	100	65	150

### Distance to Boundary - Sample Calculation

The equation for the distance to the boundary is:

$$d = \sqrt{\frac{4k\Delta t}{\gamma\phi\mu c_t}} \text{ in consistent units.}$$

For the system of units used in the examples in this work, the equation becomes:  $d = \sqrt{\frac{k\Delta t}{7.036 \times 10^4 \phi \mu c_t}}$ .

Using Figure 4.5.2 as an example, the following reservoir parameters were used to create the figure:

$$k = 7 \text{ md}$$

$$\phi = 12\%$$

$$\mu = 1.461 \text{ mPa}\cdot\text{s}$$

$$c_t = 8.25 \times 10^{-6} \text{ kPa}^{-1}$$

From Figure 4.5.2 the first maximum is located at  $\Delta t = 5.8 \text{ hr}$

Substituting these values in the above equation, distance to the boundary is calculated as:

$$d = \sqrt{\frac{k\Delta t}{7.036 \times 10^4 \phi \mu c_t}} = \sqrt{\frac{(7)(5.8)}{7.036 \times 10^4 (0.12)(1.461)(8.25 \times 10^{-6})}}$$

$$d = 20 \text{ m.}$$



## Computer Program Listings

```

SUBROUTINE EI(X,E1)
C
C   DEFINITION: E1(X) = -EI(-X)
C   IBM SCIENTIFIC SUBROUTINE PACKAGE (VERSION III)
C   PROGRAMMER'S MANUAL, H20-0205 (1968) PAGES 368-369
C   FROM Ramey, Kumar, AGA Book
C

      DOUBLE PRECISION X,DEXP,DLOG,ARG,RES,E1
      IF (X.GT.60.) GO TO 120
      IF (X.LE.4.) GO TO 100
      ARG=4./X
      RES=(0.249999999+ARG*(-0.062498588+ARG*(0.031208561+ARG
1*(-0.022951979+ARG*(0.020412099+ARG*(-0.017555779+ARG*(0.011723273
2+ARG*(-0.0049362007+ARG*(0.00094427614))))))))))
      RES=DEXP(-X)*ARG*RES
      GO TO 130
100 IF (X.LT.0.) GO TO 120
      IF (X.EQ.0.) GO TO 110
      RES=-DLOG(X)-.57721586+X*(1.0+X*(-0.25+X*(0.05555552+X*(-0.0104166
162+X*(.0016666906+X*(-.00023148392+X*(2.833759D-05+X*(-3.099604D-0
26+X*(3.0726221D-07+X*(-2.763583D-08+X*(2.1915699D-09+X*(-1.6826592
3D-10+X*(1.5798675D-11+X*(-1.0317602D-12))))))))))))))
      GO TO 130
110 RES=1.D75
      GO TO 130
120 RES=0
130 E1=RES
      END

```

```

PROGRAM EIINFINI

    REAL MU,L,K
    DOUBLE PRECISION ARG1A,ARG1,ARG2A,ARG2

    OPEN (5,FILE='SIN.TXT')
    OPEN (6,FILE='EIIN150')

    READ (5,910) PI,PHI,MU,K,RW,TP,Q,B,H,L,CT
    910 FORMAT (10F10.4,E10.3)
C
    9000 WRITE (6,910)PI,PHI,MU,K,RW,TP,Q,B,H,L,CT
C
    CONST1=933.1*Q*B*MU/(K*H)
    CONST2=7.036E4*PHI*MU*CT*RW**2/K
C
C   FOR DT=0
C
    ARG1A=CONST2/TP
    CALL EI(ARG1A,ARG1)
    ARG1=ARG1*(-1.0)
    PWS=PI+CONST1*ARG1

    WRITE (6,920) DT,PWS
C
C   FOR DT>0
C
    DO 100 I=1,10000
        READ (5,915) DT
    915 FORMAT (F10.4)
        IF (DT.EQ.-5.0) GO TO 999

        ARG1A=CONST2/(TP+DT)
        CALL EI(ARG1A,ARG1)
        ARG1=ARG1*(-1.0)

        ARG2A=CONST2/DT
        CALL EI(ARG2A,ARG2)
        ARG2=ARG2*(-1.0)

        PWS=PI+CONST1*(ARG1-ARG2)

        WRITE (6,920) DT,PWS
    920 FORMAT (5X,F10.4,3X,F10.2)

    100 CONTINUE

    999 CONTINUE
    STOP
    END

```

SUBROUTINE EI(X,E1)

C

C   DEFINITION:  $E1(X) = -EI(-X)$

C    IBM SCIENTIFIC SUBROUTINE PACKAGE (VERSION III)

C    PROGRAMMER'S MANUAL, H20-0205 (1968) PAGES 368-369

C    FROM Ramey, Kumar, AGA Book

C

DOUBLE PRECISION X,DEXP,DLOG,ARG,RES,E1

IF (X.GT.60.) GO TO 120

IF (X.LE.4.) GO TO 100

ARG=4./X

RES=(0.249999999+ARG\*(-0.062498588+ARG\*(0.031208561+ARG  
1\*(-0.022951979+ARG\*(0.020412099+ARG\*(-0.017555779+ARG\*(0.011723273  
2+ARG\*(-0.0049362007+ARG\*(0.00094427614)))))))))

RES=DEXP(-X)\*ARG\*RES

GO TO 130

100 IF (X.LT.0.) GO TO 120

IF (X.EQ.0.) GO TO 110

RES=-DLOG(X)-.57721586+X\*(1.0+X\*(-0.25+X\*(0.05555552+X\*(-0.0104166  
162+X\*(.0016666906+X\*(-.00023148392+X\*(2.833759D-05+X\*(-3.099604D-0  
26+X\*(3.0726221D-07+X\*(-2.763583D-08+X\*(2.1915699D-09+X\*(-1.6826592  
3D-10+X\*(1.5798675D-11+X\*(-1.0317602D-12))))))))))

GO TO 130

110 RES=1.D75

GO TO 130

120 RES=0

130 E1=RES

END

PROGRAM EISINGLE

```
      REAL MU,K,L
      DOUBLE PRECISION ARG1A,ARG2A,ARG3A,ARG4A,ARG1,ARG2,ARG3,ARG4

      OPEN (5, FILE='SIN.TXT')
      OPEN (6, FILE='PWSOU150')

      READ (5,910) PI,PHI,MU,K,RW,TP,Q,B,H,L,CT
      910 FORMAT (10F10.4,E10.3)
C
      9000 WRITE (6,910) PI,PHI,MU,K,RW,TP,Q,B,H,L,CT
C
      CONST1=PHI*MU*CT/K
      CONST2=CONST1*RW**2.0
      CONST3=CONST1*(2.0*L)**2.0
      CONST4=933.1*Q*B*MU/(K*H)

      ARGB=7.036E4*CONST2
      ARGC=7.036E4*CONST3

C
C  FOR THE CASE OF DT=0
C
      DT=0.0
      ARG1A=ARGB/TP
      CALL EI(ARG1A,ARG1)
      ARG1=ARG1*(-1.0)
      ARG3A=ARGC/TP
      CALL EI(ARG3A,ARG3)
      ARG3=ARG3*(-1.0)

      PWS=PI+CONST4*(ARG1+ARG3)
      WRITE (6,950) DT,PWS

C
C  FOR DT>0
C
      DO 100 I=1,10000
      READ (5,920) DT
      920 FORMAT (F10.4)
      IF (DT.EQ.-5.0) GO TO 999
      ARG1A=ARGB/(TP+DT)
      CALL EI(ARG1A,ARG1)
      ARG1=ARG1*(-1.0)
      ARG2A=ARGB/DT
      CALL EI(ARG2A,ARG2)
      ARG2=ARG2*(-1.0)

      ARG3A=ARGC/(TP+DT)
```

```

CALL EI(ARG3A,ARG3)
ARG3=ARG3*(-1.0)

ARG4A=ARGC/DT
CALL EI(ARG4A,ARG4)
ARG4=ARG4*(-1.0)

PWS=PI+CONST4*(ARG1-ARG2+ARG3-ARG4)

WRITE (6,950) DT,PWS
950 FORMAT (5X,F10.4,3X,F10.2)

100 CONTINUE

999 CONTINUE
END

SUBROUTINE EI(X,E1)
C
C DEFINITION: E1(X) = -EI(-X)
C IBM SCIENTIFIC SUBROUTINE PACKAGE (VERSION III)
C PROGRAMMER'S MANUAL, H20-0205 (1968) PAGES 368-369
C FROM Ramey, Kumar, AGA Book
C

DOUBLE PRECISION X,DEXP,DLOG,ARG,RES,E1
IF (X.GT.60.) GO TO 120
IF (X.LE.4.) GO TO 100
ARG=4./X
RES=(0.24999999+ARG*(-0.062498588+ARG*(0.031208561+ARG
1*(-0.022951979+ARG*(0.020412099+ARG*(-0.017555779+ARG*(0.011723273
2+ARG*(-0.0049362007+ARG*(0.00094427614))))))))))
RES=DEXP(-X)*ARG*RES
GO TO 130
100 IF (X.LT.0.) GO TO 120
IF (X.EQ.0.) GO TO 110
RES=-DLOG(X)-.57721586+X*(1.0+X*(-0.25+X*(0.05555552+X*(-0.0104166
162+X*(.0016666906+X*(-.00023148392+X*(2.833759D-05+X*(-3.099604D-0
26+X*(3.0726221D-07+X*(-2.763583D-08+X*(2.1915699D-09+X*(-1.6826592
3D-10+X*(1.5798675D-11+X*(-1.0317602D-12))))))))))))))
GO TO 130
110 RES=1.D75
GO TO 130
120 RES=0
130 E1=RES

RETURN
END

```

PROGRAM RTANGLE

```
      REAL MU,K,LE,LS,LSE
      DOUBLE PRECISION ARG1A,ARG2A,ARG3A,ARG4A,ARG5A,ARG6A,ARG7A,ARG8A
      DOUBLE PRECISION ARG1,ARG2,ARG3,ARG4,ARG5,ARG6,ARG7,ARG8

      OPEN (5, FILE='RTANG.TXT')
      OPEN (6, FILE='RTANGOUT')

      READ (5,910) PI,PHI,MU,K,RW,TP,Q,B,H,LE,LS,CT
910  FORMAT (11F10.4,E10.3)
C
9000 WRITE (6,910) PI,PHI,MU,K,RW,TP,Q,B,H,LE,LS,CT
C
      LSE=(4*LE**2.0+4*LS**2)**0.5
      CONST1=933.1*Q*B*MU/(K*H)
      CONST2=PHI*MU*CT/K
      CONST3=CONST2*RW**2.0
      CONST4=CONST2*(2.0*LE)**2.0
      CONST5=CONST2*(2.0*LS)**2.0
      CONST6=CONST2*LSE**2.0

      ARGB=7.036E4*CONST3
      ARGC=7.036E4*CONST4
      ARGD=7.036E4*CONST5
      ARGE=7.036E4*CONST6

C
C  FOR THE CASE OF DT=0
C
      ARG1A=ARGB/TP
      CALL EI(ARG1A,ARG1)
      ARG1=ARG1*(-1.0)

      ARG3A=ARGC/TP
      CALL EI(ARG3A,ARG3)
      ARG3=ARG3*(-1.0)

      ARG5A=ARGD/TP
      CALL EI(ARG5A,ARG5)
      ARG5=ARG5*(-1.0)

      ARG7A=ARGE/TP
      CALL EI(ARG7A,ARG7)
      ARG7=ARG7*(-1.0)

      PWS=PI+CONST1*(ARG1+ARG3+ARG5+ARG7)
      WRITE (6,950) DT,PWS
```

```

C
C FOR DT>0
C
  DO 900 I=1,10000
    READ (5,920) DT
920  FORMAT (F10.4)
    IF (DT.EQ.-5.0) GO TO 999

    ARG1A=ARGB/(TP+DT)
    CALL EI(ARG1A,ARG1)
    ARG1=ARG1*(-1.0)

    ARG2A=ARGB/DT
    CALL EI(ARG2A,ARG2)
    ARG2=ARG2*(-1.0)

    ARG3A=ARGC/(TP+DT)
    CALL EI(ARG3A,ARG3)
    ARG3=ARG3*(-1.0)

    ARG4A=ARGC/DT
    CALL EI(ARG4A,ARG4)
    ARG4=ARG4*(-1.0)

    ARG5A=ARGD/(TP+DT)
    CALL EI(ARG5A,ARG5)
    ARG5=ARG5*(-1.0)

    ARG6A=ARGD/DT
    CALL EI(ARG6A,ARG6)
    ARG6=ARG6*(-1.0)

    ARG7A=ARGE/(TP+DT)
    CALL EI(ARG7A,ARG7)
    ARG7=ARG7*(-1.0)

    ARG8A=ARGE/DT
    CALL EI(ARG8A,ARG8)
    ARG8=ARG8*(-1.0)

    PWS=PI+CONST1*(ARG1-ARG2+ARG3-ARG4+ARG5-ARG6+ARG7-ARG8)

    WRITE (6,950) DT,PWS
950  FORMAT (5X,F10.4,3X,F10.2)

900  CONTINUE

999  CONTINUE
    STOP
    END

```

```

SUBROUTINE EI(X,E1)
C
C  DEFINITION:  $E1(X) = -EI(-X)$ 
C    IBM SCIENTIFIC SUBROUTINE PACKAGE (VERSION III)
C    PROGRAMMER'S MANUAL, H20-0205 (1968) PAGES 368-369
C    FROM Ramey, Kumar, AGA Book
C

DOUBLE PRECISION X,DEXP,DLOG,ARG,RES,E1
IF (X.GT.60.) GO TO 120
IF (X.LE.4.) GO TO 100
ARG=4./X
RES=(0.24999999+ARG*(-0.062498588+ARG*(0.031208561+ARG
1*(-0.022951979+ARG*(0.020412099+ARG*(-0.017555779+ARG*(0.011723273
2+ARG*(-0.0049362007+ARG*(0.00094427614))))))))))
RES=DEXP(-X)*ARG*RES
GO TO 130
100 IF (X.LT.0.) GO TO 120
IF (X.EQ.0.) GO TO 110
RES=-DLOG(X)-.57721586+X*(1.0+X*(-0.25+X*(0.05555552+X*(-0.0104166
162+X*(-.0016666906+X*(-.00023148392+X*(2.833759D-05+X*(-3.099604D-0
26+X*(3.0726221D-07+X*(-2.763583D-08+X*(2.1915699D-09+X*(-1.6826592
3D-10+X*(1.5798675D-11+X*(-1.0317602D-12))))))))))))))
GO TO 130
110 RES=1.D75
GO TO 130
120 RES=0
130 E1=RES

RETURN
END

```



PROGRAM PARALLEL

```

REAL MU,K,LE,LW
DOUBLE PRECISION ARG1A,ARG2A,ARG3A,ARG4A,ARG5A,ARG6A,ARG7A,ARG8A
DOUBLE PRECISION ARG1,ARG2,ARG3,ARG4,ARG5,ARG6,ARG7,ARG8

OPEN (5, FILE='PARAL.TXT')
OPEN (6, FILE='PARAOUT')

READ (5,910) PI,PHI,MU,K,RW,TP,Q,B,H,LE,LW,CT
910 FORMAT (11F10.4,E10.3)
C
WRITE (6,910) PI,PHI,MU,K,RW,TP,Q,B,H,LE,LW,CT
C
CONST1=933.1*Q*B*MU/(K*H)
CONST2=PHI*MU*CT/K
CONST3=CONST2*RW**2.0

ARGA=7.036E4*CONST3
ARGB=7.036E4*CONST2

C
C FOR THE CASE OF DT=0
C
DT=0.0
ARG1A=ARGA/TP
CALL EI(ARG1A,ARG1)
ARG1=ARG1*(-1.0)

SUM=ARG1

DO 100 I=1,10000

ARG3A=(ARGB*(2*I*LE+2*(I-1)*LW)**2)/TP
ARG5A=(ARGB*(2*I*LW+2*(I-1)*LE)**2)/TP

IF(ARG3A.GT.10.AND.ARG5A.GT.10) GO TO 199

CALL EI(ARG3A,ARG3)
CALL EI(ARG5A,ARG5)

ARG3=ARG3*(-1.0)
ARG5=ARG5*(-1.0)
SUM=SUM+ARG3+ARG5

ARG7A=(ARGB*(2*I*(LE+LW))**2)/TP
IF(ARG7A.GT.10) GO TO 199
CALL EI(ARG7A,ARG7)
ARG7=ARG7*(-1.0)
SUM=SUM+2*ARG7

```

```

100 CONTINUE

199 PWS=PI+CONST1*SUM
   WRITE (6,950) DT,PWS

C
C   FOR DT>0
C
   DO 300 J=1,10000
   READ (5,920) DT
920 FORMAT (F10.4)
   IF (DT.EQ.-5.0) GO TO 999
   SUM=0.0

   ARG1A=ARGA/(TP+DT)
   RG2A=ARGA/DT

   CALL EI(ARG1A,ARG1)
   CALL EI(ARG2A,ARG2)

   ARG1=ARG1*(-1.0)
   ARG2=ARG2*(-1.0)
   SUM=ARG1-ARG2

   DO 200 I=1,10000
   DIST1=ARGB*(2*I*LE+2*(I-1)*LW)**2
   DIST2=ARGB*(2*I*LW+2*(I-1)*LE)**2
   DIST3=ARGB*(2*I*(LE+LW))**2

   ARG3A=DIST1/(TP+DT)
   ARG4A=DIST1/DT
   ARG5A=DIST2/(TP+DT)
   ARG6A=DIST2/DT

   IF (ARG3A.GT.10.AND.ARG5A.GT.10) GO TO 299

   CALL EI(ARG3A,ARG3)
   CALL EI(ARG4A,ARG4)
   CALL EI(ARG5A,ARG5)
   CALL EI(ARG6A,ARG6)

   ARG3=ARG3*(-1.0)
   ARG4=ARG4*(-1.0)
   ARG5=ARG5*(-1.0)
   ARG6=ARG6*(-1.0)

   SUM=SUM+ARG3-ARG4+ARG5-ARG6

   ARG7A=DIST3/(TP+DT)

```

```

ARG8A=DIST3/DT

IF (ARG7A.GT.10) GO TO 299

CALL EI(ARG7A,ARG7)
CALL EI(ARG8A,ARG8)

ARG7=ARG7*(-1.0)
ARG8=ARG8*(-1.0)

SUM=SUM+2*ARG7-2*ARG8

200 CONTINUE

299 PWS=PI+CONST1*SUM

WRITE (6,950) DT,PWS
950 FORMAT (5X,F10.4,3X,F10.2)

300 CONTINUE

999 CONTINUE
STOP
END

SUBROUTINE EI(X,E1)
C
C DEFINITION: E1(X) = -EI(-X)
C IBM SCIENTIFIC SUBROUTINE PACKAGE (VERSION III)
C PROGRAMMER'S MANUAL, H20-0205 (1968) PAGES 368-369
C FROM Ramey, Kumar, AGA Book
C

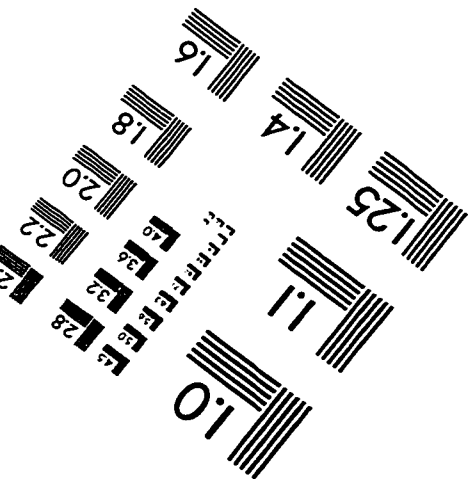
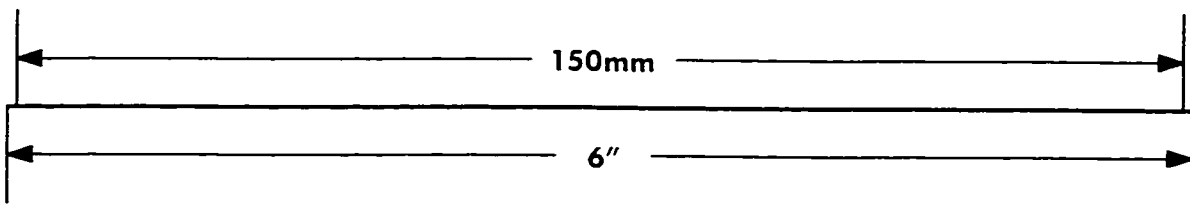
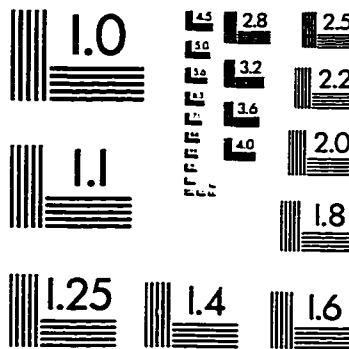
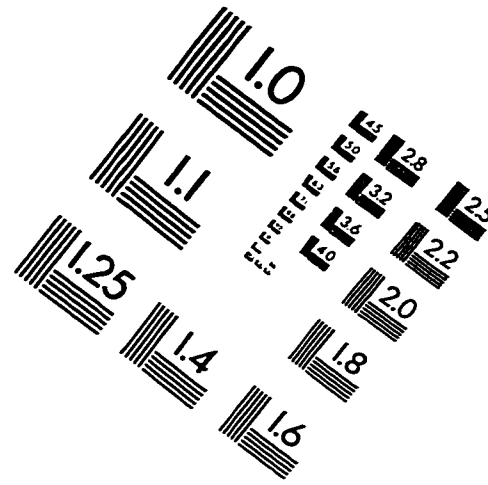
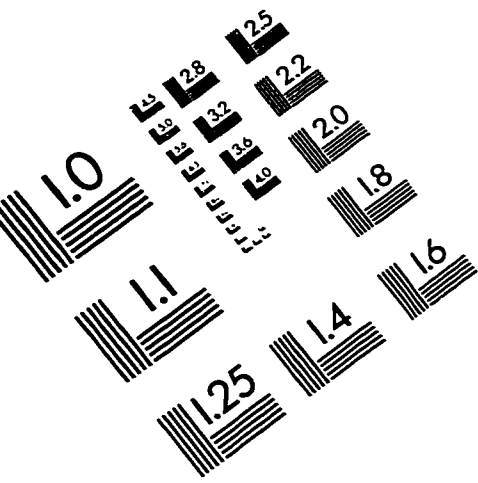
DOUBLE PRECISION X,DEXP,DLOG,ARG,RES,E1
IF (X.GT.60.) GO TO 120
IF (X.LE.4.) GO TO 100
ARG=4./X
RES=(0.24999999+ARG*(-0.062498588+ARG*(0.031208561+ARG
1*(-0.022951979+ARG*(0.020412099+ARG*(-0.017555779+ARG*(0.011723273
2+ARG*(-0.0049362007+ARG*(0.00094427614)))))))))
RES=DEXP(-X)*ARG*RES
GO TO 130
100 IF (X.LT.0.) GO TO 120
IF (X.EQ.0.) GO TO 110
RES=-DLOG(X)-.57721586+X*(1.0+X*(-0.25+X*(0.05555552+X*(-0.0104166
162+X*(.0016666906+X*(-.00023148392+X*(2.833759D-05+X*(-3.099604D-0
26+X*(3.0726221D-07+X*(-2.763583D-08+X*(2.1915699D-09+X*(-1.6826592
3D-10+X*(1.5798675D-11+X*(-1.0317602D-12)))))))))))))

```

```
      GO TO 130
110 RES=1.D75
      GO TO 130
120 RES=0
130 E1=RES

      RETURN
      END
```

# IMAGE EVALUATION TEST TARGET (QA-3)



APPLIED IMAGE, Inc  
1653 East Main Street  
Rochester, NY 14609 USA  
Phone: 716/482-0300  
Fax: 716/288-5989

© 1993, Applied Image, Inc., All Rights Reserved

